uOttawa

L'Université canadienne
Canada's university

FACULTÉ DES ÉTUDES SUPÉRIEURES ET POSTOCTORALES

uOttawa

L'Université canadienne
Canada's university

FACULTY OF GRADUATE AND POSDOCTORAL STUDIES

Xianjie Li

AUTEUR DE LA THÈSE / AUTHOR OF THESIS

M.A.Sc. (Mechanical Engineering)

GRADE / DEGREE

Department of Mechanical Engineering

FACULTÉ, ÉCOLE, DÉPARTEMENT / FACULTY, SCHOOL, DEPARTMENT

Investigation into Spongy Bone Remodeling Through a Semi-mechanistic Bone Remodeling Theory Using Finite Element Analysis

TITRE DE LA THÈSE / TITLE OF THESIS

Gholamreza Rouhi

DIRECTEUR (DIRECTRICE) DE LA THÈSE / THESIS SUPERVISOR

CO-DIRECTEUR (CO-DIRECTRICE) DE LA THÈSE / THESIS CO-SUPERVISOR

Zin Wang

Marianne Fenech

Gary W. Slater

Le Doyen de la Faculté des études supérieures et postdoctorales / Dean of the Faculty of Graduate and Postdoctoral Studies

Investigation into Spongy Bone Remodeling through a Semi-mechanistic Bone Remodeling Theory Using Finite Element Analysis

by

Xianjie Li

A thesis submitted to

the Faculty of Graduate and Postdoctoral Studies

in partial fulfillment of

the requirements for the degree of

MASTER OF APPLIED SCIENCE

in Mechanical Engineering

Ottawa-Carleton Institute for Mechanical and Aerospace Engineering

UNIVERSITY of OTTAWA

Your file Votre référence
ISBN: 978-0-494-74187-0
Our file Notre référence
ISBN: 978-0-494-74187-0

Investigation into Spongy Bone Remodeling through a Semi-mechanistic Bone Remodeling Theory Using Finite Element Analysis

Xianjie Li

Department of Mechanical Engineering, University of Ottawa

Submitted in December, 2010

Master thesis abstract

Computer simulation provides a useful approach for the studies on the issues related to living bone. Here, we performed two simulation studies on the spongy bone remodeling through Huiskes et al.'s semi-mechanistic bone remodeling theory. In the first study, a 2D finite element (FE) model was developed. The simulation results suggested that decreasing osteocyte density could cause spongy bone loss in healthy old adults, and reduction in osteocyte mechanosensitivity might contribute to excessive bone loss in osteoporotic bones. In the second study, we extended Huiskes et al.'s theory for overloading condition with respect to clinical findings and proposed a 3D FE model. It was the first 3D simulation which showed the spongy bone loss caused by overload. It supported our hypotheses that overload increased osteoclastic activities and reduced osteocyte influence distance. The simulation results in both two studies are in agreement with existing experimental evidences, also with Wolff's Law.

Abstract

Computer simulation provides a useful approach for the studies on the issues related to living bone. Here, we performed two simulation studies on the spongy bone remodeling through Huiskes et al.'s semi-mechanistic bone remodeling theory. In the first study, a 2D finite element (FE) model was developed. The simulation results suggested that decreasing osteocyte density could cause spongy bone loss in healthy old adults, and reduction in osteocyte mechanosensitivity might contribute to excessive bone loss in osteoporotic bones. In the second study, we extended Huiskes et al.'s theory for overloading condition with respect to clinical findings and proposed a 3D FE model. It was the first 3D simulation which showed the spongy bone loss caused by overload. It supported our hypotheses that overload increased osteoclastic activities and reduced osteocyte influence distance. The simulation results in both two studies are in agreement with existing experimental evidences, also with Wolff's Law.

Acknowledgements

First of all, I would like to express my gratitude immensely to my supervisor Dr. Gholamreza Rouhi for his guidance, support, hard work and dedication throughout my graduate studies. His continuous encouragement and his passion for research motivated me all the time when I experienced any challenge and obstacle in my studies and research.

I would like to thank the University of Ottawa's FGPS for providing the conference travel grant and thank the University of Ottawa's GSAED for providing additional financial support.

I am grateful to all of my research group mates. In particular, I would like to thank Kwan-Ching Geoffrey Ng and Kristina Haase who have always been happy to lend a hand or share their knowledge. As well, thanks go to Ali Vahdati for his useful feedbacks. Furthermore, I would like to acknowledge Dr. Michel Labrosse for his advice on my studies.

Last but not least I would like to give a special thank you to my parents, Ziqiu Li and Ling Lin, and my sisters, Xianxian Li and Xianli Li, who have always encouraged me to purse my interest. Their endless love, support and patience enabled me to complete my study.

Contents

List of Tables

List of Figures

Nomenclature

a	Empirical constant
$[B]$	Strain-nodal displacement matrix
b	Constant
C	Compliance tensor
C_e	Proportionality constant
C_{ij}	Generalized matrix of remodeling coefficients
C_x	Remodeling rate coefficient
c	Constant
D	Osteocyte influence distance (or decay constant)
D_{ol}	Osteocyte influence distance under overload
$[D]$	Stress-strain matrix
$d_i\,(x)$	Distance between osteocyte i and location x
$\frac{dm}{dt}$	Rate of bone remodeling
$\frac{dm_{ob}}{dt}$	Rate of formation by osteoblasts
$\frac{dm_{oc}}{dt}$	Rate of resorption by osteoclasts
$\frac{dX}{dt}$	Rate of bone growth perpendicular to the surface
E	Elastic modulus of the material
E_{max}	Maximum Young's modulus
F	Loading amplitude
F_{ol}	Critical load value for overload
F'	Static external stress

$\{F\}$ Global force vector

f Loading frequency

$f_i(x)$ Decay function of bone formative stimulus sent from osteocyte i to location x

$[K]$ Global stiffness matrix

$[K^e]$ Element stiffness matrix

k_{ol} Threshold stimulus for calculating bone resorption probability under overload

k_{lr} Bone formation threshold

m Relative density

m_T Mass of total bone

N Number of osteocytes within the influence region

P Porosity

$P(x,t)$ Total bone formative stimulus

p Bone resorption probability

$p_{ol}(x,t)$ Bone resorption probability under overload

$R_i(t)$ Strain energy density rate in the location of osteocyte i

r_{oc} Relative amount of mineral resorbed by each osteoclast resorption

$r_{oc\text{-}ol}$ Amount of mineral resorbed by each osteoclast resorption under overload

S Stiffness tensor

s Half width of the lazy zone

t Time

U Strain energy density

U^* Equilibrium value of strain energy density that determines the boundary between apposition and resorption

$\{U\}$ Vector of global displacement

$\{U^e\}$ Vector of element nodal displacement

V_B The volume of bone tissue

V_T The volume of total bone

V_V The volume of void (or marrow) parts

x Surface location

Greek symbols

γ Power that relates Young's modulus and relative density

ε Strain tensor

ε_{ij}^{*} Homeostatic strain tensor

ε_{ij} Actual strain tensor

μ_i Osteocyte mechanosensitivity of osteocyte i

ν Poisson ratio

ρ Apparent density

σ Stress tensor

τ Proportionality factor that determines the bone formation rate

Acronyms

2D Two-dimensional

3D Three-dimensional

BMD Bone mineral density

BMUs Basic multicellular units

DEXA Dual energy x-ray absorptiometry

DOFs Degrees of freedom

FEA Finite element analysis

MES Minimum effective strain

PBM Peak bone mass

PGE_2 Prostaglandin E_2

SED Strain energy density

μFEA Micro-finite element analysis

Chapter 1

Introduction

Bone is the main component of the musculoskeletal system. It is characterised physically by hardness, moderate elasticity, and very limited plasticity. The bone tissue is classified as either cortical (compact or Haversian) or spongy (trabecular or cancellous) bone. Cortical bone is a rather dense tissue which forms the outside of the bone as a solid structure. Spongy bone is porous and primarily found near joint surfaces, at the end of long bones and within vertebrate. It has a complex three-dimensional structure consisting of struts and plates of trabeculae. Although bone cells make up a small percentage of bone volume, they play a critical role in the adaptation of its structure. There are four main types of bone cells. They are: osteoclasts, which resorb old bone; osteoblasts, which form new bone; osteocytes, which is believed that act as mechanosensors (Cowin et al., 1991; Burger, 2001; Burger and Klein-Nulend, 1999, Nijweide, et al., 1996) and bone lining cells, which are inactive cells on the resting surfaces of bone.

Although bones may seem like hard and lifeless structures, bone is a living, continuously self-renewing tissue (Elisabeth et al., 1994). This tissue is able to adapt itself to the variation of mechanical environment. Apart from skeletal growth and fracture healing, bone maintains and adapts its mass and internal structure by a process called bone remodelling process. Bone remodeling is a repair mechanism targeted to increase the lifetime of bone tissue by removing microdamage and substituting it with new bone (Laoise and Patrick, 2007). It consists of two distinct stages: bone resorption by osteoclasts, and bone formation by

osteoblasts. Ostoclasts and osteoblasts which carry out bone remodeling process are called *basic multicellular units* or BMUs. Usually, the resorption and formation are in balance and skeletal strength and integrity are maintained. In cortical bone, BMUs form cylindrical canals through the bone. In spongy bone, the remodeling process is a surface event. Due to spongy bone's large surface-to-volume ration, spongy bone is more actively remodeled than cortical bone (Huiskes and van Rietbergen, 2005).

For restoring normal function and relieving the pain caused by trauma or disease, the implants are used to replace or augment bone. For example, orthopaedic implants are artificial devices incorporated into bones and joints, often acting as joint replacements in cases where the hip, knee, shoulder or elbow have been damaged by injury or by diseases such as osteoarthritis. In the bone-implant system, bone remodeling plays an important role in the adaptation of its structure to the changes in the mechanical environment. In order to estimate the long-term impacts of implants and prostheses on bone tissue, numerical analyses have been performed for the latest developments of these devices. Furthermore, bone diseases, especially osteoporosis, are caused by the interruption of bone remodeling process (Thompson, 2007; Rouhi et al., 2007). Osteoporosis is a disease characterized by low bone mass and deterioration of bone tissue caused by bone loss. This leads to increased bone fragility and risk of fracture (broken bones), particularly of the hip, spine and wrist. Bone diseases have severe impacts in terms of human cost and socioeconomic burden (Osteoporosis Canada, 2008). In Canada, one in four women and at least one in eight men over the age of 50 have osteoporosis and it is estimated that as many as two million Canadians may be at risk of osteoporotic fractures. The cost to the Canadian health care system of treating osteoporosis and the fractures it causes is currently estimated to be $1.9 billion annually (Osteoporosis Canada,

2008). Because of these severe impacts caused by bone diseases, it is of great importance to understand the mechanism of bone remodeling process, and so propose a mathematical model and also simulate this process.

Since Wolff (1892) proposed that bone adapted to mechanical loading in accordance with mathematical law during its growth and development, numerous researchers have been encouraged to propose mathematical models for the bone remodeling process. In 2000, Huiskes and co-workers developed a semi-mechanistic model for bone remodelling theory. The semi-mechanistic bone remodeling theory (Huiskes et al., 2000) includes the experimental findings in bone cells' physiology, such as a separate description of osteoclastic resorption and osteoblastic formation (Burger and Klein-Nulend, 1999); an osteocyte mechanosensory system (Aarden et al., 1994; Cowin et al., 1991); and role of microdamage (Pazzaglia et al., 1997; Taylor, 1997; Martin, 2000). In this semi-mechanistic bone remodeling theory (Huiskes et al., 2000), osteocytes are assumed to be sensitive to the maximal rate of the strain energy density (SED) in a recent loading history and to recruit the osteoblasts, bone forming cells which form new bone, to fill the cavities caused by osteoclast resorption. Osteoclast resorption by microdamage is supposed to occur spatially random.

1.1. Motivation

An imbalance in the regulation of bone remodeling's two sub-processes, i.e. bone resorption and bone formation, results in many metabolic bone diseases. When the amount of bone resorption is more than that of bone formation for a long period of time, a net reduction in bone apparent density, or bone loss, will occur. The serious bone loss leads to osteoporosis. Bone loss usually starts after maturation and accelerates in osteoporotic bones. It is known

that in healthy adults the number of osteocytes decreases significantly with aging (Frost, 1960; Mullender et al., 1996; Qiu et al., 2002). On the other hand, it is found that osteoporotic patients have a greater osteocyte density than healthy old adults (Mullender et al., 1996). In modern time, it was suggested that osteocytes regulated the recruitment of basic multicellular units (BMUs) in response to mechanical stimuli (Kenzora et al., 1978; Marotti et al., 1990; Lanyon, 1993). Furthermore, Mullender et al. (1994) and Mullender and Huiskes (1995) suggested that osteocyte density may affect the trabecular morphology and that reduced osteocyte mechanosensitivity, sensitivity of osteocyte to mechanical stimulus, may cause bone loss in a similar way as did disuse. According to the above findings, the changes of osteocyte density in aging and osteoporotic individuals and the effects of osteocyte density and osteocyte mechanosensitivity on spongy bone remodeling led us to hypothesize that decreasing osteocyte density causes spongy bone loss in the case of healthy adults and that a reduction in osteocyte mechanosensitivity is one of the main contributing factors for the bone loss in the osteoporotic bones. In order to investigate the validity of our hypothesis, we built a two-dimensional spongy bone model for simulating spongy bone remodelling. In the case of the healthy adults, we decreased the model's osteocyte densities with aging according to the experimental data to test the effects of reduced osteocyte densities on the aging spongy bone remodeling. In the case of osteoporotic individuals, we increased the model's osteocyte densities for osteoporotic bone compared to the healthy adults' bone, but decreased the osteocyte mechanosensitivities to test the effects of reducing osteocyte mechanosensitivities on the osteoporotic spongy bone remodeling. To the best of our knowledge, this research is the first computer simulation study investigating the effects of osteocyte mechanosensitivity on the osteoporotic spongy bone remodeling.

Looseness at the bone-implant system caused by bone resorption is a major problem in prosthetic implantation (Huiskes et al., 1987; McNamara et al., 1997). Besides stress-shielding which is well accepted as a reason for bone resorption, some researchers (Huiskes and Nunamaker, 1984; Quirynen et al., 1992) have suggested that bone loss around some implants was associated with overload. In spongy bone, osteoclast resorption is activated at the bone surface where inhibitive osteocyte signals no longer reach (Burger and Klein-Nulend, 1999). This can occur not only when external loads are reduced, but also when the osteocytic network is blocked because of the presence of microcracks caused by overloading (Martin, 2003; Tanck et al., 2006). If the loading is so high that the self-repair mechanism cannot keep pace with the increasing damage, overload resorption will occur (Li et al., 2007). Many mathematical models have been proposed to describe bone remodeling process, but very few attempts were made to study bone resorption due to overload. In this study, in order to investigate the spongy bone remodeling under overload, an extension to Huiskes and co-workers' semi-mechanistic bone remodeling theory (2000) was made. Based on the previous theoretical and experimental results, we hypothesized that the osteoclast resorption activity, including the bone resorption probability and also the amount of resorbed bone, will increase under overload. Furthermore, we assumed that microdamages caused by overload reduce the osteocyte influence distance. We also simulated the spongy bone remodelling, when is under overload, with a three-dimensional finite element model, which promising results have been gained.

1.2. Objectives

The general goal of this study is to investigate the spongy bone remodeling using the semi-mechanistic bone remodeling theory (Huiskes et al., 2000). The specific objectives of this study are:

1) To develop a two dimensional finite element model of spongy bone and investigate the effects of osteocyte density and osteocyte mechanosensitivity on the spongy bone remodeling for aging healthy adults and also osteoporotic patients, respectively.

2) To propose a new mathematical model for overloaded bone resorption. Using our new formulation and a three-dimensional computer model, investigation will be made on the spongy bone remodelling under overload.

1.3. Thesis organization

First, chapter 1 briefly states the motivation and objectives of this thesis. Chapter 2 provides background information on bone physiology and anatomy, bone structure, bone cells, bone mechanics, bone adaptation, and also literature review on the most popular theories related to bone remodeling. Chapter 3 introduces the general method used in this thesis, including a brief introduction on a semi-mechanistic bone remodeling theory and the particular finite element methods' applications in our researches. Chapters 4 and 5 address the specific objectives of the thesis in order. The thesis closes with Chapter 6 that provides final conclusions and recommendations for future work.

Chapter 2

Background and Literature Reviews

Bone is one of the most important components of the musculoskeletal system. It is characterised physically by hardness, moderate elasticity, and very limited plasticity. Although apparently immobilized in a petrified state, it is a rather unique tissue with many functions. Bone forms supportive framework for the body and sites for muscle attachment. Bone also serves to protect vital organs (brain) and tissue (bone marrow). A number of ions such as calcium and phosphate are reserved by bone which helps maintain the homeostasis of these minerals in the blood (Elisabeth et al., 1994).

2.1. Components of bone matrix

Bone is a highly heterogeneous tissue. Its composition and structure both vary in a way that depends on skeletal site, physiological function, the age and sex of subjects. In contrast with this heterogeneity, the basic components of the tissue are remarkably consistent (Yuehuei and Robert, 2000). By volume, bone consists of relatively few cells and much intercellular substances formed of mineral substances, organic matrix, and water.

By weight, approximately 65% of the bone tissue is made by mineral phase. The feature that distinguishes bone from other connective tissue is the mineralization of the matrix. This produces a hard and strong type of tissue capable of providing mechanical integrity for efficient body motion and also protection for the internal organs. Approximately 95% of the mineral phase is composed of a specific crystalline hydroxyapatite ($Ca_{10}(PO_4)_6(OH)_3$).

The organic phase comprises approximately 30% of the total mass of bone. About 90% of the organic phase is composed of collagen fibres (mainly Type I collagen); Approximately 8% of the organic phase are a variety of non-collagenous proteins such as osteopontin, osteonectin, bone sialoprotein, and osteocalcin ; cells accounting for the remaining 2% of the organic phase (Buckwalter et al. 1995; Einhorn, 1996; Gorski, 1998). The arrangement of the fibrils is important in determining bone's mechanical properties.

Water comprises approximately 5% of the total weight of bone and is located within collagen fibres, in the pores, and bound in the mineral phase. Water plays an important role in determining the mechanical properties of bone. For example, it has been shown that dehydrated bone samples have increased strength and stiffness, but decreased ductility (Nyman et al., 2006; Smith and Walmsley, 1959).

2.2. Bone structure

On the basis of shape, bones can be classified into four groups, long bones (e.g. the tibia and the femur), short bones (e.g. carpal bones of the hand), flat bones (e.g. the sternum), and irregular bones (e.g. vertebra). Long bones have one dimension much longer than the other two, short bones have similar extensions in all dimensions, and flat bones have one dimension much shorter than the other two. Figure 2.1 depicts the human skeleton and thus examples for each kind of bone.

Figure 2.1 Human skeleton (Sohit and Parma, 2007).

At macroscopic level, according to the level of porosity and location within the skeleton, bone is categorized as either cortical (haversian, or compact) bone or spongy (cancellous, or trabecular) bone (Figure 2.2), easily distinguished by their degree of porosity. Individual bones in the body can be formed from both of these types of bone tissue. Almost 80% of the skeletal mass in the adult human skeleton is cortical bone, while the remaining 20% is spongy bone (Jee, 2001). Cortical bone, which is a low porosity solid material, forms the outer wall of all bones and is largely responsible for the supportive and protective function of the skeleton. Spongy bone is a porous structure and is mainly found in the interior of bones, such as vertebral bodies, and in the end of long bones. The porosity of spongy bone ranges from 40 to 95% depending on the anatomic site (Kuhn et al., 1990; Mosekilde et al., 1989), far greater than that of cortical bone which is 30% or less (Hayes and Bouxsein, 1997). The main

function of spongy bone is to support the articular surfaces of the joint, and to transfer joint and muscle load to long bones. Spongy bone also provides shock absorption due to its porous structure.

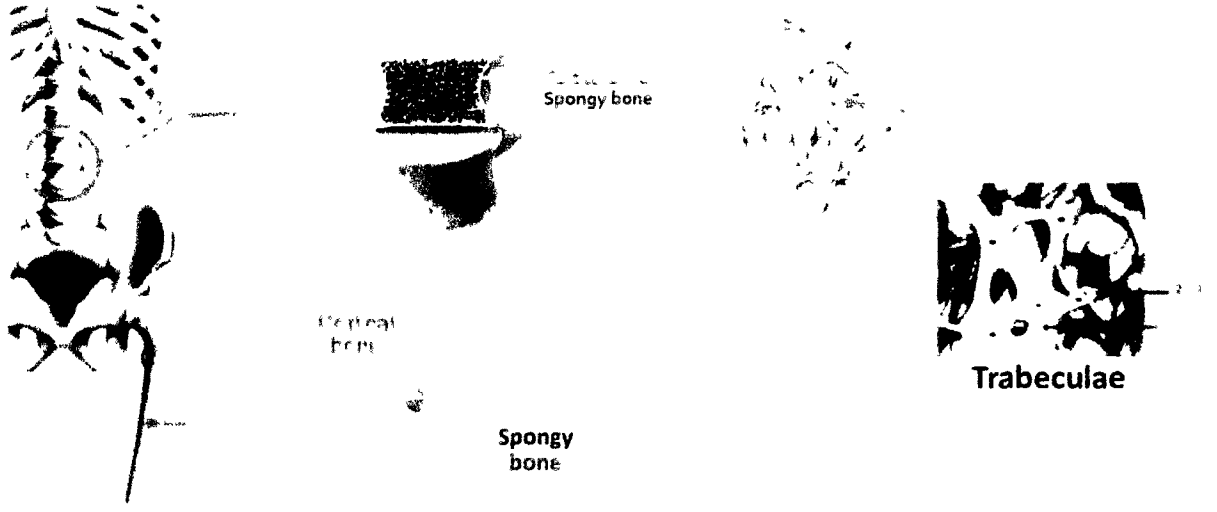

Figure 2.2 A cutaway view of the human vertebrae and femur, showing the regions of cortical and spongy bone (Wang, 2004).

One can state that a given volume of bone consists of two parts:

$$V_T = V_B + V_V \tag{2.1}$$

where V_T, V_B and V_V are the total bone volume, bony part's volume, volume of the void (or marrow), repectively. With the definition of the volume parts, the term porosity, P, can be defined as:

$$P = V_V/V_T = 1 - V_B/V_T \tag{2.2}$$

where V_B/V_T is often referred to as the bone volume fraction.

Another important quantity is the apparent density, ρ, described by:

$$\rho = \frac{m_T}{v_T} \tag{2.3}$$

where m_T is the mass of total bone.

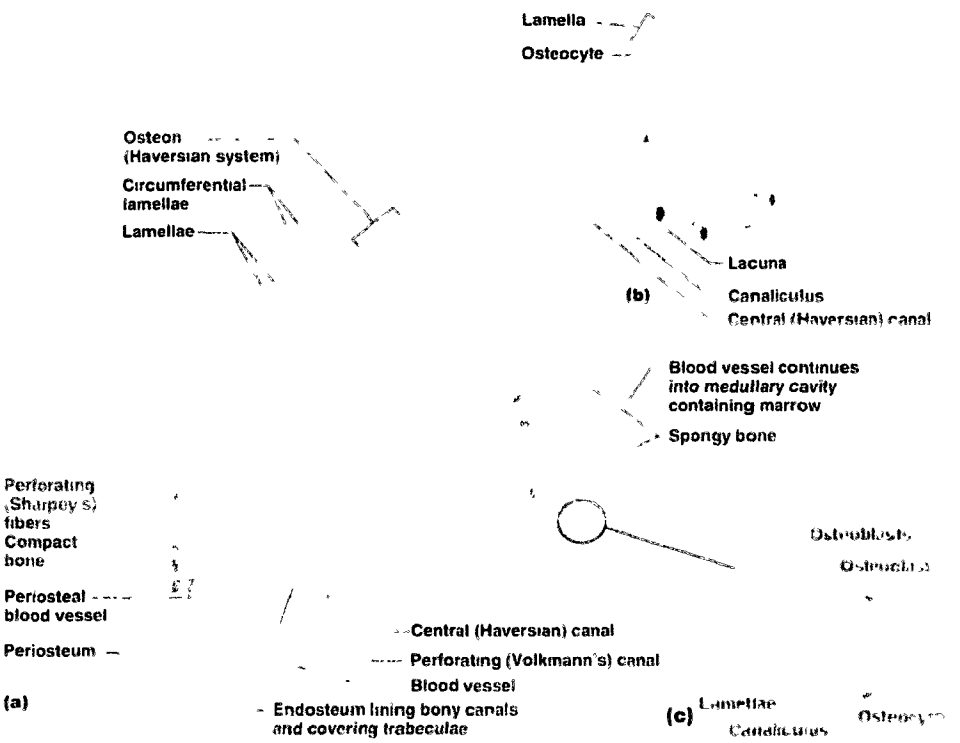

Figure 2.3 Cortical and spongy bones (Fischer, 2007).

Cortical bone is a dense, solid mass with only microscopic channels (Figure 2.3) and with a maximal density of about 1.8 g/cm^3. In cortical bone the main structural unit is the osteon or Haversian system. Osteons form approximately two thirds of the cortical bone volume; the remaining one third is interstitial bone. A typical osteon is a cylinder about 200 or 250 μm in diameter and 1 to 2 cm long. Haversian canals are interconnected by transverse Volkmann's canals. Within the central canal run blood vessels, lymphatic, nerves and loose connective tissue that continue through the bone marrow and the periosteum. The wall of an osteon is made up of 20 to 30 concentric lamellae approximately 70 to 100 μm thick.

Surrounding the outer border of each osteon is a cement line, a 1 to 2 μm thick layer of mineralized matrix deficient in collagen fibres.

Spongy bone has a cellular structure and is made up of a connected network of rods and plates (70 to 200 μm in thickness) of calcified bone tissue called trabeculae (Figure 2.3). Spongy bone accounts for 20% of total bone mass, but it has nearly ten times the surface area of compact bone. The high surface area of the trabecular network allows for energy absorption and dissipation from loads on the joint. The trabeculae are usually oriented in a way that produces an anisotropic structure (Turner, 1997). The trabeculae are surrounded by marrow that is vascular and provides nutrients and waste disposal for the bone cells. Individual trabeculae have a plate or rod shape and are composed primarily of interstitial bone of varying composition. Analogous to an osteon in cortical bone, the structural unit of spongy bone is the trabecular packet which consists of sheets of non-concentric lamellae (Figure 2.3.C). The ideal trabecular packet is shaped like a shallow crescent with a radius of 600 μm and is about 50 μm thick and 1 mm long. As with cortical bone, cement lines hold the trabecular packet together.

Spongy bone tissue is a non-homogeneous and anisotropic porous structure. The symmetry of the structure in spongy bone depends upon the direction of the applied loads. If the stress pattern in spongy bone is complex, the structure of the network of trabeculae is also complex and highly asymmetric. In bones where the loading is largely uniaxial, such as the vertebrae, the trabeculae often develop a columnar structure with cylindrical symmetry (Weaver and Chalmers, 1966; Whitehouse et al., 1971).

Tiny cavities in the bone matrix called lacunae are observed throughout both cortical and spongy bone. A single cell known as an osteocyte is trapped within each lacuna. Osteocytes form a network with adjacent lacunae allowing for nutrient diffusion and cell to

cell communication via a system of cell processes located in canaliculi (Figure 2.3.b, Figure 2.3.c and Figure 2.4).

At the microstructural level, according to the arrangement of the collagen fibrils, both compact and spongy bone can be of woven or lamellar bone (Yuehuei and Robert, 2000). Woven bone has a small number of randomly oriented collagen fibres and is mechanically weak. Lamellar bone has a regular parallel alignment of collagen into sheets (lamellae) and is mechanically strong. In cortical bone, lamellae are arranged either concentrically in quasi-cylindrical osteons or circumferentially near the outer and inner surfaces of the compact bone (Cowin et al., 1991). The trabeculae of spongy bone generally are composed of a collection of parallel lamellae. In cross-section, the fibres run in opposite directions in alternating layers, much like in plywood, assisting in the bone's ability to resist torsion forces. During skeletal embryogenesis, woven bone is the bone formed first. After birth, it is gradually removed by the process of bone remodeling and is substituted by lamellar bone. In adults, woven bone is created after fractures or in Paget's disease. Woven bone forms quickly. It is soon replaced by lamellar bone (Yuehuei and Robert, 2000).

2.3. Bone cells

Although bone cells make up a small percentage of the volume of bone, they play a critical role in the adaptation of its structure. There are four main types of bone cells (Figure 2.4). They are osteoclasts, which resorb old bone, osteoblasts, which form new bone, osteocytes, which is believed that they act as mechanosensors (Cowin et al., 1991; Burger, 2001; Burger and Klein-Nulend, 1999, Nijweide, et al., 1996) and bone lining cells, which are inactive cells on the resting surfaces of bone.

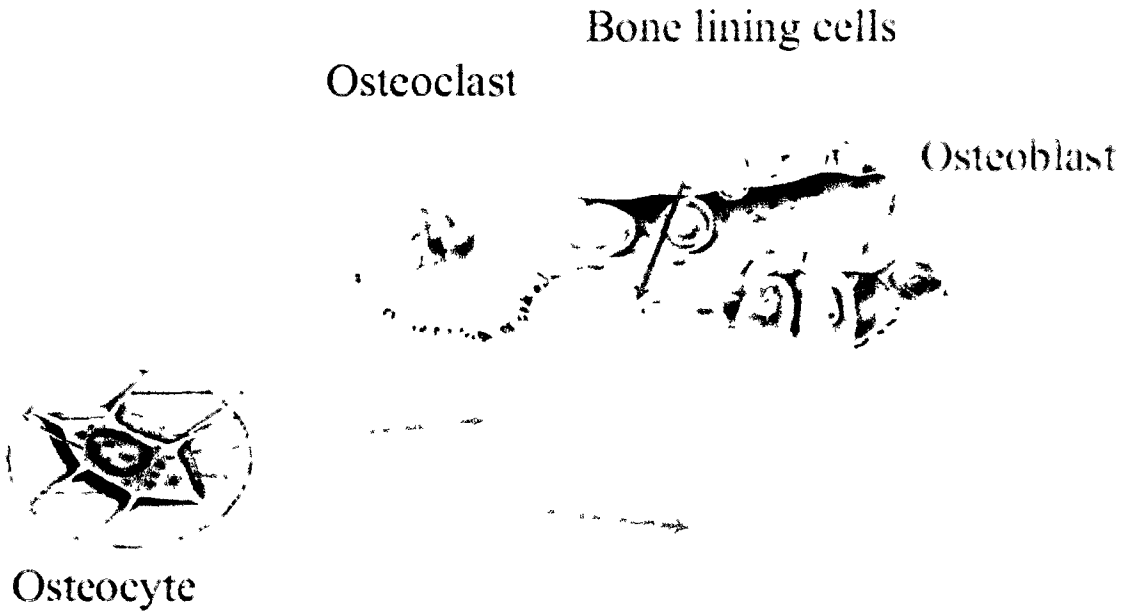

Figure 2.4 Diagram of bone cells (Roche Facets)

Osteoclasts, bone resorbing cells, are multi-nucleated giant cells that contain from 1 to more than 50 nuclei and range in diameter from 20 to over 100 μm (Figure 2.4). Osteoclasts are derived from precursor cells circulating in the blood. Active osteoclasts are usually found in cavities on bone surfaces, called resorption cavities or Howship's lacunae. These cells secrete acids and enzymes to break down the mineralized bone matrix. They erode bone structure as they make their way through the bone matrix at a rate of about 40 μm per day

(resorption rate). Debris, both organic and mineral, are packed into little vesicles and pass through the cell body of the osteoclast and are dumped into the space above. When osteoclasts have done their job, they disappear and presumably die (Bilezikian et al., 1996).

Osteoblasts are bone forming cells which have a cuboidal form, and are tightly packed against each other at the tissue surface (Figure 2.4). They are mono-nucleated cells, up to 10 μm in diameter. Osteoblasts secrete both the collagen and the ground substance that constitutes the initial un-mineralized bone or osteoid. During bone remodeling, these cells refill the gap opened by the osteoclasts at a rate of about 1 μm per day (apposition rate). Initially, the osteoid has a very low elastic modulus, but its value increases when mineralization takes place. A great number of osteoblasts disappear by a yet unknown process after their lifespan (Buckwalter et al. 1995). But, some become buried in the tissue and survive as osteocytes.

Osteocytes are former osteoblasts that have become buried in the mineralize bone matrix (Bilezikian et al. 1996). They are the most abundant cell type which makes up more than 90-95% of all bone cells in the adult animal bone (Parfitt, 1977). Osteocytes are regularly dispersed throughout the mineralized matrix within caves called lacunae, connected to each other and cells on the bone surface through slender, cytoplasmic processes or dendrites passing through the bone in thin tunnels (100-300 nm) called canaliculi (Figure 2.3 and 2.4). The cell processes are on the order of fifty emanating from each cell, and they are surrounded by a bone fluid space. Comparing to osteoblasts and osteoclasts, no clear functions have been ascribed to osteocytes (Bonewald, 2006a). For a long time, osteocytes were considered as the quiescent cells that merely acted as place holders in bone (Bonewald, 2006b; Heino et al., 2009). Since osteocytes were proposed to be multifunctional cells decades ago (Bonewald,

2006b), both theoretical considerations and experimental results have constantly strengthened the knowledge of the role of osteocytes in mechanosensing and in the consequent regulation of bone mass and structure, which is accomplished by the process of bone remodeling (Frost, 1960; Cowin et al., 1991; Burger et al., 1995; Burger and Klein-Nulend, 1999; Cheng et al., 2001; Klein-Nulend and Bakker, 2007) (see section 2.4).

Bone lining cells are flattened, inactive osteoblasts that lay on the bone surface (Figure 2.4). In adult bone, lining cells cover the surface of trabeculae in trabecular bone, the periosteum and endosteum of cortical bone, and the Haversian and Volkmann's channels of the osteons. Bone lining cells maintain communication with each other and the osteocytes and are believed to be hormonal receptors and chemical messengers (Bilezikian et al., 1996). Like osteocytes, bone lining cells are also thought to initiate bone remodeling in response to various chemical and mechanical stimuli (Buckwalter et al., 1995).

2.4. Osteocyte mechanosensing

Mechanosensing is the process by which mechanical loads is sensed by mechanosensor cells. The osteocyte is the most abundant cell type of bone (Klein-Nulend and Bakker, 2007). Osteocytes are embedded in the mineralized matrix of bone and spaced regularly throughout the calcified matrix. The number of osteocytes and their particular location in bone make them seem to be one of the best candidates for the job of detecting mechanical signals in the bone matrix. *In vivo* experiments show that loading produces rapid changes in the metabolic activity of osteocytes and suggest that osteocytes function as mechanosensors in bone (Skerry et al., 1989; El-Haj et al., 1990; Dallas et al., 1993; Lean et al., 1995; Forwood et al., 1998; Terai et al., 1999).

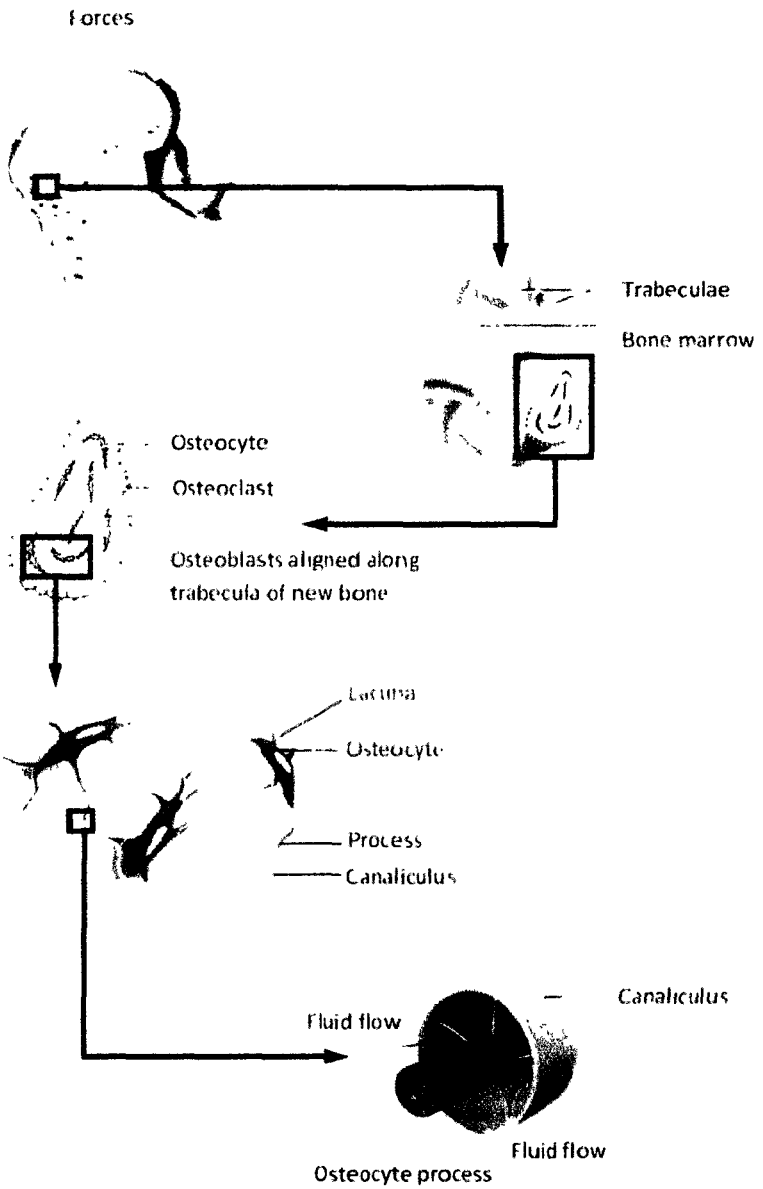

Figure 2.5 Schematic of the osteocyte mechanosensing. Osteocytes are dispersed throughout the bone matrix. An osteocyte resides in a lacuna, contacting with other osteocytes through its processes within the channels known as canaliculi. Mechanical loads on bone are assumed to induce fluid flow in the lacunar-canalicular network. Osteocytes are supposed to detect the mechanical signal via the fluid flow.

Mature osteocytes are located in lacunae and contact with each other, osteoblasts and bone lining cells covering the surface of bone via their long cell processes located in canaliculi, forming a large lacuno-canalicular network which is fluid-filled. It is currently believed that when bones are loaded, the resulting deformation will drive the thin layer of interstitial fluid surrounding the network of osteocytes to flow from regions under high pressure to regions under low pressure (Figure 2.5). Evidence has been increasing steadily for the flow of canalicular interstitial fluid as the likely factor that informs the osteocytes about the level of bone loading (Cowin et al., 1991; Weinbaum et al., 1994; Klein-Nulend et al., 1995; Burger and Klein-Nulend, 1999; Knote-Tate et al., 2000). Subsequently, it could be that mechanically induced osteocyte signals, soluble signalling molecules, are transferred through the canaliculi to the bone surface where they regulate osteoblast activity by affecting osteoblast proliferation and differentiation (Vezeridis et al., 2005). Recently, *in vitro* studies suggest that mechanical loading decreases the osteocyte's potential to induce osteoclast formation (You et al., 2008). You et al.' research's results (2008) indicate that osteocytes may function as mechanotransducers by inhibiting osteoclastogenesis via soluble signals.

2.5. Spongy bone mechanics

In general, bone is a non-homogeneous, anisotropic, and multi-phasic material. The spongy bone tissue modulus is 20 to 30% lower than that of cortical bone tissue. The preliminary results in human vertebrate indicate that both spongy and cortical bone tissue from young adults (age 20 to 40) have significantly higher moduli than the tissue from older aging adults aged 55 to 65 and 75 to 85 (Edward Guo, 2001).

The mechanical behaviour of spongy bone is best described as viscoelastic due both to the viscous properties of the tissue material and to the marrow in the pores. The elastic part of this behaviour is demonstrated by the ability of spongy bone to recover its initial geometry fully after release of an applied load that did not exceed the elastic limit. The viscous part is responsible for the dependency of stiffness on strain rate (Carter and Hayes, 1977; Linde et al., 1991) and for phenomena such as stress relaxation and creep behaviour of spongy bone (Zilch et al., 1980; Lakes, 2001). It should be noted that for strain rates as they occur during normal activities (~ 1 Hz), spongy bone could be well described as an elastic material (van Rietbergen and Huiskes, 2001).

Elastic properties of continua are fully described by the stiffness tensor, S, or by the compliance tensor, C, in the generalize Hooke's Law:

$$\sigma_{ij} = S\varepsilon_{ij}, \qquad \varepsilon_{ij} = C\sigma_{ij}, \qquad S = C^{-1} \tag{2.4}$$

where σ_{ij} is the stress tensor, and ε_{ij} is the strain tensor.

The stiffness and compliance tensors are usually represented by symmetric six-by-six matrices which consist of 21 independent components that must be determined from experiments. For example, the compliance tensor can be depicted as below (van Rietbergen and Huiskes, 2001):

$$C = \begin{bmatrix} C_{11} & C_{12} & C_{13} & C_{14} & C_{15} & C_{16} \\ C_{12} & C_{22} & C_{23} & C_{24} & C_{25} & C_{26} \\ C_{13} & C_{23} & C_{33} & C_{34} & C_{35} & C_{36} \\ C_{14} & C_{24} & C_{34} & C_{44} & C_{45} & C_{46} \\ C_{15} & C_{25} & C_{35} & C_{45} & C_{55} & C_{56} \\ C_{16} & C_{26} & C_{36} & C_{46} & C_{56} & C_{66} \end{bmatrix} \tag{2.5}$$

Spongy bone is anisotropic based on its very complex internal structure. The elastic modulus of spongy bone varies over a wide range and is dependent on the direction in which

the bone is loaded. It is shown that an orthotropic (three orthogonal planes are plane of symmetry) assumption can be made for the spongy bone (Gibson, 1985).

Using standard engineering test methods such as tensile tests, three- or four-point bending tests, and buckling tests, it is far more difficult to measure mechanical properties of spongy bone tissue than to measure those properties of cortical bone tissue. The technical difficulties are due to the extremely small dimension (thickness, 100 to 200 μm; length, 1 to 2 mm) and irregular shape of individual trabeculae in spongy bone (van Rietbergen and Huiskes, 2001; Edward Guo, 2001). In order to overcome these chanllenges an alternative method so-called micro-finite-element analysis (μFEA) have been developed to calculate the elastic constants of spongy bone directly from computer models by simulating experimental tests on bone specimens (Hollister et al., 1994; van Rietbergen et al., 1995 and 1996). In these simulations, many uncertainties that play a role in real tests (e.g., bone-platen interface conditions, protocol errors) can be eliminated or well controlled (van Rietbergen and Huiskes, 2001). Using the μFEA model, it was found that the anisotropic elastic properties of spongy bone can be well neglected, and so spongy bone can be represented with isotropic tissue properties. This effective isotropic tissue modulus can be determined by comparing the results of μFEA with those of experimental tests for the same specimen (Kabel et al., 1999). The values found for the tissue Young's modulus are generally in the range of 4 to 8 GPa (van Rietbergen et al., 1995; Ladd et al., 1998; Kabel et al., 1999).

Supposing that a given bone specimen is a homogeneous and isotropic material, one can describe the constitutive behaviour with two material parameters, i.e. the Young's modulus, E, and the Poisson ratio, ν. In the case of isotropy, the compliance tensor, C, can be written as (van Rietbergen and Huiskes, 2001):

$$C = \begin{bmatrix} \frac{1}{E} & \frac{-\nu}{E} & \frac{-\nu}{E} & 0 & 0 & 0 \\ \frac{-\nu}{E} & \frac{1}{E} & \frac{-\nu}{E} & 0 & 0 & 0 \\ \frac{-\nu}{E} & \frac{-\nu}{E} & \frac{1}{E} & 0 & 0 & 0 \\ 0 & 0 & 0 & \frac{2+2\nu}{E} & 0 & 0 \\ 0 & 0 & 0 & 0 & \frac{2+2\nu}{E} & 0 \\ 0 & 0 & 0 & 0 & 0 & \frac{2+2\nu}{E} \end{bmatrix} \tag{2.6}$$

Carter and Hayes (1977) observed a cubic relation between local elastic modulus and apparent density in spongy bone. Martin et al. (1998) proposed the relation between the material stiffness, represented by local elastic modulus, E, and the apparent density, ρ, in a more general form as:

$$E=c\rho^{b} \tag{2.7}$$

with constants c and b, where the power b has a value between 2 and 3.

Obeying the general form, but more elaborate is the model of the Stanford method (Jacobs, 1994, Doblaré and García, 2002):

$$E = \begin{cases} 0.002014\rho^{2.5} & if \ \ \rho \leq 1200 \\ 0.001763\rho^{3.2} & if \ \ \rho > 1200 \end{cases} \tag{2.8}$$

with E in GPa and ρ in kg/m^3.

A more sophisticated approach is provided by Hernandez and coworkers (Hernandez, 2001; Hernandez et al., 2001). The material stiffness varies as a function of both the bone volume fraction, V_B/V_T (see Eq. 2.2), and the mineralization fraction, α. The mineralization fraction, α, ranges from 0.42 to 0.7, and the bone volume fraction ranges from 0 to 1. The formula is as follows:

$$E = 84.37\left(\frac{V_B}{V_T}\right)^{2.58} \alpha^{2.74} \tag{2.9}$$

with units in GPa.

For the Poisson ratio, ν, most studies consider that ν=0.3 is sufficient in the context of a qualitative analysis for the isotropic cases (van Rietbergen and Huiskes, 2001).

2.6. Bone remodeling process

Bone is a living tissue which continually alters its structure in response to changes in the physical environment through the process of bone adaptation. It is believed that bone adaptation enables bone to perform its mechanical functions with a minimum mass. There are three major methods of bone adaptation: osteogenesis, modeling, and remodeling.

Osteogenesis is the formation of either new soft bone tissue or cartilage. This is the way in which bones are formed during embryonic development, early stages of growth, healing at the site of an injury, for example fracture. In osteogenesis, osteoblasts and osteoblasts generally act independently, and large amounts of woven bone are rapidly formed.

Bone modeling is the reshaping of bone structure on existing bone (see Figure 2.6). During bone modeling, osteoblastic and osteoclastic activities occur independently at different bone surfaces. Mineralize bone tissue is resorbed in some regions, while new bone is formed in others. Large changes in bone structure may occur specially during growing periods in young individuals or initial healing stage.

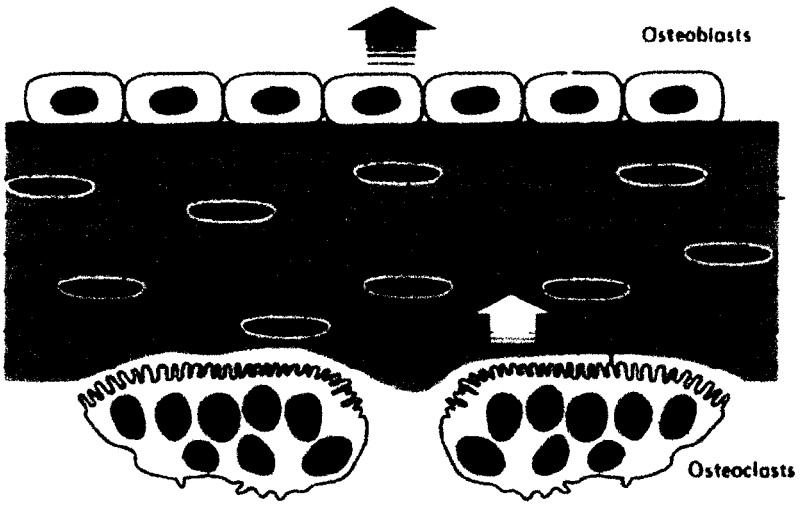

Figure 2.6 Bone modeling. Osteoblast and osteoclast action are not linked and rapid changes can occur in the amount, shape, and position of bone (Rauch and Glorieux, 2004).

Bone remodeling is a life-long process of ongoing replacement of old bone by new bone (Huiskes and van Rietbergen, 2005). In human adults, 5% of cortical bone and 25% of trabecular bone is replaced per year by remodeling (Martin et al., 1998). Bone remodeling serves to adjust bone architecture to meet changing mechanical needs and it helps to repair microdamages in bone matrix preventing the accumulation of old bone (Hadjidakis and Androulakis, 2006). Bone remodeling differs from osteogenesis and modeling in that osteoclasts and osteoblasts do not act independently, but are coupled and bone resorption and formation occur at the same spot on a bone surface (see Figure 2.7). As with modeling, bone remodeling occurs on existing bone surfaces (Buckwalter et al., 1995). However, unlike modeling, remodeling cannot cause large changes in bone structure at a given site. At best, remodeling maintains the current amount of bone structure. When age is over 25-30, the amount of new added bone starts to slightly lag the amount of bone resorbed, leading to a gradual decline in bone mass (Mullender et al., 1996).

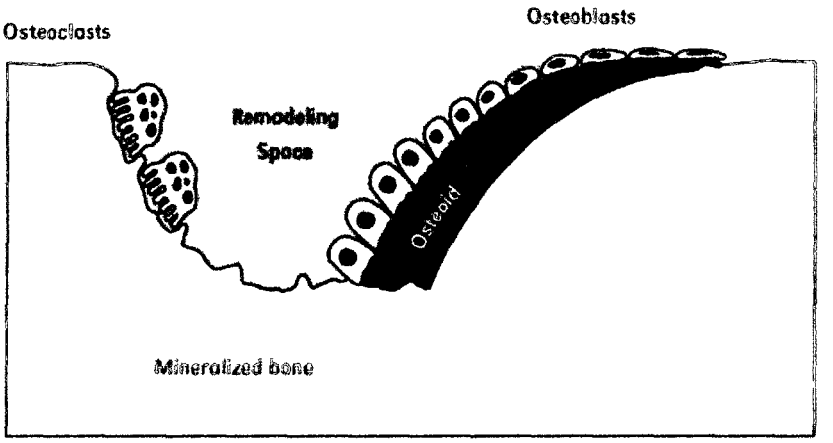

Figure 2.7 Bone remodeling. Osteoblast action is coupled to prior osteoclast action. Net changes in the amount and shape of bone are minimal unless there is a remodelling imbalance (Rauch and Glorieux, 2004).

There are six stages in bone remodeling (Figure 2.8). Remodeling starts from the stage of activation by which the osteoclastic precursors become osteoclasts. This activation takes about three days (Martin et al., 1998). After activation, newly formed osteoclasts begin to resorb bone throughout the process of tunneling in cortical bone (Figure 2.9.A) and surface erosion in trabecular bone (Figure 2.9.B). The osteoclasts attach to the bone surface, dissolve the mineral, and later the organic phase of the bone, opening a hole that is subsequently filled by a number of osteoblasts, which produce the collagen matrix and secrete a protein which stimulates the calcium phosphate deposition (Rouhi, 2006). Resorption takes about three to four weeks. The stage of reversal, the transition from osteoclastic to osteoblastic activity, takes about several days. After reversal, a single layer of mineralized tissue (cement line) formed by osteoblasts covers the surface of resorption cavity. Osteoblasts begin to refill the cavity by deposition of consecutive layers of osteoid. The formation stage in adult humans averages about three months. During formation, osteoid mineralization starts after a period of about ten days (Bilezikian et al., 1996). Once mineralization begins, approximately 60% of the

mineralization occurs within a few days. Full mineralization is suspected to take up to six months (Tovar, 2004). When the mineralization is finished, the osteoblasts disappear or become osteocytes or bone lining cells during the quiescence stage.

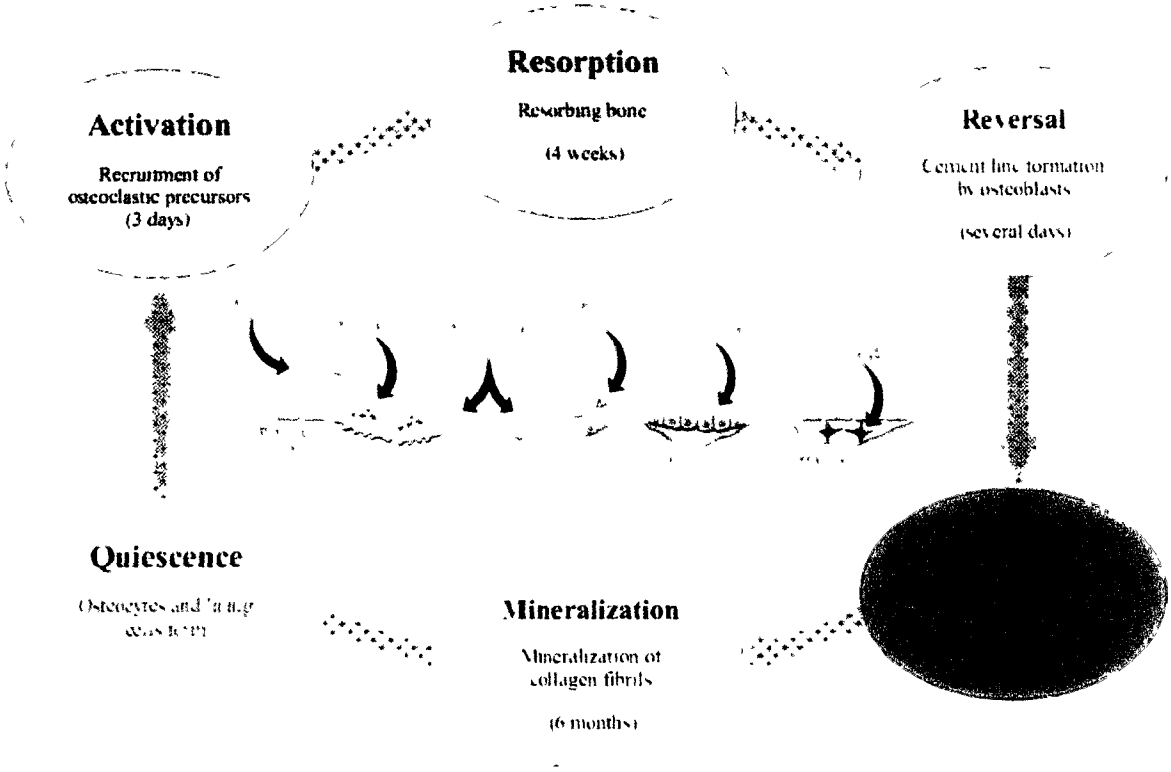

Figure 2.8 Bone remodeling sequence (Landrigan et al., 2006).

In bone remodeling process, osteoclasts and osteoblasts closely collaborate as a team called *basic multicellular units* (or BMUs). In cortical bone a BMU forms a cylindrical tunnel about 2000 μm long and 150-200 μm wide (Figure 2.9.A). In its tip on the order of ten osteoclasts dig a circular tunnel (cutting zone) at a speed of 20-40 μm/day. They are followed by several thousands of osteoblasts that fill the tunnel (closing zone) to produce an osteon of renewed bone (Parfitt, 1994). In spongy bone, bone remodeling process occurs on the spongy bone surface (Figure 2.9.B). Because of its large surface-to-volume ratio, spongy bone is more actively remodeled than cortical bone, with remodeling rates up to ten times higher (Lee and

Einhorn, 2001). Along the trabecular surface, osteoclasts dig a trench with depths of 40-60 μm. Subsequently, osteoblasts form new bone at the same site. The area of the trench varies from 50×20 to 1000×1000 μm^2 (Mosekilde, 1990).

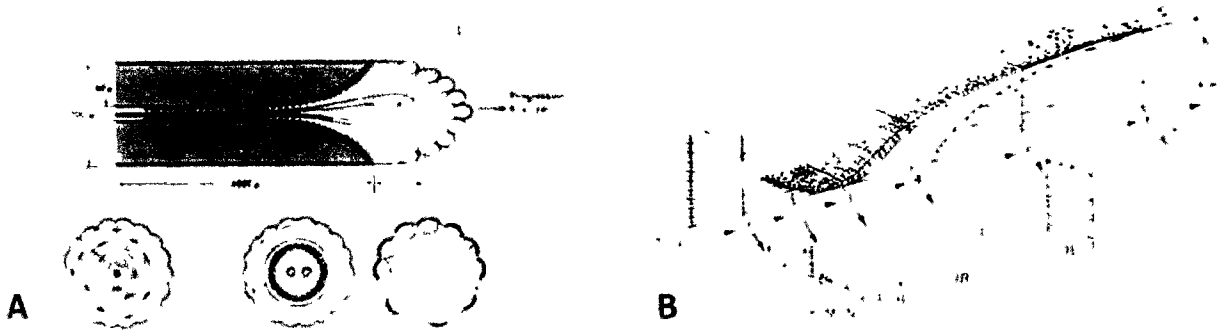

Figure 2.9 Schematic drawings of cortical and spoongy bone remodeling. (A) A cortical bone remodeling, and (B) a spongy bone remodeling (Parfitt, 1994).

2.7. Bone diseases related to bone remodeling

When osteoclastic resorption and subsequent osteoblastic formation are in balance, there is no net change in the structure and mass of bone after bone remodeling. Many diseases are related to a global shift in the remodelling balance. For example, osteoporosis is the bone loss caused by increased osteoclast activity; osteopetrosis is an abnormal increase in bone density by reduced osteoclast activity; osteopenia is the bone loss by decreased osteoblast activity (Rouhi, 2006). The treatment of these diseases is based on drugs that intend to restore the remodelling equilibrium. Most of the work on osteoporosis, probably the most important and common of these diseases, seems to be currently in the osteoclast inhibition side (Rodan and Martin, 2000; Teitelbaum, 2000).

Bone diseases, especially osteoporosis, are caused by the interruption of bone remodeling process (Thompson, 2007). Bone diseases have severe impacts in terms of human

cost and socioeconomic burden. In Canada one in four women and at least one in eight men over the age of 50 have osteoporosis and it is estimated that as many as two million Canadians may be at risk of osteoporotic fractures. The cost to the Canadian health care system of treating osteoporosis and the fractures it causes is currently estimated to be $1.9 billion annually (Osteoporosis Canada, 2008). Because of these severe impacts caused by bone diseases and failure of implants and prostheses, it is of great importance to understand how bone remodeling works, with the hope of finding practical ways to keep the balance between the bone resorption and formation.

During childhood and teenage years, the amount of new bone added is more than the amount of old bone removed. This tendency continues until peak bone mass (PBM) is reached between 20 and 30 years of age (Compston & Rosen, 2002). Hereditary factors account for about 80% of the PBM, while about 20% depends on environmental stimuli (Gunnes, 1995). After age 30, bone resorption exceeds bone formation and it is difficult to build more bone mass. At that stage, hormonal changes (Ahlborg et al., 2001; Bendavid et al., 1996), nutrition (Dawson-Hughes et al., 1997) and lifestyle (Hollenbach et al., 1993; Holbrook and Barrett-Connor, 1993; Greendale et al., 1995) are the main factors that determine bone loss. At every age, but especially after PBM is reached, eating well and providing the proper mechanical stimuli to the bone are critical to reduce the risk of problems related to low bone mineral density (BMD) such as osteopenia and osteoporosis (Chan et al., 2003). Bone mineral density refers to the amount of mineral per square centimetre of bone and is most frequently measured by dual energy x-ray absorptiometry (DEXA). Osteoporosis occurs over time when the amount of bone broken down greatly exceeds the amount of bone replaced by new bone cells.

At this point, bone mineral density decreases, and so can cause a reduction in the bone mass. The ultimate results are that bones become more porous, less stiff and more prone to fracture.

Bone responds to mechanical stimuli with changes in the structure and, consequently, alteration of the BMD. Immobilization and weightlessness are associated with reduction in bone mass (Vogel, 1975; Whalen, 1993; Lang et al., 2004; Silva et al., 2004). Conversely, weight-bearing exercises (work against gravity) help build stronger bones (Calbet et al., 1998, 1999; Oleson et al., 2002; Faulkner et al., 2003). Figure 2.10 shows the internal structural effect of mass reduction in trabecular bone.

Figure 2.10 Bone mass reductions in spongy bone. Micrograph of normal bone (left), thinning bone (center) and osteoporotic bone (right) (Tovar, 2004).

The insertion of an orthopaedic prosthesis dramatically can alter bone's physical environment. Whenever an implant is inserted into the body, existing bone has to be removed for the implant to take its place. This alters the load path and the strain distribution for the bone tissue in the vicinity of the implant, causing a redistribution of bone mass at the implant-bone interface. The complex stress transfer between the external device and the host bone might cause an undesired structural remodeling around the implant. For instance, while the deposition of higher density bone material near the implant is desirable for good fixation, gradual resorption of bone tissue around the stem may affect the performance of the prosthesis

(Tavor, 2004; Haase, 2010). The degenerative adaptation process might result in loosening of the implant, causing pain for the patient and eventually fracture of the bone (Figure 2.11).

Figure 2.11 Loosening of a long-stem prosthesis of the left hip with major bone loss (Wagner, H. and Wagner, M.).

2.8. Bone remodeling theories

Based on Wolff's Law (1892) indicating that bone adapts to mechanical loading in accordance with mathematical law during its growth and development, numerous researchers have been encouraged to propose mathematical models for the bone remodeling process. In 1987, Frost developed mechanostat theory which was the starting point for many mathematical theories of bone remodeling (Frost, 1987). The mechanostat theory states that a minimum effective strain (MES) should be exceeded in order to trigger an adaptive response in bone. Cowin and Hegedus developed adaptive elasticity theory (Cowin and Hegedus, 1976; Hegedus and Cowin, 1976), which considered strain as mechanical stimulus to initiate the bone remodeling process. However, the attempt to adjust the tensor of remodeling constants ended up in a variation of data, and yet the exact values of the remodeling constants are not available

(Cowin, 2003; Vahdati and Rouhi, 2009). Huiskes et al. (1987) proposed a scalar quantity, strain energy density (SED), as a mechanical stimulus for bone remodeling and incorporated the concept of lazy zone, which was introduced by Carter (1984), into their model. Later, Huiskes and co-workers (2000) developed a semi-mechanistic model for bone remodelling. The semi-mechanistic bone remodeling theory (Huiskes et al., 2000) includes the experimental findings in bone cells' physiology (Vahdati and Rouhi, 2009), such as a separate description of osteoclastic resorption and osteoblastic formation (Burger and Klein-Nulend, 1999), an osteocyte mechanosensory system (Aarden et al., 1994; Cowin et al., 1991), and role of microdamage (Pazzaglia et al., 1997; Taylor, 1997; Martin, 2000). Recently, a few remodeling theories considered both mechanical stimuli and microdamage (Rouhi et al., 2006; McNamara and Prendergast, 2007). Each of the proposed theories of bone remodeling sheds some lights on this multifactorial and complex process. For example, van der Linder and co-workers' models have been used to predict changes in bone structure due to the effect of anti-resorptive drugs (van der Linden et al., 2003), and Foldes et al.'s model and Cowin's model have shown the effects of immobilization or microgravity exposure on the bone structure (Foldes et al., 1990; Cowin, 1998). However, none of them could predict all different features of the very complex process of bone remodeling. The following is a review of major theoretical studies and computational models related to the bone remodelling process.

2.8.1. Trajectorial theory and Wolff's Law

The earliest observations directed at uncovering the influence of mechanical environment on trabecular structure date back to the drawings of the internal structure of the proximal femur (trajectories of trabecular bone) (Figure 2.12.A) by a Swiss anatomist, von Meyer (1867). By chance, a German civil engineer, Karl Culmann, the father of the method of graphical statistics (Culman, 1866), studied von Meyer's sketches and found that the direction of internal stresses in a Fairbairn crane (Figure 2.12.B) were remarkably similar to the trabecular architecture in the proximal femur.

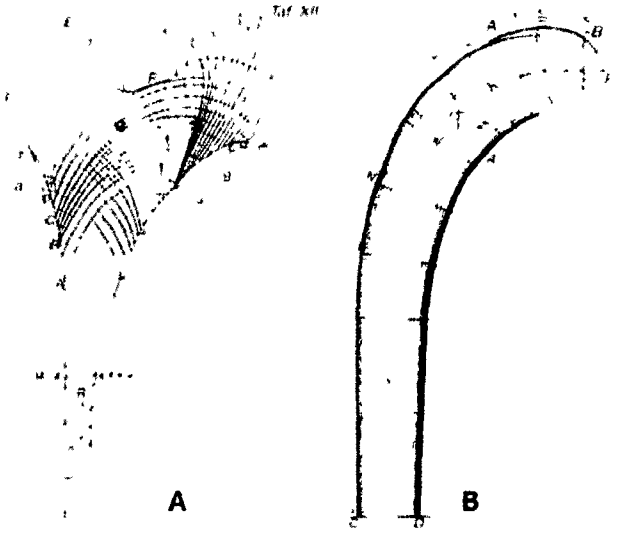

Figure 2.12 (A) von Meyer's sketch of the trajectories of trabecular bone in proximal femur; (B) Culmann's graph of the principal stress trajectories in a Fairbairn crane (Wageningen ur, 2009).

The first cooperation in the field of bone biomechanics between von Meyer and Culmann (Roesler, 1987) suggested that trabecular alignment is regulated by internal stress patterns (Jacobs, 2000). In 1870, their work laid the foundation for a German orthopaedic surgeon, Julius Wolff, to discover that trabecular architecture matches the principal stress

trajectories, known as the Trajectorial Theory of trabecular alignment (Jacobs, 2000). Wolff (1892) declared the most widely accepted theory on bone remodeling which now bear his name, Wolff's Law: "the law of bone remodelling is the law according to which alterations of the internal architecture clearly observed and following mathematical rules, as well as secondary alterations of the external form of the bones following the same mathematical rules, occur as a consequence of primary changes in the shape and stressing ... of the bones." He believed that bone adapted to mechanical loading during its growth and development, and that the same adaptation process took place during healing after fracture. Even though Wolff hypothesized that the adaptation is governed by a mathematical law, he never attempted to formulate a mathematical theory (Martin et al., 1998).

2.8.2. Frost's mechanostat theory

In 1987, Frost developed Mechanostat Theory. Instead of speculating that strains below a certain threshold are trivial and evoke no adaptive response, Frost suggested that there is an equilibrium range of strain values which elicits no response. Strains above this range will evoke deposition of bone, while strains below this range will induce bone resorption. In the model postulated by Frost (1987), the equilibrium range was defined between 200 and 2500 μm/m for compression and between 200 and 1500 μm/m for tension. Strains over 4000 μm/m (tension and compression) can cause damage and, consequently, woven bone formation. Frost is commonly credited with providing the conceptual framework from which many of the current mechanical theories have been guided (Grosland et al., 2001).

2.8.3. Cowin and Hegedas' adaptive elasticity theory

The adaptive elasticity theory developed by Cowin and Hegedus (Cowin and Hegedus, 1976; Hegedus and Cowin, 1976) was recognized as the mathematically rigorous and potentially powerful theory which was able to describe the adaptive behaviour of bone (Jacobs, 2000). In this model, bone is defined as a chemically reacting porous elastic solid whose porosity is modified through mass deposition or resorption controlled by strain (Cowin and Hegedus, 1976).

2.8.4. Huiskes el al.'s strain energy density model

Please see section 3.1

2.9. Open questions related to bone remodeling

There are many open questions related to bone remodeling process which need urgent attention. Some of them are listed below:

What is the actual mechanical stimulus to initiate the bone remodelling process? A variety of mechanical stimuli associated with ambulation (at a frequency of 1 to 2 Hz) have been considered for bone remodeling (Burger, 2001). The mechanical stimuli suggested include strain (Cowin and Hegedus, 1976; Frost, 1987), stress (Wolff, 1892; Frost, 1964b), strain energy density (Huiskes et al., 1987), strain rate (Hert et al, 1969; Fritton et al., 2000), and fatigue microdamage (Martin and Burr, 1982).

What are the mechanosensors of bone? Although it is believed that osteocytes are the most suitable candidate for the mechanosensor, there is no consensus on this yet. This is an

extremely important question which should be addressed in the future. Moreover, how osteocytes signal effector cells (osteoclasts and osteoblasts) and initiate bone turnover are not well understood (You et al., 2008).

In bone remodeling process there is a phase of reversal, which is a 1 to 2 weeks interval between the completion of resorption and beginning of formation. The cellular and hormonal mechanisms involved in reversal stage are unclear as well (Rouhi, 2006).

Osteocyte apoptosis as a potential signal source for osteoclastic bone resorption has been identified. The molecular links between damaged induced apoptosis and targeted osteoclast activity are unknown and need to be studied further (Noble, 2003; Heino et al., 2009).

Physical loading and routine activities have been proven to inhibit bone resorption. However, the cellular mechanism underlying this phenomenon remains largely unknown (You et al., 2008).

Chapter 3

General Methods

This chapter will introduce a semi-mechanistic bone remodeling theory (Huiskes et al., 2000) and finite element methods employed in this study.

3.1. A semi-mechanistic bone remodeling theory

3.1.1. A phenomenological model developed by Huiskes and co-workers (1987)

Cowin's adaptive elasticity theory (Cowin and Hegedus, 1976; Hegedus and Cowin, 1976), which considers strain as mechanical stimulus to initiate the bone remodeling process, has been extended by Huiskes et al. (1987) with two main differences. They incorporated the concept of lazy zone (Figure 3.1), proposed by Carter (1984), into their model. Furthermore, the strain energy density (SED), a scalar quantity, is taken as the mechanical stimulus in their remodelling equation. However, as other early models, the model relates mechanical signals to bone adaptation without direct consideration of the underlying cell-biological mechanisms (Ruimerman, 2005). Strain energy density, the strain energy per unit volume, is defined as:

$$U = \frac{1}{2}\varepsilon\sigma \tag{3.1}$$

where U is the SED, ε and σ are the strain tensor and stress tensor, respectively.

The use of strain tensor, as the remodeling stimulus, makes it difficult to determine the remodeling rate coefficients (Cowin, 2003; Rouhi, 2006). In order to overcome this problem,

Huiskes and coworkers (1987) suggested the SED, a scalar quantity, as a suitable mechanical stimulus for both surface remodeling (cortical bone) and internal remodeling (spongy bone). For the surface remodeling (cortical bone), the bone can either add or remove material according to:

$$\frac{dX}{dt} = C_x(U - U^*) \tag{3.2}$$

where $\frac{dX}{dt}$ is the rate of bone growth perpendicular to its surface, C_x is the remodelling rate coefficient, U is the SED, U^* is the equilibrium value of SED that determines the boundary between apposition and resorption.

For internal remodeling, there will be changes in bone apparent density. By assuming a modulus-density relationship (Eq. 2.1), one can write:

$$\frac{dE}{dt} = C_e(U - U^*) \tag{3.3}$$

where E is the local elastic modulus, C_e is a proportionality constant.

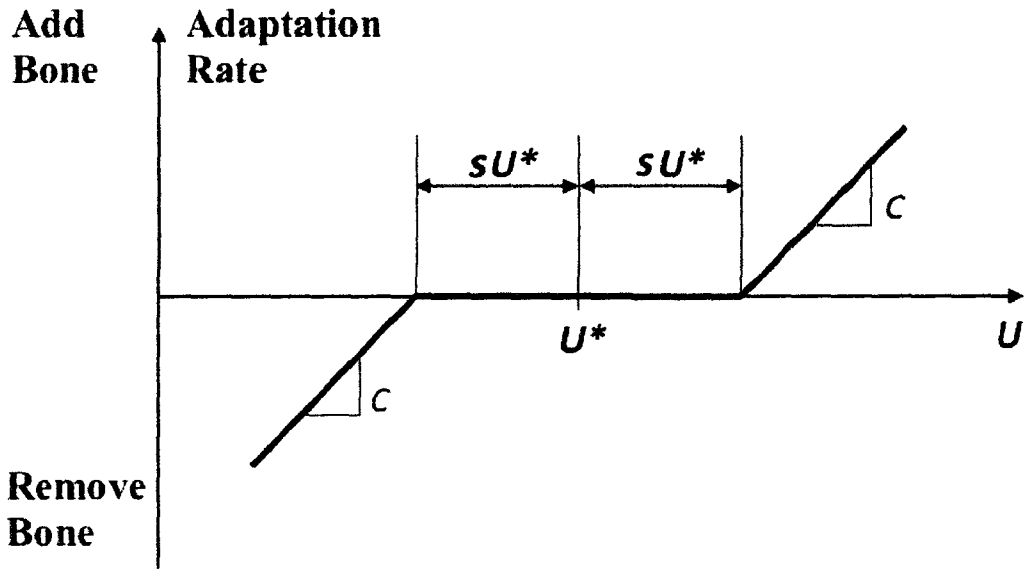

Figure 3.1 The assumed bone adaptation as a function of the strain energy density (SED, U) incorporating lazy zone ($(1-s)U^* \leq U \leq (1+s)U^*$) (MichiganEngineering).

Carter (1984) proposed the concept of lazy zone. A lazy zone, in which no bone adaptation occurs, separates the domains of bone formation and resorption (Figure 3.1). Huiskes et al. (1987) applied the concept of lazy zone to their model. For instance, the new remodeling equation for internal remodeling (spongy bone) is written as:

$$\frac{dE}{dt} = \begin{cases} C_e[U-(1+s)U^*] & \text{for } U > (1+s)U^* \\ 0 & \text{for } (1-s)U^* \leq U \leq (1+s)U^* \\ C_e[U-(1-s)U^*] & \text{for } U < (1-s)U^* \end{cases} \quad (3.4)$$

where s denotes the extent rate of the lazy zone around the U^*, and $2sU^*$ is the width of the lazy zone.

This phenomenological theory was applied to predict bone adaptation for both surface remodeling (shape changes) (Huiskes et al., 1987) and internal remodeling (density changes) (van Rietbergen et al., 1993; Weinans et al., 1993) after implantation of prostheses. For

instance, in the two-dimensional simulation of cortical bone adaptation after hip-prosthetic implantation, Huiskes et al. (1987) predicted the effect of stress shielding successfully.

3.1.2. A semi-mechanistic bone remodeling theory (Huiskes et al., 2000)

Huiskes et al.'s first model (1987) was able to explain bone adaptation on a macroscopic level (Ruimerman, 2005). In order to investigate possible mechano-biological pathways, Huiskes et al. (2000) proposed a new bone remodeling theory, a semi-mechanistic bone remodeling theory, which includes the experimental findings in bone cells' physiology (Vahdati and Rouhi, 2009), such as a separate description of osteoclastic resorption and osteoblastic formation (Burger and Klein-Nulend, 1999), role of microdamage (Pazzaglia et al., 1997; Taylor, 1997; Martin, 2000), and an osteocyte mechanosensory system (Aarden et al., 1994; Cowin et al., 1991). The proposed regulatory process of spongy bone remodeling is shown in Figure 3.2. Spongy bone remodeling is depicted as a coupling process of bone resorption and bone formation on the bone free surfaces. Osteoclasts are assumed to resorb bone stochastically. It is suggested that osteocytes locally sense the SED rate perturbation generated by either the external load or by cavities made by osteoclasts (bone resorbing cells), and then recruit osteoblasts (bone forming cells) to form bone tissue to fill the resorption cavities.

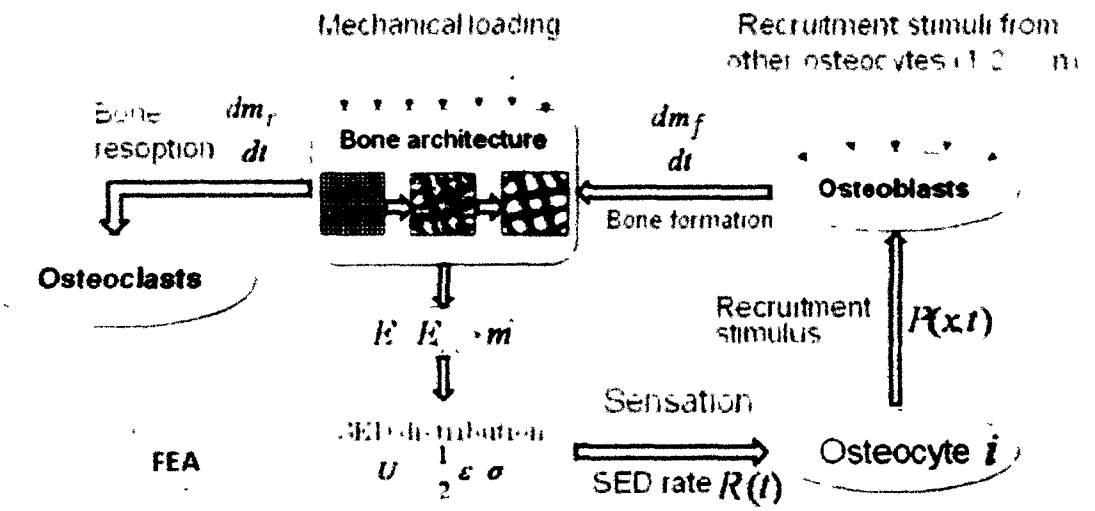

Figure 3.2 Regulation mechanism of the semi-mechanistic bone remodeling process (Huiskes et al., 2000).

3.1.2.1. Separation of osteoclastic and osteoblastic activities

In maturity, local bone resorption and subsequent formation in a process called bone remodeling continuously renew the structure of bone (Frost, 1990). Huiskes et al. (2000) considered bone mass and form are, at any time, determined by a balance between osteoclast resorption and osteoblast formation. They assumed that the change in bone mass at a particular spongy bone surface location x at time t is the result of osteoclastic bone resorption and osteoblastic bone formation, thus:

$$\frac{dm(x,t)}{dt} = \frac{dm_f(x,t)}{dt} + \frac{dm_r(x,t)}{dt} \tag{3.5}$$

where $\frac{dm_f(x,t)}{dt}$ is the local change of relative bone density caused *(m)* by osteoblast formation at trabecular surface location x, and $\frac{dm_r(x,t)}{dt}$ shows the local change of relative bone density *(m)* caused by osteoclast resorption at trabecular surface location x.

3.1.2.2. Osteoclastic resorption caused by the presence of microdamage

Huiskes et al. (2000) assumed that the probability, p, of osteoclast activation per surface site at any time is regulated either by the presence of microdamage within the bone matrix or by disuse. In this study, for the sake of simplicity, only the incidence of the micro-cracks is considered. Supported by experimental evidence (Fazzalari et al., 2002), microdamages are assumed to occur spatially random and microdamage can occur anywhere at any time. Thus, the probability of resorption by microcracks can be considered stochastic and was expressed as:

$$p(x,t) = constant \tag{3.6}$$

where this constant was selected to be 10%.

In their theory (Huiskes et al., 2000), it is assumed that osteoclasts are attracted towards the bone surface by microdamage. When activated, each osteoclast is assumed to remove a fixed amount of mineral. Hence, bone resorption is described by:

$$\frac{dm_r(x,t)}{dt} = -r_{oc} \tag{3.7}$$

where r_{oc} represents the relative amount of mineral resorbed by osteoclasts, and r_{oc} is assumed to be constant.

3.1.2.3. Osteocyte mechanosensory system and osteoblastic formation

Another basic assumption of Huiskes et al.'s theory (2000) is that osteocytes within the bone matrix are mechanosensitive cells capable of sensing the mechanical stimulus and transmitting bone remodeling signals to the bone surface to attract and activate basic multi-cellular units

(BMUs, osteoclasts and osteoblasts, which control resorption and formation at the bone surface, respectively).

The signal sent to the surface by an osteocyte was assumed to decay exponentially with increasing distance, d_i, between osteocyte i and location x according to:

$$f_i(x) = e^{-d_i(x)/D} \tag{3.8}$$

where parameter D [μm] represents the osteocyte influence distance (or the decay constant), which controls average trabecular thickness, for a given external force. It should be noted that the function, $f_i(x)$, was just based on pure speculation. Huiskes and coworkers did not present any specific reason for this decay function. Their assumption is based on rough experimental evidence, so a more mechanistic approach is needed to make this model more accurate and reliable (Rouhi, 2006).

The total bone formation stimulus (osteoblast recruitment stimulus) at the trabecular surface location, x, are contributed by all the N osteocytes located within the influence region. So, the osteoblast recruitment stimulus derived from all the osteocytes in the neighbourhood of the bone surface location x can be written as:

$$P(x,t) = \sum_{i=1}^{N} f_i(x)\mu_i R_i(t) \tag{3.9}$$

where $P(x,t)$ is the total bone formation stimulus value at trabecular surface, x; μ_i is the mechanosensitivity of osteocyte i; and $R_i(t)$ is the SED-rate in the location of osteocyte i. In this theory, the stimulus sensed by osteocytes is assumed to be a typical strain energy density rate (SED-rate), $R_i(t)$, in a recent loading history.

Cyclic loading conditions characterized by frequency and magnitude were imposed, and it was assumed that osteocytes reacted to the maximum SED-rate during the loading cycle. It is showed that the maximum SED-rate was related to the SED value for some substitute static

load and that it could be calculated by static finite element analysis (Ruimerman et al., 2001). It seems that considering a scalar quantity such as strain energy density or its rate has a disadvantage that cannot make any difference between compressive and tensile form of loadings.

Osteoblast formation at the trabecular surface is assumed to be controlled by the osteoblast recruitment stimulus, $P(x,t)$. If the stimulus value, sent by neighbouring osteocytes, is greater than a bone formation threshold, k_{tr}, bone formation at the trabecular surface will take place. But, if the stimulus value is less than the threshold value, k_{tr}, there will be no bone formation (Huiskes et al., 2000). So, one can express the bone formation's governing equation as follows:

$$\frac{dm_f(x,t)}{dt} = \begin{cases} \tau[P(x,t) - k_{tr}] & for \quad P(x,t) > k_{tr} \ , \\ 0 & for \quad P(x,t) \leq k_{tr} \end{cases} \tag{3.10}$$

where τ is a proportionality factor that determines the bone formation rate. The values of the bone formation threshold, k_{tr}, and the proportionality factor, τ, are chosen empirically.

As stated earlier, the change in the relative density at a particular trabecular surface location x and at time t is determined by osteoblast bone formation and osteoclast bone resorption. Substituting Eqs. 3.7- 3.10 into Eq. 3.5, one can write the mathematical expression of the bone remodeling process as follows:

$$\frac{dm(x,t)}{dt} = \begin{cases} \tau\left[\sum_{i=1}^{N} e^{-\frac{d_i(x)}{D}} \mu_i R_i(t) - k_{tr}\right] - r_{oc} & for \quad P(x,t) > k_{tr} \ , \\ -r_{oc} & for \quad P(x,t) \leq k_{tr} \end{cases} \tag{3.11}$$

According to Currey's relationship (Currey, 1988), the Young's modulus, $E(x, t)$ [GPa], at each location depends on the relative density of bone, m, and can be obtained using:

$$E(x,t) = E_{max} \times m(x,t)^{\gamma} \quad (3.12)$$

where the maximum Young's modules, E_{max}, and the exponent, γ, are empirical constants.

3.2. Finite element analysis (FEA)

The semi-mechanistic bone remodeling theory used in our study assumed that strain energy density (SED) was the mechanical stimulus and supposed that the bone remodeling was coupled with two separate processes: bone resorption and subsequent bone formation. Osteocytes were assumed to be sensor cells which can sense the SED and recruit osteoblasts at the bone surface to fill the cavities formed by osteoclasts. The semi-mechanistic bone remodeling theory was expressed by numerical algorithms. FEA codes were developed in this research (see Appendix II). The purpose of the FEA codes is to calculate each bone element's SED. Figure 3.3 shows the finite element analysis flow chart for the calculation of bone elements' SED.

The computer simulation was conducted as an iterative process, during which each bone element's relative density, m, was regulated between 0.01 (no bone) and 1.0 (fully mineralized bone). In the beginning of the iteration, Young's modulus of each bone element E can be determined from the relative density of bone using $E(x,t) = E_{max} \times m(x,t)^{\gamma}$ (Eq. 3.12), with E_{max} =5.0 GPa and γ=3. As the tissue Poisson's ratio, ν, is 0.3 using Eq. I.16 (Appendix I) or Eq. I.44 (Appendix I), the stress-strain matrix, $[D]$, for two- or three-dimensional computer bone model can be formed.

From Eq. I.21 (Appendix I) and Eq. I.50 (Appendix I), we know that the strain-nodal displacement matrix, $[B]$, can be expressed as a matrix with respect to the local coordinates.

$[B]^T[D][B]$ is a function of local coordinates, r and s. Referred to Table I.1 (Appendix I) or Table I.2 (Appendix I), we can find the local coordinates of the integrating point and weighting coefficients. According to Eq. I.27 (Appendix I) and Eq. I.56 (Appendix I), the approximation of the element stiffness matrix, $[K^e]$, for two- and three-dimensional mesh can be evaluated, respectively.

As soon as the element stiffness matrix, $[K^e]$, has been formed, it can be assembled into the global stiffness matrix, $[K]$. Since external forces are given, we can form the global force vector, $\{F\}$, directly. Following the assembled global equations:

$$[K]\{U\} = \{F\} \tag{3.13}$$

with $\{U\}$ representing the vector of global displacement, the global nodal displacement can be obtained. Once $\{U\}$ is known, the element nodal displacements,$\{U^e\}$, are retrieved.

The strain tensor, $\{\varepsilon\}$, at the center of the element is given by the strain-nodal displacement relations, Eq. I.20 (Appendix I) or Eq. I.49 (Appendix I). According to Eq. I.28 (Appendix) or Eq. I.57 (Appendix I), the SED, u^e, at the center of the two- or three-dimensional element can be obtained.

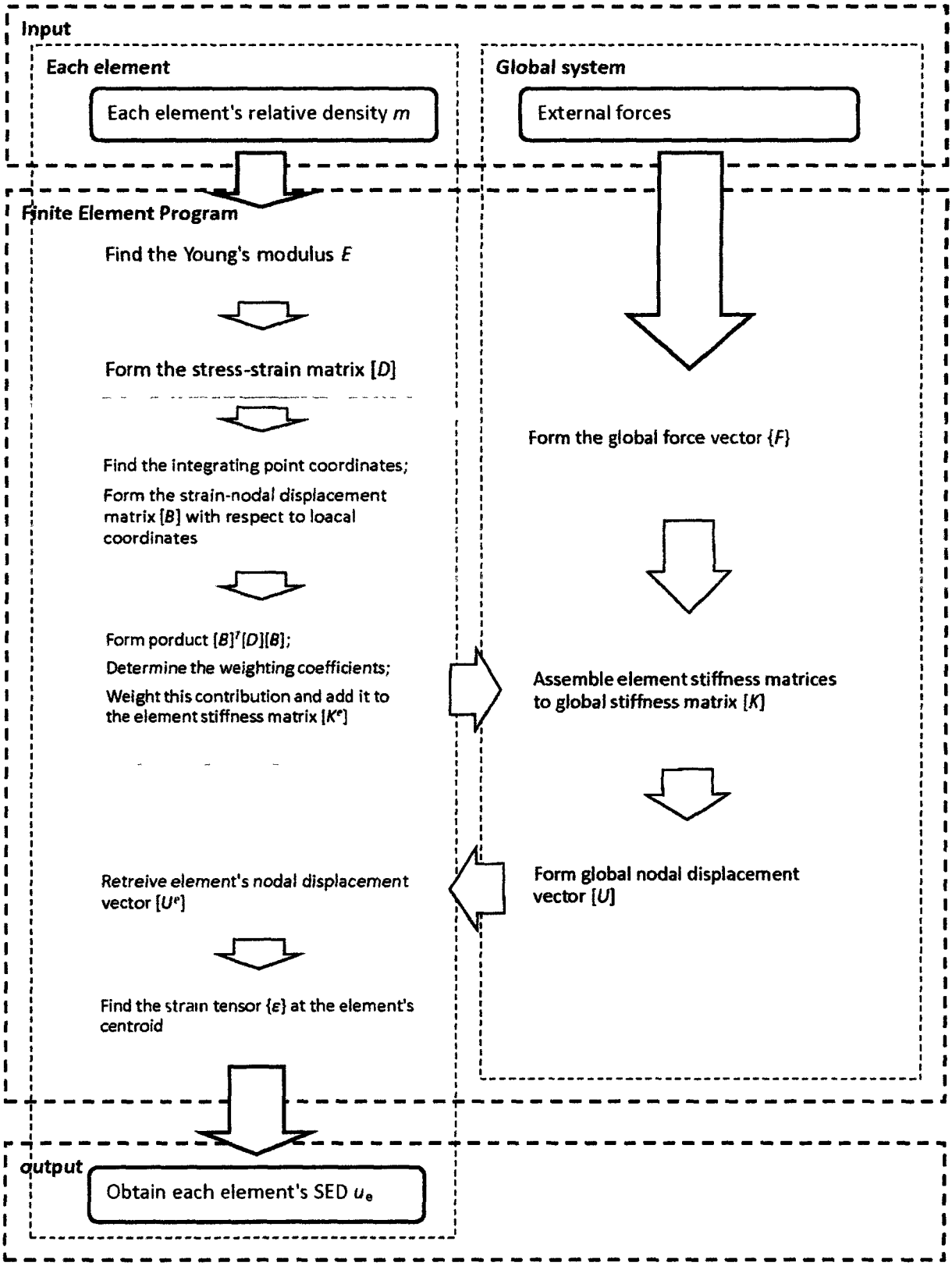

Figure 3.3 The finite element analysis flow chart for calculation of the bone elements' SED.

Chapter 4

An Investigation into the Reasons for Bone Loss in Aging and Osteoporotic Individuals Using a Two-Dimensional Computer Model

4.1. Introduction

Bone is a dynamic tissue which adapts its mass and architecture to the external loads constantly. Bone's adaptation is finished through a coupled process of bone resorption by osteoclasts, and subsequent bone formation by osteoblasts, which is so-called bone remodeling process (Ruimerman and Huiskes, 2005; Ruimerman et al., 2005). When the amount of bone resorption is more than the added newly formed bone for a long period of time, bone loss, a net reduction in bone apparent density which is defined as bone mass per total volume of bone sample, and so a decrease in bone modulus of elasticity and also its strength appear. Bone loss usually starts after maturation and accelerates in osteoporotic bones. For instance, after the age of 25-30 years, a slightly negative balance between bone resorption and formation may cause progressive bone loss (Mullender et al., 1996). Usually, in the case of a minor reduction in bone density, mechanical integrity is maintained (Mullender et al., 1996). However, in the case of osteoporosis or very major bone loss, a substantial reduction can be seen in both bone modulus of elasticity and strength (Parfitt et al., 1983), in which

bone can fail even with lifting a light weight (Dickenson et al., 1981; Bono and Einhom, 2003; Yuan et al., 2004; Slomka et al., 2008).

In the beginning of 21st century, Huiskes and co-workers (2000) developed a semi-mechanistic model for bone remodelling. The semi-mechanistic bone remodeling theory includes the experimental findings in bone cells' physiology (Vahdati and Rouhi, 2009), such as a separate description of osteoclastic resorption and osteoblastic formation (Burger and Klein-Nulend, 1999), an osteocyte mechanosensory system (Aarden et al., 1994; Cowin et al., 1991), and the role of microdamage (Pazzaglia et al., 1997; Taylor, 1997; Martin, 2000). In this theory, osteocytes are assumed to be sensitive to the maximal rate of the strain energy density (SED) in a recent loading history and send out signals to recruit the osteoblasts, bone forming cells, which form new bone to fill the cavities caused by osteoclast resorption. Osteoclast resorption caused by microdamage is supposed to occur spatially random.

Based on the experiments, it is known that osteocyte density (the number of osteocytes per unit surface of bone) changes with aging and also in osteoporotic bones (Mullender et al., 1996). It has been found that osteocyte density declines significantly with aging in healthy adults from 30 to 91 years of age (Frost, 1960; Mullender et al., 1996; Qiu et al., 2003). On the other hand, Mullender et al. (1996) interestingly found that the osteocyte density increases in osteoporotic patients compared to healthy adults, although excessive bone loss and reduced spongy bone wall thickness have been described as characteristic of osteoporotic bones.

It was suggested that osteocytes regulate the recruitment of basic multicellular units (BMUs) in response to mechanical stimuli (Kenzora et al., 1978; Marotti et al., 1990; Lanyon, 1993). Based on the fact that the number of osteocytes per unit surface of bone changes in

aging healthy adults and also in osteoporotic patients, here we hypothesize that bone loss is correlated with the reduction of either the number of osteocytes in the aging healthy adults' bone or the strength of the recruitment signal sent by osteocytes to the bone making cells (osteoblasts) in the osteoporotic bone. The former part of our hypothesis is raised because of the evidence indicating that osteocyte density can likely affect the trabecular bone morphology (Mullender et al., 1994; Mullender and Huiskes, 1995). The later part of our hypothesis is raised since one may ask: "If the bone loss with aging is provoked and driven by a decrease in osteocyte density, then what is the explanation for rapid bone loss in osteoporotic bones wherein there is an increase in osteocyte density?". Since the changes in bone structure because of osteoporosis are similar to changes resulting from disuse (Frost, 1988; Rodan, 1991; Mullender et al., 1994; Mullender and Huiskes, 1995), we assumed that one of the causes for bone loss in osteoporotic bones is the reduction in osteocyte mechanosensitivity. To investigate our hypotheses we employed Huiskes and co-workers' (2000) semi-mechanistic bone remodeling theory to build computer models for simulating the spongy bone remodeling.

4.2. Methods

4.2.1. A semi-mechanistic bone remodeling theory

Please see section 3.1.2.

4.2.2. A two-dimensional computer model

A two dimensional finite element model of spongy bone, which was a square domain of 1.52×1.52 mm^2, was created by implementing the mathematical expressions of the semi-mechanistic bone remodeling theory (Huiskes et al., 2000). This domain was divided into 38 $\times$ 38 rectangular four-node elements. Relative bone density (m) per element is considered to alter between 0.01 (no bone, so just bone marrow) and 1.0 (no void, fully solid mineralized bone) (see Figure 4.1). In order to apply external loads to our 2D computer model, the perimeter of the square domain was assumed to be surrounded by a band. The thickness of the band was one element, equal to 40 μm. This band did not participate in the bone remodeling process, and the load was applied at the edge of the bone model. In order to minimize the effect of stress shielding caused by continuous band corners, no external load was imposed on the corner of the band (see Figure 4.1), and the material properties of the band were the same as those of a fully mineralized trabecular bone tissue, which were given a Young's modulus of 5 GPa and a Poisson ratio of 0.3. The structure was loaded by a sinusoidal stress, cycling between 0 and 2 MPa, and at frequency of 1 Hz. The semi-mechanistic bone remodelling theory assumed that the stimulus sensed by osteocytes is the maximal SED-rate during one loading cycle. It has been shown that the maximum SED-rate can be substituted by the SED value for some static load (Ruimerman et al., 2001). Hence, the bone remodeling can be evaluated by static finite element analysis. In this study, the SED value was calculated using a substitute static stress of 4 MPa.

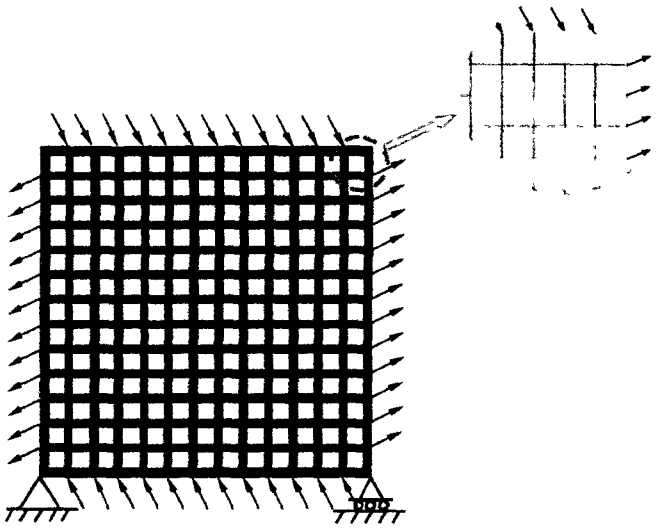

Figure 4.1 Initial geometry of spongy bone model used in computer simulation. In the circular region, grey and white elements show bone matrix and bone marrow, respectively. No load was imposed on the corners of the computer model with plates.

It is known that both cortical and spongy bones are anisotropic materials (van Rietbergen and Huiskes, 2001). Moreover, both cortical and spongy bones show viscoelastic behaviour when the external loads are out of the physiological range (van Rietbergen and Huiskes, 2001). In this study, however, for the sake of simplicity, the bone model's elements were assumed to be isotropic and linearly elastic material. The Young's modulus of each element changed per iteration according to the modulus-density relationship which was determined from empirical data for trabecular bone with E_{max} = 5 GPa and γ = 3 (Eq. 3.12). Other model parameters were set in Table 4.1.

Table 4.1 Parameter settings for the two-dimensional spongy bone remodeling simulations

Variable	Symbol	Value	Unit[a]
Osteocyte mechanosensitivity	μ	1	$nmolmmJ^{-1}s^{-1}day^{-1}$
Osteocyte influence distance	D	100	μm
Formation threshold	k_{tr}	0001	$nmolmm^{-2}day^{-1}$
Proportionality factor	τ	20	mm^5nmol^{-1}
Resorption probability	p	10	%
Relative mineral amount per resorption	r_{oc}	0.3	voxel
Maximal elastic modulus	E_{max}	5.0[b]	GPa
Poisson ration	v	0.3[b]	-
Exponent gamma	γ	3[c]	-
Loading amplitude	F	2.0	MPa
Loading frequency	f	1	Hz

[a]Ruimerman et al., 2005.

[b]Mullender and Huiskes, 1995.

[c]Currey, 1988.

Bone resorption and formation in each bone element were determined according to Eq. 3.11, leading to a new configuration after each iteration of computer simulation. The whole simulation process is repeated until equilibrium is reached, when bone resorption and formation are balanced and no significant structural change is observed. In this study, in order to have a stable configuration, 3000 iterations were performed for each simulation.

4.2.3. Computer simulations of spongy bone remodeling

Three series of simulations were performed in this study. The purpose of the first series was to test whether the configuration of our computer model is adaptive to the environmental loading condition, such as loading magnitude and direction. In the first series, osteocytes were assumed to be distributed uniformly within the domain. Each element has an osteocyte in its center. The magnitude and direction of the load acting on the edge of the model were changed in this series. In process A (see Figure 4.2), the orientation of the external loads was 30

degrees counter-clockwise, with respect to vertical axis. In process B (see Figure 4.3), the magnitude of the external loads was increased by 20% compared to that of the loads used in process A, and the direction of the external loads was kept the same as in process A. In process C (see Figure 4.4), the magnitude of the external loads were reduced by 20% compared to that of process A, and the direction of the external loads was maintained the same as in process A. In process D (see Figure 4.5), the orientation of the external loads was rotated by 30 degree in clockwise direction.

The purpose of the second series was to investigate the effects of decreased osteocyte density on spongy bone remodeling. As stated before, it is found that osteocyte density decrease in healthy adults as one ages (after the age of 30). As can be seen in Table 4.2, osteocyte density is 172.8±34.9 mm^{-2} in the healthy adults who are younger than 55 years, and 135.1±38 mm^{-2} in the adults who are older than 55 years (Mullender et al., 1996). There is a 21.82% reduction with aging in osteocyte density for the whole spongy bone. Based on the experimental evidence, it is well known that the number of empty lacunae and lacunae with degenerated osteocytes is increasing with age, and also with the distance from the vascular sources (Marotti et al., 1985; Baiotto and Zidi, 2004). Thus, it is reasonable to assume that some elements in our 2D computer model (see Figure 4.1) have no sensor cells (osteocytes) at their centers. In this series of simulations, osteocytes were non-uniformly distributed in the bone region. In order to mimic the non-uniform osteocyte distribution, a random distribution of osteocytes within different elements was considered in our computer model. Some elements had three sensor cells (osteocytes), but others had either 2, or 1, and some others did not have any sensor cells at their centers. In the first step, osteocyte density was the same as that used in the first series of simulations. Starting from the initial configuration, the spongy bone

remodeling of the healthy adults under the age of 55 years was simulated (see process E, Figure 4.7). In the second step, starting from the final configuration of process E, the spongy bone remodeling of the healthy adults over 55 years was simulated (see process F, Figure 4.7). In process F, the osteocyte number per bone area was reduced by 21.82%, and the external loads were kept the same as those used in process E (see Figure 4.7).

Table 4.2

Osteocyte density of healthy adults and osteoporotic patients (Mullender et al., 1996)

		Number of osteocytes/bone area (mm^{-2})	**Combined number of osteocytes/bone area (mm^{-2})**
Healthy individuals	≤55 years	172.8±34.9	150.7±40.7
	>55 years	135.1±38.0	
Osteoporotic patients >55years	Hip fracture	158.3±23.6	164.5±24.2
	Vertebrae fracture	176.0±21.6	

The third series were performed to test the probability of bone loss in osteoporotic bones caused by a reduction in osteocyte mechanosensitivity. Experimental observations show that in the observed osteoporotic group older than 55 years, osteocyte density has a significant increase relative to the healthy adults (Mullender et al., 1996). As can be seen in Table 4.2, the osteocyte density in healthy adults over the age of 55 is 135.1±38.0 mm^{-2}, whereas that of the osteoporotic patients for the same age group is 164.5±24.2 mm^{-2}. Thus, the osteocyte density in osteoporotic patients (older than 55 years) increased by 21.76% compared to the osteocyte density in healthy adults above 55 years. In the third series of simulations, based on the

experimental evidence (Marotti et al., 1985; Baiotto and Zidi, 2004), osteocytes were randomly distributed in the bone region. We considered that an adult was healthy when he (or she) was under 55 years, but was affected by osteoporosis when he (or she) got older than 55 years. So, in order to model the spongy bone remodeling for the osteoporotic patients, in the first step, starting from the initial configuration, the spongy bone remodeling for a healthy adult younger than 55 years was simulated (see process E, Figure 4.7). Then, in the second step, since osteoporotic patients were assumed to be older than 55 years, we decreased the osteocyte density in the healthy young adults by 21.82% to get the osteocyte density in the healthy adults over the age of 55 years, and then increased the osteocyte density by 21.76% to get the osteocyte density in the osteoporotic patients. The loading conditions, magnitude and direction, were kept the same for the first and second steps. To investigate the effects of mechanosensitivity on the spongy bone remodeling in osteoporotic patients, we decreased the mechanosensitivity of osteocytes from 1 to 0.1 gradually for each simulation in the second step (see Figure 4.9). The simulations with different osteocyte mechanosensitivities all started from the structure obtained from the first step, i.e. from process E (see Figure 4.7).

4.3. Results

In the first series of simulations, trabeculae-like structures were obtained from the initial configuration. Trabeculae were lined up with the loading direction (see Figure 4.2). A 20% increase in the external loading magnitude increased the trabecular thickness (see Figure 4.3) which resulted in a 12.5% increase in the bone mass (see process A and B, Figure 4.6). Reduction in the external loading magnitude by 20% has led to a decrease in trabecular

thickness (see Figure 4.4) and a decreased bone mass by 12.5% (see process A and C, Figure 4.6). When the directions of external loads were changed to horizontal and vertical, the trabeculae were realigned to the new loading directions as well (see Figure 4.5). Even though the direction of trabeculae changed as the direction of external load had been altered, there is no considerable mass change in the final simulation result (see process A and D, Figure 4.6). The results were similar to the results published by Ruimerman et al. (2001).

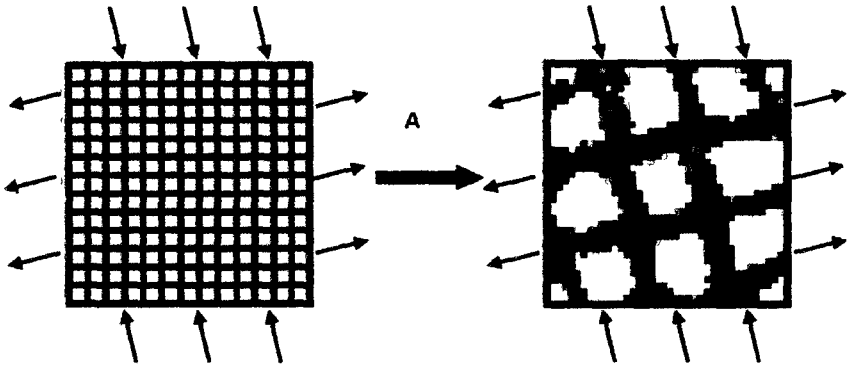

Figure 4.2 Trabecular structure was developed and the trabeculae were aligned with the loading direction (Process A). Black (and grey) represents bone matrix and white shows bone marrow. Black elements have higher densities than grey elements.

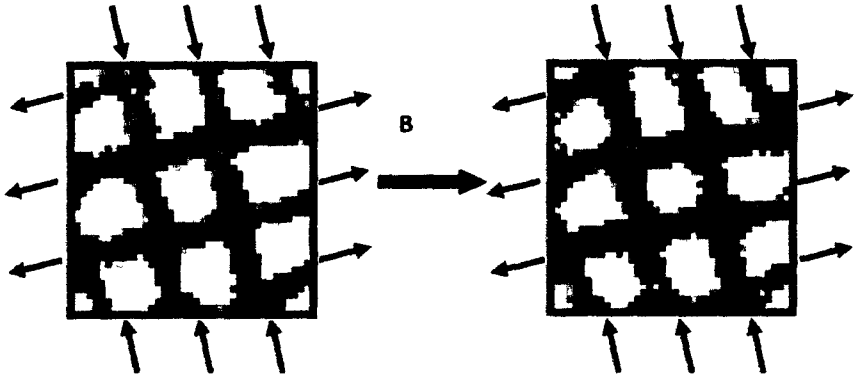

Figure 4.3 Increased loading magnitude leads to increased trabeculae thickness (Process B). The left structure is the result of process A from Figure 4.2.

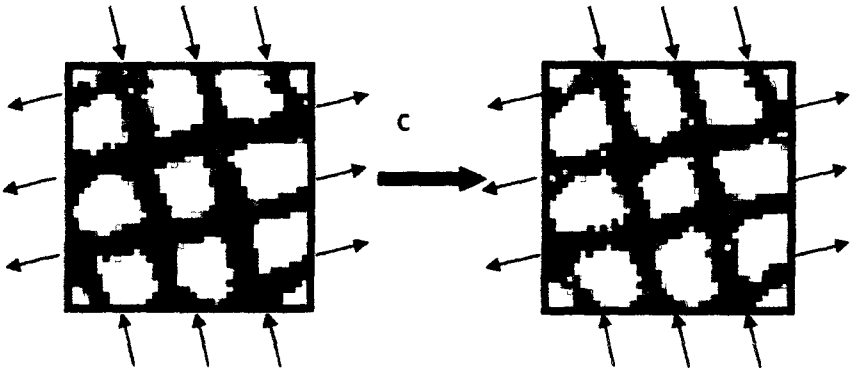

Figure 4.4 Decreased loading magnitude leads to a reduction in the thickness of trabeculae (Process C). The left structure is the result of process A from Figure 4.2.

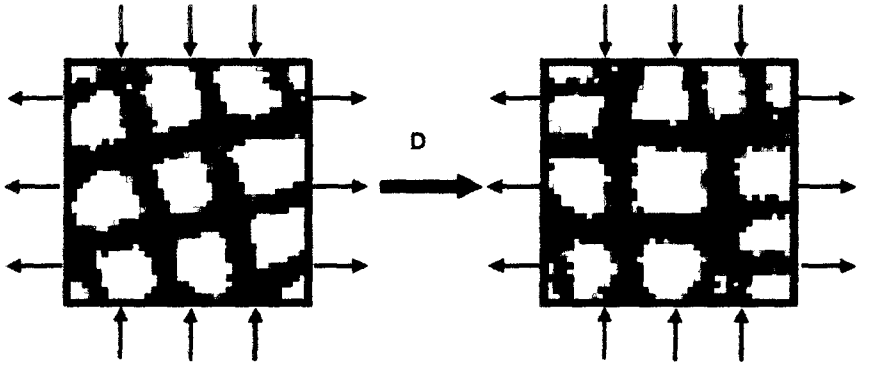

Figure 4.5 Rotating the external loading direction realigned the trabeculae accordingly (Process D). The left structure is the result of process A from Figure 4.2.

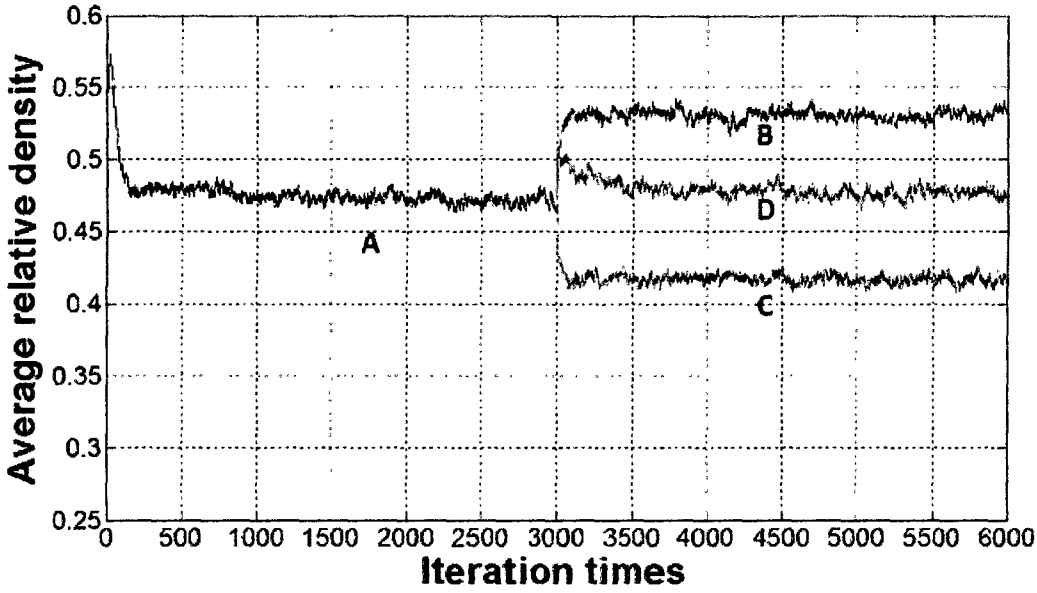

Figure 4.6 The mean relative density changes caused by different external loading environments: increasing the external loads magnitude (Process B, Figure 4.3, a 20% increase in the load magnitude compared to Process A, Figure 4.2), reducing the external loads magnitude (Process C, Figure 4.4, a 20% decrease in the load magnitude compared to Process A, Figure 4.2), and rotating the load direction (Process D, Figure 4.5).

In the second series of simulations, by comparing the circular and square region in Figure 4.7, it is obvious that bone loss has occurred in healthy older spongy bone model (result of process F, Figure 4.7) compared to the healthy young bone model (result of process E, Figure 4.7). The bone loss in the spongy bone of the healthy old adults was also proved by the decreasing average relative bone density (see Figure 4.8). For the non-uniform osteocyte distribution in the bone region, the decreased osteocyte density of the old adults (older than 55 years, process F, Figure 4.8) compared to that of healthy young adults (younger than 55 years, process E, Figure 4.8) has led to a decreased average relative bone density of the model by 5.34%.

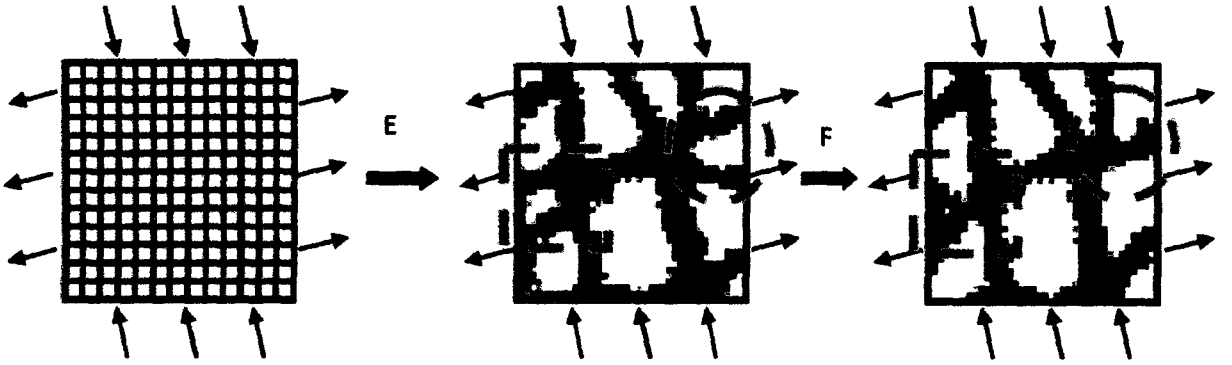

Figure 4.7 Left: The initial configuration. Middle: The result of the spongy bone remodeling simulation (Process E) for the healthy young group (younger than 55 years). The right structure is the result of the simulation (Process F) for the healthy old group (older than 55 years).

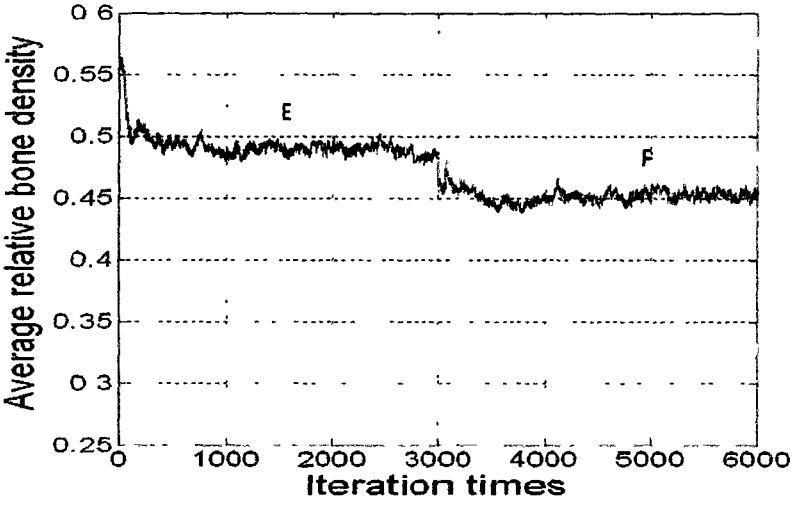

Figure 4.8 The variation of the relative density of the healthy model with randomly distributed osteocytes. Process E (Figure 4.7) corresponds to the remodeling of the spongy bone in healthy young adults (younger than 55 years). Process F (Figure 4.7) relates to the remodeling of the spongy bone in healthy old adults (older than 55 years). The spongy bone model in the healthy old adults has lower number of osteocytes per unit area than that of healthy young adults.

In the third series of simulations, the results of the simulations with different osteocyte mechanosensitivities can be seen in Figure 4.9. All started from the spongy bone configuration in healthy young adults (result of process E, Figure 4.7). The osteocyte mechanosensitivity was decreased gradually from 1 to 0.1 for each simulation. It should be noted that the same osteocytes' number and also the same form of osteocyte distribution were considered for all cases in Figure 4.9. To exclude the effects of age on spongy bone apparent density, only subjects older than 55 years were used for the comparison between the healthy adults and the osteoporotic patients. Here, we compared the average relative (or apparent) bone density between the healthy old adults and the osteoporotic patients. Stars (*) in Figure 4.10 represent the average relative bone densities of structures with different mechanosensitivities. The trend of the density change shows that average relative spongy bone density decreases when osteocyte mechanosensitivity is reduced. When osteocyte mechanosensitivity was less than 0.87, the average relative density in the osteoporotic bone was less than that of the healthy old adult, even though more osteocytes per unit area were considered in the osteoporotic case. In order to make sure about our simulations' results, osteoporotic spongy bone remodeling with different osteocyte mechanosensitivities was simulated one more time. In Figure 4.10, square points (□) represent the new average relative bone densities of structures with different mechanosensitivities. The new trends of the density changes are very close to the former one (see Figure 4.10).

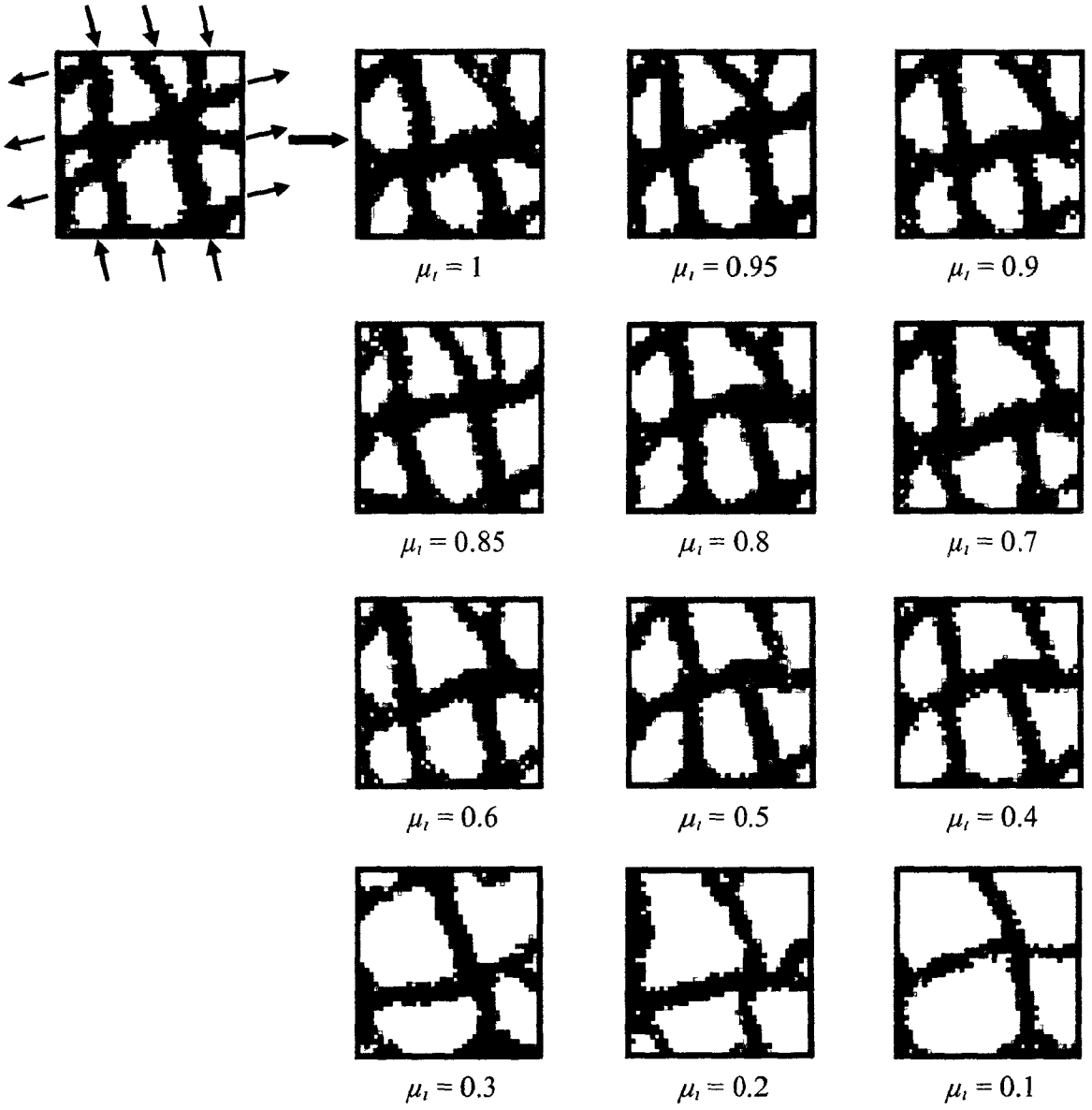

Figure 4.9 Results of simulation of the spongy bone remodeling for different values of osteocyte mechanosensitivity (μ_l), representing the level of activity of bone sensor cells. The osteocytes numbers in each simulation with different osteocyte mechanosensitivities are unchanged. The left structure is the result of the process E (see Figure 4.7).

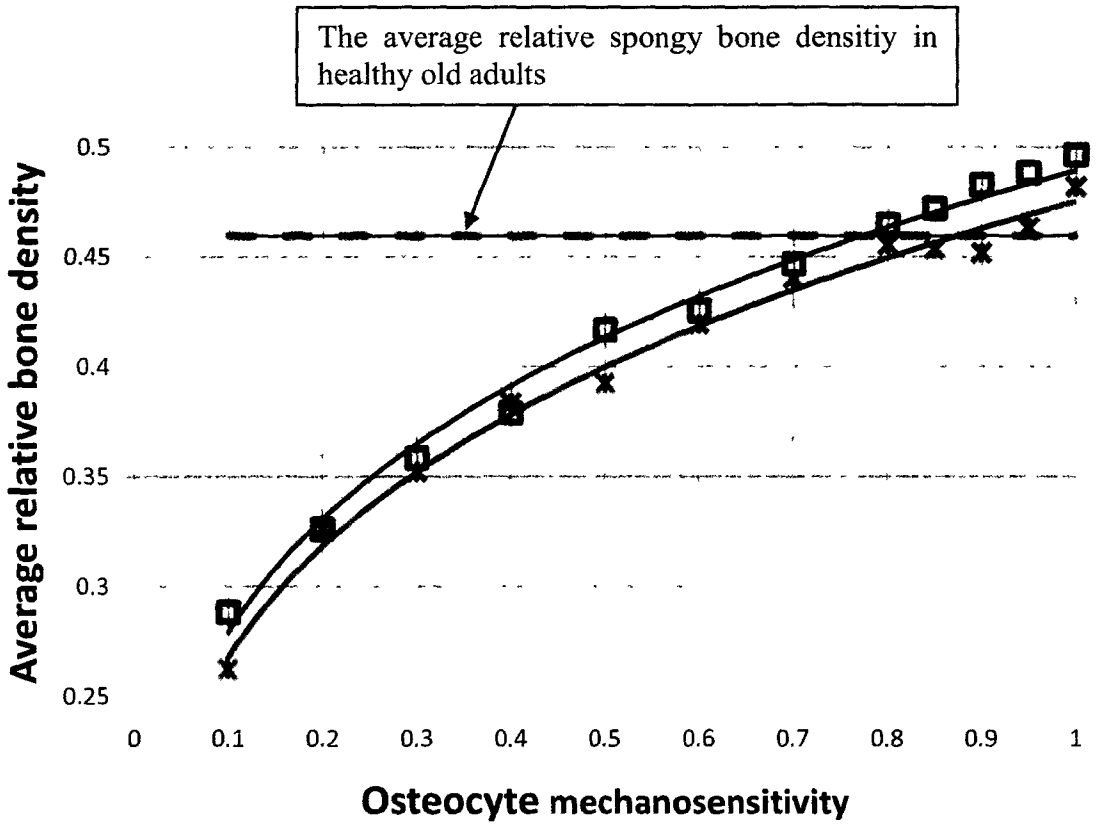

Figure 4.10 Comparison of relative densities of osteoporotic spongy bone models with those of healthy old adults' bone model. Solid lines are the tendency of the variation of the relative density of the osteoporotic bone model with different osteocyte mechanosensitivities. Dashed red line shows the average relative spongy bone density in healthy old adults which is 0.4595. The osteocyte mechanosensitivities in healthy adults are assumed to be 1 here. This figure shows that bone loss occurs in the osteoporotic bones when the activity of an osteocyte is less than a certain level, even though the osteocyte density in osteoporotic patients is greater than that of the healthy old adults. The trends of these two solid curves are very close. It can be said that our model is stable.

4.4. Discussion and conclusions

The spongy bone remodeling simulation results of our computer model in this study are in agreement with the general statement of Wolff's law (Wolff, 1892). In the first series of simulations, when osteocytes are uniformly distributed in the bone region, trabeculae-like architectures are obtained in our computer simulations (see Figures 4.2-4.6). Although the strain energy density (SED), which is used here as the mechanical stimulus for the initiation of the bone remodeling process, is a scalar quantity, the simulation results still showed that the spongy bone structure were adaptive to not only external loading magnitude, but also to the loading direction. The thickness of the trabeculae in the final configuration decreased when the magnitude of the external loading was reduced and vice versa (see Figures 4.3 and 4.4). Moreover, the directions of the trabeculae are aligned with the direction of the external loads (see Figure 4.5).

Results of this study also show that the osteocyte density has a significant role in the final shape of spongy bone in the bone remodeling process. In the second series of simulations, with the same parameter settings as the first series of simulation, including the same mechanosensitivity for osteocytes, it is shown that by decreasing the osteocyte density (knowing that the osteocyte density decrease as a healthy adult ages), bone loss will occur and there will be a decrease in bone apparent density (see Figures 4.7 and 4.8). These results are in favour of our first hypothesis which says that "by decreasing osteocyte density, there will be a net bone loss with aging in the healthy adults".

The third series of simulations showed that when osteocyte mechanosensitivity is less than a certain level, osteoporotic patients lose more spongy bone than healthy old adults, even

though osteoporotic patients have more osteocytes than healthy old adults (see Figure 4.9). If bone loss because of aging in healthy old adults be considered as a normal bone loss process (due to the reduction in the osteocyte density, based on experimental evidence), the bone loss in osteoporotic patients with osteocyte mechanosensitivity less than some certain levels should be deemed as an abnormal process and a pathological state. These results also show that our second hypothesis saying that "by decreasing the osteocyte mechanosensitivity (as is the case in an osteoporotic bone), bone apparent density will also decrease, even by increasing the number of osteocytes" makes a good sense and seems reasonable.

It should also be noted that in both second and third series of simulations, a non-uniform osteocyte distribution was used. The final structures of these two series of simulations are not as regular as those in the first series of simulation in which uniform osteocyte distribution was used (compare Figures 4.7 and 4.9 with Figures 4.2-4.5). Thus, one can conclude that not only the osteocytes number and mechanosensitivity, but also their spatial distribution can have a considerable effect on the final geometry, configuration, and anisotropy of spongy bone at the micro-scale.

Experimental evidence for an altered mechanosensitivity of osteocytes derived from osteoporotic patients has also been reported. Sterck et al. (1998) tested response of normal and osteoporotic human bone cells to mechanical stress *in vitro*. In their test, bone cells (osteocytes, osteoblasts, and lining cells) were mechanically stressed by treatments with pulsating fluid flow to mimic the stress-driven flow of interstitial fluid through the bone canaliculi, which is likely the stimulus for mechanosensation in bone *in vivo*. They observed that bone cells from non-osteoporotic bones responded to pulsating fluid flow with enhanced release of prostaglandin E_2 (PGE_2). Sterck and co-workers (1998) also found that the PGE_2

release is significantly reduced in the bone cells from osteoporotic patients compared with age-matched individuals, as well as with the non-osteoporotic group. Recently, Mulvihill and Prendergast (2008), based on a theoretical approach, suggested that a lower bone tissue mechanosensitivity, caused either by a genetic effect or age, could be responsible for the rapid bone loss observed in an osteoporotic bone. They simulated the bone remodelling cycles using a finite element model, but just for a trabecular strut. In their simulations, mechanical strain was considered as the remodeling stimulus, in accordance with the mechanostat theory of Frost (1987).

Some of the other possible explanations for the abnormal bone loss in an osteoporotic bone suggested by different researchers are: (1) a higher percentage of the bone forming cells is embedded in bone matrix as osteocytes (Mullender et al., 1996); (2) the bone forming activity of osteoblasts is reduced (Mullender et al., 1996; Ruimerman et al., 2001); and (3) the average life-span of osteoblasts is reduced (Eriksen and Kassem, 1992; Mullender et al., 1996). It seems reasonable to assume that bone loss in the case of osteoporosis is the result of a combination of all the above mentioned factors, and likely some other factors which are not known yet.

This research, as a preliminary investigation on the relation between the number and the activity of bone sensor cells and the bone apparent density, needs further efforts on both experimental and theoretical grounds in order to shed more light on the complex bone remodelling process with the hope of finding a solution for the osteoporosis, so-called bone silent disease, which affects millions of people worldwide.

Chapter 5

A Three-Dimensional Computer Model to Simulate Spongy Bone Remodeling under Overload

5.1. Introduction

The bone remodeling process is essential for the maintenance of our skeleton. It enables adaptation of the bone mass and architecture to changes in mechanical loads (Wolff, 1892; Frost, 1987). Bone remodeling is mainly a two stage process which includes bone resorption and subsequent bone formation. The coupled bone remodeling process is performed by two types of bone cells: osteoclasts, which are multinucleated bone resorbing cells, and osteoblasts, which are bone-forming cells. Osteoclasts resorb packets of bone tissue, and osteoblasts replace the resorbed tissue with new mineralized bone tissue. Clusters of osteoclasts and osteoblasts involved in bone remodeling are known as basic multi-cellular units (BMUs).

The ends of the long bones are filled with spongy bone (or cancellous bone), a very porous bone structure made of mineralized plates and struts, the trabeculae. This spongy bone gives the bones a relatively low mass, but a relatively high stiffness. Spongy bone is also found within the interior of vertebrae, in flat bones like the skull and the pelvis and in the hand and feet. In the spongy bone, remodeling takes place at the surface of the trabeculae (Figure 2.9.B).

In order to perform the bone remodeling process, a connection between external load and the activities of BMUs must exist (Ruimerman et al., 2001). Firstly, bone requires sensors which can detect the mechanical load. Secondly, bone needs channels through which necessary

signals can be sent to effector cells (osteoblasts and osteoclasts). Osteocytes are the most abundant bone cells distributed throughout the bone matrix. They, osteocytes, are located within lacunae and are in contact with each other, also with osteoblasts, and bone lining cells via their long processes contained within channels known as canaliculi. Lacunae and canaliculi make up a fluid-filled lacuno-canalicular network. The number of osteocytes and their location in bone make them suitable candidates for mechanosensors (Cowin et al., 1991). Previous studies assumed that osteocytes detected mechanical load and converted mechanical loading information into bone-formative stimuli, transported to effector cells through the osteocytic canalicular network (Burger and Klein-Nulend, 1999). It is assumed that this stimulus recruits and activates osteoblasts to form new bone (Huiskes et al., 2000; Tanck et al., 2006).

Some researchers have also suggested that osteocytes can send out an inhibitory signal, preventing osteoclastic activity (Marotti et al., 1992; Martin, 2000; Vahdati and Rouhi, 2009). Osteoclast resorption is activated at the bone surface, where inhibitive osteocyte signals no longer reach (Burger and Klein-Nulend, 1999). This can occur not only when external loads are reduced, but also when the osteocytic network within the bone matrix is blocked due to microdamage (Martin, 2003; Tanck et al., 2006). Microdamage, in the form of microcracks, occurs in both cortical and spongy bone *in vivo* during daily activities (Schaffler et al., 1989; Wenzel et al., 1996; Vashishth et al., 2000) and *in vitro* during overloading (Fyhrie and Schaffler, 1994; Wachtel and Keaveny, 1997; Reilly and Currey, 1999).

Bone loss is a main factor that leads to failure in prosthetic implants as it causes looseness at the bone-implant interface, thus causing micromotion of the implants and decreasing the reliability of implantation (Huiskes et al., 1987; McNamara et al., 1997). While stress-shielding is commonly regarded as a reason for bone loss in the implant system,

overload at the interface has also been suggested as a contributing factor (Li et al., 2007). For instance, Huiskes and Nuanmaker (1984) reported that the loosening of and bone resorption around orthopaedic implants were associated with high peak stresses at the interface. The coupled remodeling process is capable of increasing the rate of remodeling to cope with increased damage, but this ability has substantial limits (Hazelwood et al., 2001). While moderate levels of bone microdamage may play a constructive and important role in maintaining bone structural integrity, excessive damage caused by overload can result in accumulation of unrepaired damaged regions (Hazelwood et al., 2001). Bone formation cannot keep pace with bone resorption experiencing overload, thus bone loss due to overload will occur (Li et al., 2007). Other possible effects of overload include the degradation of mechanical properties and development of skeletal fragility, particularly in spongy bone (Frost, 1994; Turner, 2002; Martin, 2003; Schaffler, 2003; Nagaraja et al., 2005).

More than one hundred years ago, Wolff's Law (1892) was proposed. It explained that bone adapted its structure to mechanical loadings in accordance with mathematical law. In 1964, the first mathematical expression of bone remodeling was developed by Frost (1964b). In the last 4 decades, several mathematical models of bone remodeling have been proposed to describe bone remodeling process. However, it is still not clear what the actual mechanical stimulus of the bone adaptation is. Stress (Wolff, 1892; Frost, 1964b), strain (Cowin and Hegedus, 1976; Frost, 1987), and strain rate (Hert et al, 1969; Fritton et al., 2000) have been usually assumed to be the mechanical stimulus. Recently, Huiskes and co-workers (2000) developed a semi-mechanistic model for bone remodeling theory which used strain energy density (SED) as mechanical stimulus. The semi-mechanistic bone remodeling theory (Huiskes et al., 2000) includes the experimental findings in bone cells' physiology (Vahdati

and Rouhi, 2009), such as a separate description of osteoclastic resorption and osteoblastic formation (Burger and Klein-Nulend, 1999), an osteocyte mechanosensory system (Aarden et al., 1994; Cowin et al., 1991), and role of microdamage (Pazzaglia et al., 1997; Taylor, 1997; Martin, 2000).

Although many mathematical models governing bone's mechanical adaptation have been proposed, few can consider bone resorption due to overload (Li et al., 2007). In this study, we investigated the effects of microdamage caused by overload on the bone remodeling process (section 5.2.2) and implemented these effects in the extension of the pre-existing semi-mechanistic bone remodeling theory (Huiskes et al., 2000). A three-dimensional (3D) computational model was developed here to test our mathematical model for spongy bone remodeling under overload.

5.2. Methods

5.2.1. A Semi-mechanistic bone remodeling theory

Please see section 3.1.2.

5.2.2. Hypotheses for the effects of overload on bone remodeling

We proposed two hypotheses for the effects of overload on the spongy bone remodeling and extended the semi-mechanistic bone remodeling theory of Huiskes and coworkers (Huiskes et al., 2000).

5.2.2.1. The bone resorption probability and resorption amount increase under overload

Huiskes et al. (2000) stated that the microcracks produced by the dynamic forces of daily normal physical activities could occur anywhere at any time, and suggested that osteoclast resorption was activated by microdamage. Hence, osteoclast resorption would be spatially random. In the semi-mechanistic bone remodeling theory (Huiskes et al, 2000), a probability function of osteoclastic resorption, *p(x,t)*, was defined and included in their model. The *p(x,t)* caused by microcracks was considered to be spatially random and selected to be a constant. They also assumed that each osteoclast resorption removed a fixed amount of mineral. Bone resorption is described by:

$$\frac{dm_r(x,t)}{dt} = -r_{oc} \tag{5.1}$$

where $\frac{dm_r(x,t)}{dt}$ was the local change of relative bone density *(m)* caused by osteoclast resorption at trabecular surface location *x*; r_{oc} represented the relative amount of mineral resorbed by each osteoclast resorption, and it was supposed to be a constant.

It has been suggested that microdamage trigger resorption in order to remove those damaged regions (Noble, 2003; Vahdati and Rouhi, 2009) and that signals transported to the bone surface through osteocytic network inhibit osteoclast activation (Huiskes et al., 2000). Since overload accumulates microdamages (Hazelwood et al., 2001) which disconnect the lacuno-canalicular network (Burger and Klein-Nulend, 1999), it is reasonable to assume that the probability of bone resorption under overload is greater than the resorption probability under normal daily activities and that the osteoclast activity increases.

In this study, we defined a critical load value and a threshold stimulus which were required to cause excessive microdamage, i.e. overload. In other words, we proposed that the

probability of bone resorption would increase when the external load was greater than the critical load value and stimulus exceeded the threshold; otherwise bone resorption probability would remain constant. Since, based on experimental results, there is a positive quadratic relationship between microdamage and local strain energy density (Nagaraja et al., 2005), we assumed that resorption probability, $p_{ol}(x,t)$, caused by overload was a quadratic function of total remodeling stimulus ($P(x,t)$). Thus, the revised resorption probability, when the external load exceeds the critical load value, can be written as follows:

$$p_{ol}(x,t) = \begin{cases} a[P(x,t) - k_{ol}]^2 + p & for \quad P(x,t) > k_{ol} \\ p & for \quad P(x,t) \leq k_{ol} \end{cases}, \tag{5.2}$$

where a is an empirical constant (Table 5.1); p is the probability of bone resorption under normal daily activities (assigned as 20% in our study similar to Ruimerman an coworkers (Ruimerman et al., 2003)); and k_{ol} is a threshold stimulus (Table 5.1). Li et al. (2007) reported the overload resorption under a stress of 9 MPa using their mathematical model; hence, we set the critical load value equals to 9 MPa in this study.

As assumed above, osteoclast activity increased under overload. It means that more relative amount of mineral is resorbed by each osteoclast under overload than the amount of mineral resorbed by each osteoclast under normal loading condition. Ruimerman et al. (2003) set the relative mineral amount per resorption to 30% of a voxel. In our study, the relative resorption amount, $r_{oc\text{-}ol}$, was set to 75% of a voxel.

5.2.2.2. Microdamages caused by overload reduce the osteocyte influence distance

In the semi-mechanistic bone remodeling theory (Huiskes et al.'s, 2000), the stimulus sent to the trabecular surfaces through canaliculi was assumed to attenuate exponentially with the increasing distance, d_i, between osteocyte i and location x according to:

$$f_i(x) = e^{-d_i(x)/D} \tag{5.3}$$

where parameter D [μm] represents the osteocyte influence distance (or the decay constant), which was proposed by Mullender and Huiskes (1995).

Overload causes an accumulation of microdamages (Hazelwood et al., 2001). Microdamages disconnect the lacuno-canalicular network (Burger and Klein-Nulend, 1999). Due to the disconnection of the osteocytic network, signals cannot be transported as far away as usual. Therefore, we assumed that the osteocyte influence distance decreased due to the accumulation of microdamages caused by overload. Ruimerman et al., (2003) set the osteocyte influence distance to be 2 times the voxel size. In our study, the voxel size was the same as the one used in Ruimerman et al. (2003) and the influence distance under overload, D_{ol}, was assumed to be 1.4 times the voxel size.

5.2.3. A three-dimensional computer model

The extended mathematical expressions of semi-mechanistic bone remodeling theory were implemented in a three-dimensional (3D) finite element model of spongy bone, which was a cubic domain divided in $23 \times 23 \times 23$ eight-nodes cubic voxels (Figure 5.1.A). The length of each voxel's side was 63 μm (Ruimerman et al., 2003). Relative bone density (m) per element fluctuated between 0.01 (void (or marrow) parts of bone) and 1.0 (fully solid mineralized bone) during the simulation. In order to apply external loads to our 3D computer model, 6 plates were added at the external surfaces of the cubic domain. The thickness of the side plates was one element, equal to 63 μm. The side plates were connected at the ribs of the cubic domain (Figure 5.2). These plates did not participate in the bone remodeling process. For minimizing

the effects of stress shielding at the model's ribs and corners, no load was added at all 12 sides of the cubic domain (circular region, Figure 5.2).

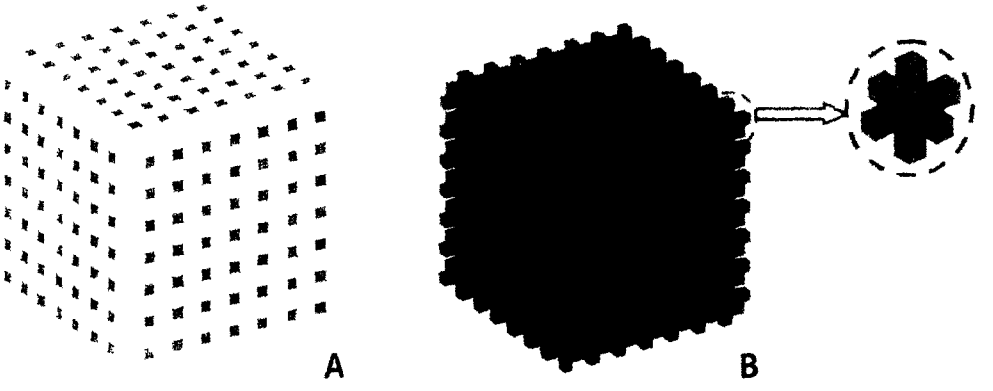

Figure 5.1 The initial three-dimensional computer simulation model. (A) The initial model is a cubic domain in which white voxels represent void (or marrow) parts of bone and grey elements are bone matrix; (B) This is the initial model when the elements, which represent void (or marrow) parts of bone, are transparent.

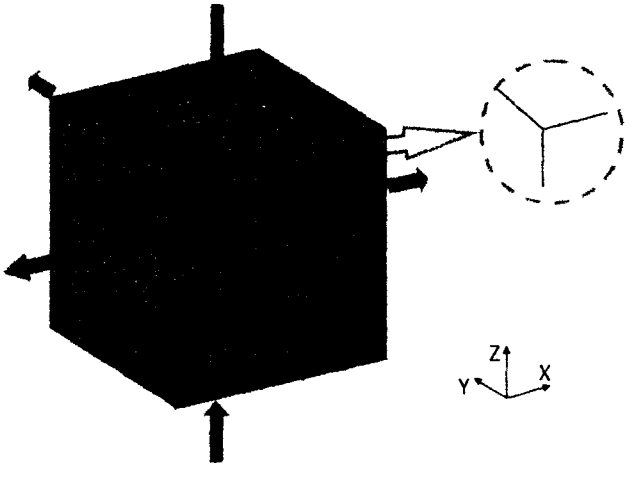

Figure 5.2 The computer model with plates for applying external loads. Red arrows are symbols of the distributed loads' directions. No load was imposed on the sides of the computer model with plates.

It is known that both cortical and spongy bones are anisotropic materials (Uten''kin and Ashkenazi, 1972; van Rietbergen and Huiskes, 2006). Moreover, both cortical and spongy bones show viscoelastic behavior when the external loads are much greater than those which are in the physiological range (Pugh et al., 1973; Carter and Hayes, 1977; van Rietbergen and Huiskes, 2006). With the intention of simplicity, the bone model's elements were assumed to be isotropic and linearly elastic material in this study. The material properties of fully mineralized bone elements (m=1.0) were given a Young's modulus of 5 GPa and a Poisson ratio of 0.3. During computer simulations, the Young's modulus of each element changed per iteration according to the modulus-density relationship which was determined from empirical data for trabecular bone with E_{max} = 5 GPa and γ = 3 (Eq. 3.12) (Mullender and Huiskes, 1995). The material properties of the plates for adding external forces were the same as those of a fully mineralized bone tissue.

Relative bone density per element was determined by the net effects of bone resorption and formation in each bone element according to Eq. 3.11. A new configuration in term of elements' relative bone densities was performed after each iteration. The whole simulation process was repeated until equilibrium state was met, i.e. when no considerable architectural change was observed. In order to have a stable configuration, 250 iterations were performed for each spongy bone remodeling simulation in this study.

In this study, osteocytes were assumed to be distributed uniformly within the domain at a density of 44,000 mm^{-3} (Mullender et al., 1996). Other parameter settings for the spongy bone remodeling are as specified in Table 5.1.

Table 5.1 Parameter settings for the three-dimensional spongy bone remodeling simulations

Variable	Symbol	Value	Unit[a]
Osteocyte density	n	44,000[b]	mm^{-3}
Osteocyte mechanosensitivity	μ	1	$nmolmmJ^{-1}s^{-1}day^{-1}$
Osteocyte influence distance	D	126	μm
Formation threshold	k_{tr}	13×10^{5}	$nmolmm^{-2}day^{-1}$
Proportionality factor	τ	8.5×10^{-9}	$mm^{5}nmol^{-1}$
Resorption probability	p	20	%
Relative mineral amount per resorption	r_{oc}	0.3	voxel
Maximal elastic modulus	E_{max}	5.0[c]	GPa
Poisson ration	v	0.3[c]	-
Exponent gamma	γ	3[d]	-
Loading amplitude	F	2.0	MPa
Loading frequency	f	1	Hz
Overload:			
Critical load	F_{ol}	9[e]	MPa
Proportionality factor in the resorption probability function (Eq. 5.2)	a	1×10^{-11}	$mm^{2}daynmol^{-1}$
Threshold stimulus in the resorption probability function (Eq. 5.2)	k_{ol}	10×10^{6}	$nmolmm^{-2}day^{-1}$
Relative mineral amount per resorption	$r_{oc\text{-}ol}$	0.75	voxel
Osteocyte influence distance	D_{ol}	88.2	μm

[a]Ruimerman et al., 2005.

[b]Mullender et al., 1996.

[c]Mullender and Huiskes, 1995.

[d]Currey, 1988.

[e]Li et al., 2007.

5.2.4. Computer simulations of spongy bone remodeling

Three series of simulations were performed in this study. The purpose of the first series was to test whether trabecular-like 3D structure could be produced using our computer model. In process A (Figure 5.3.A), the simulation started from the initial configuration (Figure 5.1), representing bone in the post-mineralized fetal stage (Ruimerman et al., 2005), until structural equilibrium was reached. The structure was loaded by a sinusoidal distributed stress, cycling between 0 and 2 MPa, which is a value in a realistic range for human spongy bone (Brown

and DiGioia III, 1984), and at frequency of 1 Hz (Ruimerman et al., 2001). The loads were compressive in vertical and tensile in horizontal directions (Figure 5.2). The semi-mechanistic bone remodeling theory assumed that the stimulus sensed by osteocytes was the maximal SED-rate during one loading cycle. It has been shown that the maximum SED-rate can be substituted by the SED value for some static load according to the following equation (Ruimerman et al., 2001):

$$F' \approx 2Ff^{\frac{1}{2}} \tag{5.4}$$

where F' is the static external load; F is the amplitude of the external load; f is the frequency (Hz). Hence, the bone remodeling can be evaluated by static finite element analysis. In this study, the SED value was calculated using a substitute static stress of 4 MPa.

The second series of simulation was performed from the resulting structure of the first series to investigate whether our model was adaptive to the alternative external loading conditions, such as loading magnitude and direction. In process B (Figure 5.3.B), the magnitude of the external loads was increased by 20% compared to that of the loads used in process A, and the direction of the external loads was maintained the same as in process A, to test whether trabecular thickness would increase. In process C (Figure 5.3.C), the external loads were reduced by 20% compared to the loads in process A, and the direction of the external loads was maintained the same as in process A, to test whether trabecular thickness would decrease. In process D (Figure 5.3.D), for testing whether the trabeculae would realign with the alternative loading direction, the orientation of the external loads was rotated by 30 degree in counterclockwise direction around Y axis and the magnitude of the external loads were maintained the same as in process A. In process E (Figure 5.3.E), the loads were

changed to be tensile in vertical and compressive in horizontal directions, to test whether the compressive or tensile loads would affect the resulting morphology.

The purpose of the third series was to test whether there would be bone resorption when external load was increased to the critical load value. We started from the homeostatic structure of the first series and performed simulation of the spongy bone remodeling under the stress of 9 Mpa, corresponding to the critical load value (Figure 5.3.F). The hypothetical effects of overload on spongy bone remodeling were mimicked by decreasing the osteocyte influence distance and increasing the bone resorption probability and each resorption amount (see Table 5.1) when the external stress was 9 MPa.

5.3. Results

In the first simulation, starting from the initial configuration, the simulation resulted in a structure composed of finite elements (Figure 5.3.A). With a program (threeD_surface.m, Output files, Appendix II) which can show the surfaces of the structure, a trabecular-like equilibrium (homeostatic) architecture with trabeculae aligned to the external loading direction (Figure 5.3.A) was obtained.

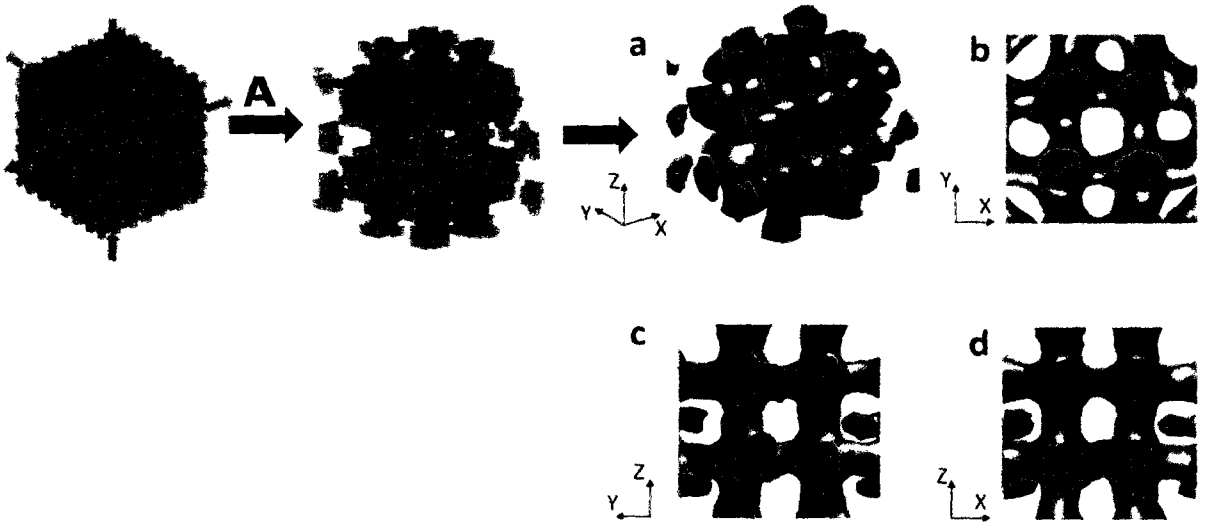

Figure 5.3.A Starting from the initial structure, trabecular-like structure was obtained after bone remodeling simulation. The external loads (sinusoidal stress: magnitude 0~2 MPa, frequency 1 Hz) were compressive in vertical and tensile in horizontal direction.

In the second series of simulations, the equilibrium structure (Figure 5.3.A.a) was used to test whether our model could adapt to new loading conditions. In process B (Figure 5.3.B), an increase in the loading magnitude by 20% increased the relative bone density by 10.45% (from 0.421 to 0.465) (process B, Figure 5.4). Trabeculae thickness increased, but no new trabeculae were formed. In process C (Figure 5.3.C), reduction in the external loading magnitude by 20% led to a decrease in trabecular thickness and a decreased relative bone density by 10.83% (from 0.421 to 0.375) (process C, Figure 5.4).

In addition to adaptation to variations in loading magnitudes, the trabecular direction also adapted to alternative load orientations. In process D (Figure 5.3.D) the external loads were rotated by 30 degree in counterclockwise direction around Y axis. Interestingly, the trabecular structure realigned completely to the new external loads, with trabeculae oriented in the new loading directions (Figure 5.3.D.d), no significant density change was found after changing the external loading direction (process D, Figure 5.4). In process E (Figure 5.3.E),

there was no significant change in the spongy bone's morphology (Figure 5.3.E) and also in its density (process E, Figure 5.4) when the directions of the loads were changed from compressive (tensile) to tensile (compressive).

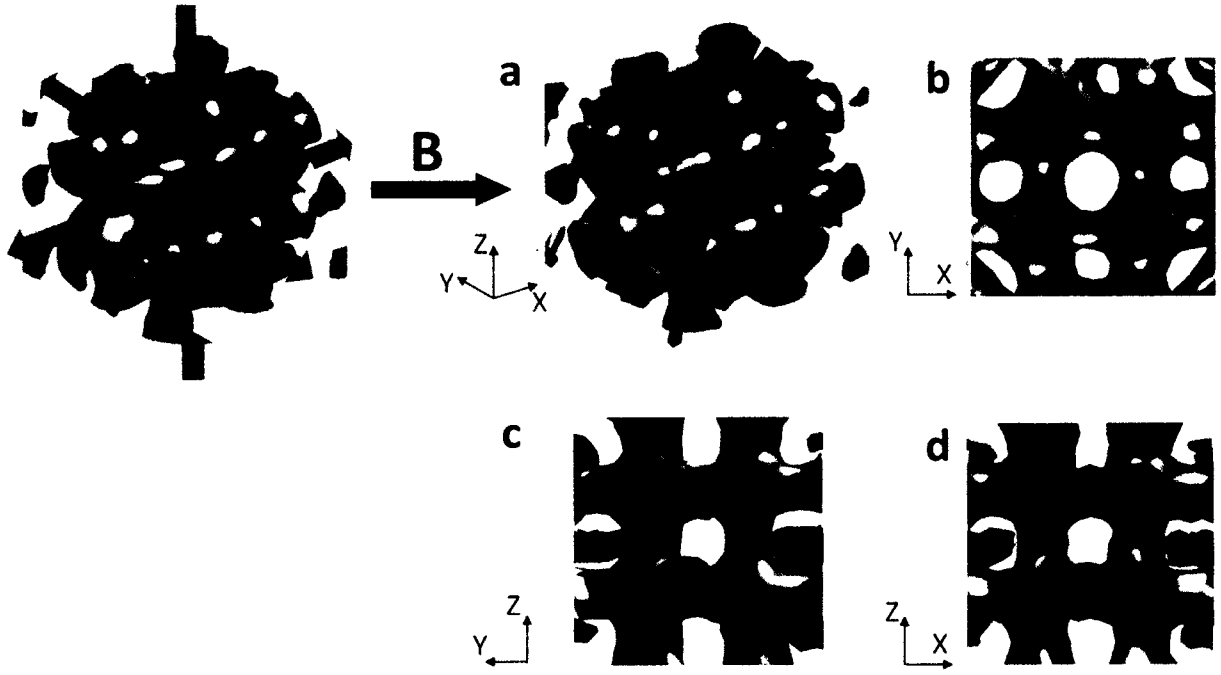

Figure 5.3.B Starting from the resulting structure of the first series (Figure 5.3.A), trabeculae got denser when external loads were increased by 20%.

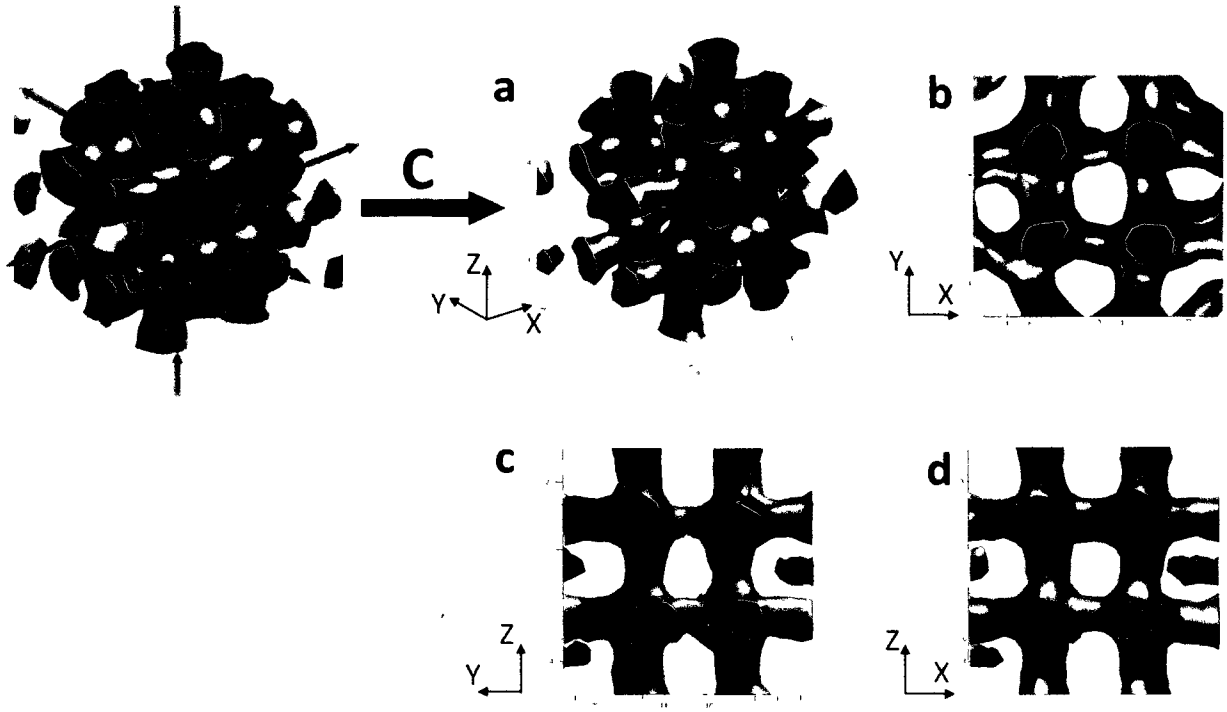

Figure 5.3.C Starting from the resulting structure of the first series (Figure 5.3.A), trabeculae became thinner when external loads were decreased by 20%.

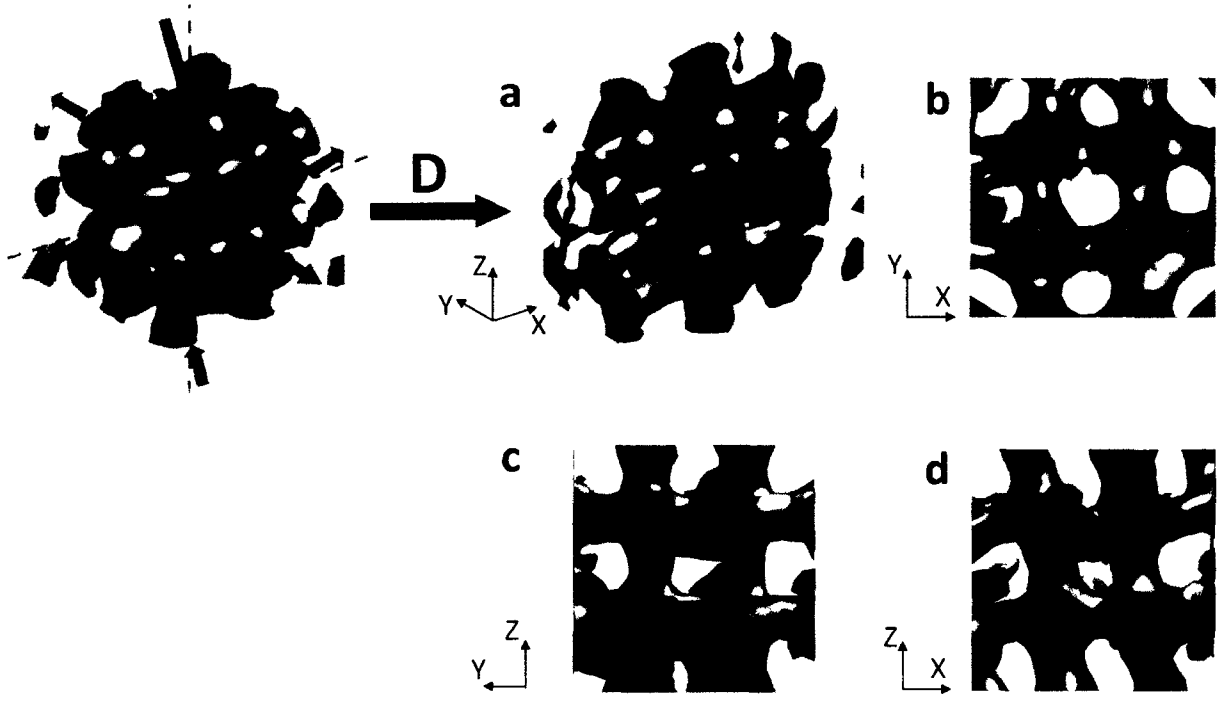

Figure 5.3.D Starting from the resulting structure of the first series (Figure 5.3.A), rotating the loads by 30 degree in counterclockwise direction around Y axis realigned the trabeculae accordingly.

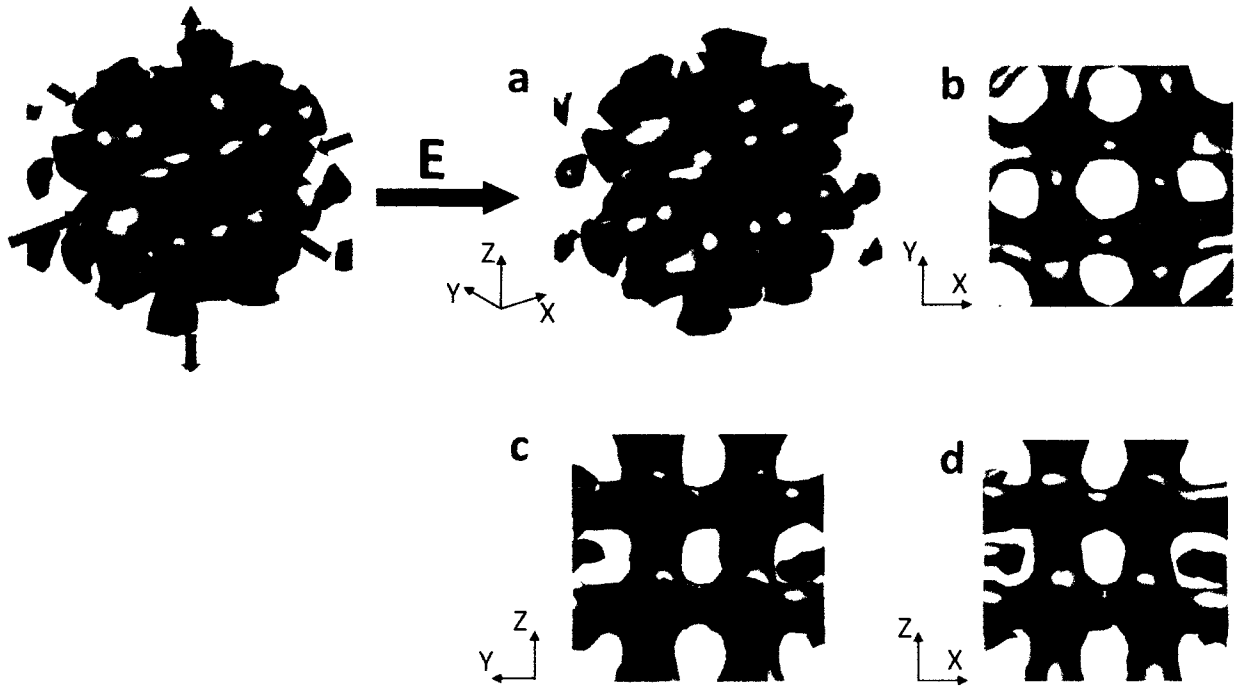

Figure 5.3.E Starting from the resulting structure of the first series (Figure 5.3.A), changing the loading direction from compressive to tensile or from tensile to compressive did not cause a significant change in the spongy bone's morphology.

In the third series of simulation, we simulated spongy bone remodeling under overload by increasing the bone resorption probability and relative amount of each bone resorption, and also by decreasing the osteocyte influence distance, in order to check our hypotheses regarding the effects of overload on spongy bone remodeling. Starting from the resulting structure of the first series of simulation (Figure 5.3.A), when we increased the magnitude of the external loads to the critical load value, i.e. 9 MPa at frequency of 1 Hz, the thickness of the resulting trabeculae reduced (Figure 5.3.F). Bone loss occurred when bone model was under overload, the average relative bone density reduced by 17.8% from 0.421 to 0.346 when the external load was increased from 2 MPa to 9 MPa, both at the frequency of 1Hz (process F, Figure 5.4).

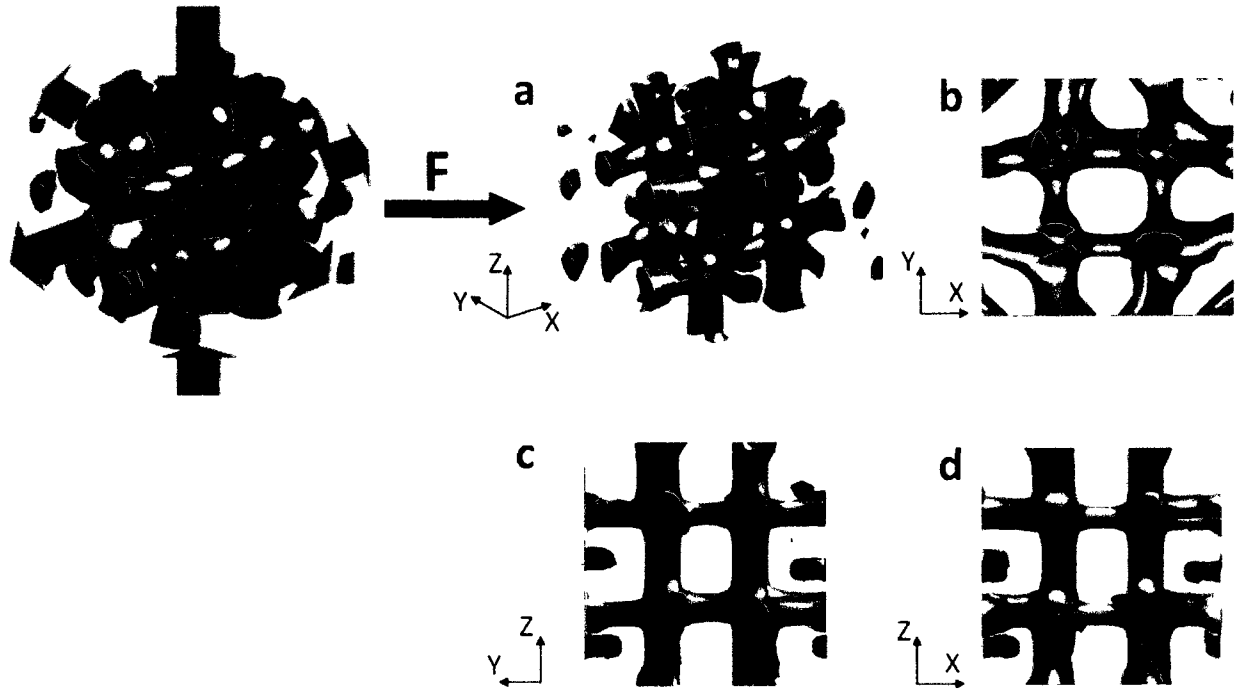

Figure 5.3.F Simulation result of spongy bone remodeling under overload. When the external load was increased from 2 MPa to 9 MPa (the critical load value), the thickness of trabeculae was decreased.

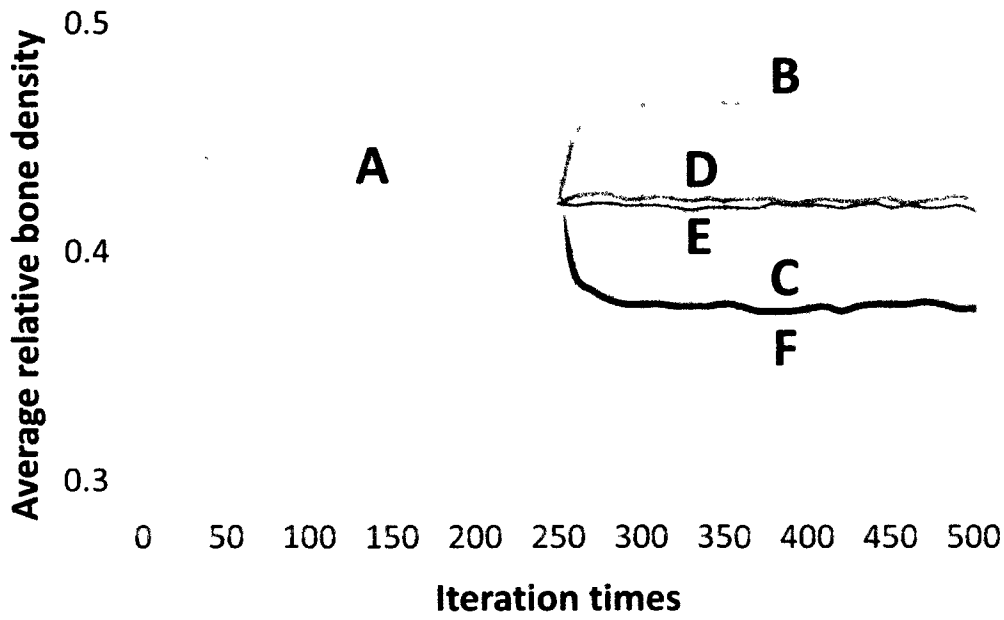

Figure 5.4 Alteration of average relative bone density during bone remodeling simulation processes. Increasing the amplitude of external loads by 20% led to an increased density by 10.45% (process B). Reducing the magnitude of external loads by 20% led to a decreased density by 10.83% (process C). Rotating the external loads did not change the density significantly (process D). Changing the tensile (compressive) loads to compressive (tensile) loads also did not cause a considerable variation in the density and morphology of spongy bone (process E). When spongy bone was under overload (9 MPa), the density of spongy bone decreased substantially (process F).

5.4. Discussion and conclusions

The results of our first and second series of simulations are similar to the simulation results performed and reported by Ruimerman et al. (2005). In the first series of our three-dimensional spongy bone remodeling simulation, when we added external loads (2 MPa, 1 Hz) to the initial model, a more-or-less realistic trabecular bone-like architecture was reproduced

and the trabeculae were aligned with the direction of the external loading (Figure 5.3.A). Process A on Figure 5.4 showed that average relative bone density first increased sharply, followed by a decrease and subsequent stabilization. A similar trend was observed in the development of trabecular bone from porcine vertebrae and tibiae (Tanck et al., 2001). In addition, this trend was also seen in cortical bone from ulnae of birds, in which the ulnae were loaded with 36 cycles/day (Rubin and Lanyon, 1984). It seems that an increase in mechanical forces initially produces excessive bone deposition. Thereafter, trabecular structure is optimized, i.e. the trabeculae better align to the main loading direction while bone mass decreases and stabilizes (Tanck et al., 2001).

The results of our second series of simulations are in agreement with Wolff's law (Wolff, 1892), known as the functional adaptation of the trabecular structure. Although the strain energy density (SED), which was used here as the mechanical stimulus to initiate the bone remodeling process, is a scalar quantity, the results of the second simulation series showed that the spongy bone structure were adaptive to not only external loading magnitude, but also to the external loading direction. Increasing the external loads caused an increase in the thickness of the trabeculae, and also the average relative bone density (Figure 5.3.B and process B, Figure 5.4). On the other hand, decreasing loading magnitude caused the opposite trend, i.e. reduced trabecular thickness and also average relative bone density (Figures 5.3.C and process C, Figure 5.4). After rotating the external loads by 30 degree, trabeculae eventually rotated by the same amount (Figure 5.3.D). However, no significant change in average relative bone density was found as a result of altering the external load's direction (process D, Figure 5.4). Moreover, Figure 5.3.E and process E in Figure 5.4 showed that no significant changes in morphology and average relative bone density of spongy bone could be

seen when we changed the compressive (tensile) loads to the tensile (compressive) loads. It implies that whether the loads are compressive or tensile does not influence the resulting structure because the local SED values in compression and tension are equal.

In the third series of simulation, and investigation was made on the spongy bone remodeling under overload. In Huiskes and co-workers' semi-mechanistic bone remodeling theory (2000), the bone resorption probability, the relative amount of mineral resorbed and the osteocyte influence distance are assumed to be constants. Compared to Huiskes et al.'s (2000), based on the previous theoretical and experimental results (Burger and Klein-Nulend, 1999; Nagaraja et al., 2005), we assumed that the local bone resorption probability is SED dependent, with a higher chance for overloading situation according to Eq. 5.2. Moreover, we assume that the accumulation of microdamages caused by overload (Hazelwood et al., 2001) increases the amount of bone resorbed and decreases the average osteocyte influence distance.

Tanck et al. (2006) kept the loading amplitude and frequency constant (2 MPa, 1 Hz) when they studied trabecular bone remodeling for both disuse and overload. Knowing that in everyday normal physical activities, both the load magnitude and frequency of loading change continuously, assuming a constant value for them does not make a good sense. Li et al. (2007) developed a new mathematical model for studying the dental implant loosening. In their theoretical study, they varied the stress magnitudes and found that bone density decreased quickly when they increased the magnitude of stress to 9 MPa. Based on Li et al.'s (2007) work, we considered the amplitude of the critical load for overload to be 9 MPa and the frequency of the load to be 1 Hz, in our work.

The results of our third series of three-dimensional simulation showed that spongy bone remodeling under overload (9 MPa, 1Hz) led to significant and sharp decreases in the

trabecular thickness (Figure 5.3.F) and also in spongy bone's relative density (process F, Figure 5.4). Our results, which considered the overloading effect, prove that the extended algorithm is sensitive to overload. Whereas, bone loss under overload cannot be shown using Huiskes et al.'s (2000) semi-mechanistic bone remodeling model, this is quite understandable due to the lack of the overload effect in their theory. A similar trend for the decrease in bone density due to overload was also found in some previous theoretical researches (Tanaka et al., 1999; Tanck et al., 2006; Li et al., 2007) which were simulated on two-dimensional models. Recently, some investigations have been performed on the overload resorptions that often occur in dental implant treatments. Li et al. (2007) used their mathematical model to study a practical case of dental implant treatment. Their FE analysis results showed that bone resorption at the neck of the implant occurred due to occlusal overload but then resorption stopped after some time, which may account for progressive implant loosening that is sometimes observed in clinical situations (Li et al., 2007; Nyström et al., 2004; Lin et al., 2009).

Similar to other theoretical studies, our study contains some limitations. In this study, bone was assumed to be isotropic and a linear elastic material. It is well known that trabecular bone is an anisotropic and viscoelastic material (van Rietbergen and Huiskes, 2001). The FEA model of spongy bone analyzed in this study was relatively small, restricted by our computer capacity. Although the trabeculae in the final architecture of our simulation were aligned with the external loads' direction, the final density of spongy bone and also its morphology were insensitive to the polarity of the external load (i.e. compression or tension). In our present study, just sinusoidal external loads with a constant frequency have been considered, which are not real loading pattern. Most parameters used in the formulation have physical meanings,

nevertheless many parameter values are assumed hypothetically due to lack of experimental data. Thus, there is a great need for experimental research on the bone remodeling process in order to find the material constants appeared in the bone remodeling theories.

In conclusion, in agreement with the clinical situations (Li et al., 2007; Nyström et al., 2004; Lin et al., 2009), our simulation for spongy bone remodeling under overload results in bone loss. The integration of our hypotheses with the pre-existing regulatory mechanisms (Huiskes et al., 2000) does not disrupt the processes. For example, the integration of our hypotheses can help form and maintain trabecular-like structure. Our hypotheses provide a direction for experimentation providing a layout for future experimental groundwork. Future simulations can incorporate physiological values and parameters into the model and simulate the bone remodeling around implants under realistic loading patterns.

Chapter 6

Summary, Conclusions and Future Directions

6.1. Summary

Bone is a very active structure and is continuously remodeled through a coupled process of bone resorption and bone formation, in a process so-called bone remodeling process. In 2000, Huiskes and co-workers developed a semi-mechanistic bone remodeling theory. Compared with other bone remodeling theories, the novelty of their theory is that it explains the effects of mechanical forces on trabecular bone remodeling by relating local mechanical stimuli in the bone matrix to assumed cells' activities actually involved in bone matabolism (Ruimerman et al., 2005). In this theory, the rate of strain energy density (SED) is used as the mechanical stimulus for bone remodeling process, and osteocytes are assumed to act as mechanosensors which can sense the rate of SED, and then activate bone making cells, i.e. osteoblasts, to form new bone, filling the cavities caused by osteoclasts' resorption. This thesis was aimed to investigate spongy bone remodeling using Huiskes et al.'s semi-mechanistic bone remodeling theory (Huiskes et al., 2000). Two studies have been done in this research. First, an investigation was made to study the reasons for spongy bone loss in aging and osteoporotic individuals, using a two-dimensional computer model. Secondly, a three-dimensional finite element model was developed to simulate spongy bone remodeling under overload. In our second study, a modification on the pre-existing semi-mechanistic bone remodeling theory was made with respect to the effects of accumulated microcracks caused by overload.

6.1.1. Investigation into the reasons for spongy bone loss in aging and osteoporotic individuals

In chapter 4, a two dimensional finite element model of spongy bone was presented with the aim of investigating the effect of osteocyte density and osteocyte mechanosensitivity on the spongy bone remodeling for aging healthy adults and osteoporotic patients. Bone loss usually starts after maturation and accelerates in osteoporotic bones. Experimental evidence shows that osteocyte density (the number of osteocytes per unit surface of bone) changes with aging and also in osteoporotic bones (Table 4.2) (Mullender et al., 1996). Osteocyte density declines significantly with aging in healthy adults who are over the age of 30 years (Frost, 1960; Mullender et al., 1996; Qiu et al., 2003). On the other hand, osteocyte density increases in osteoporotic patients compared to healthy adults. Moreover, *in vitro* experiments show that the mechanosensitivity of osteocytes derived from osteoporotic patients is significantly reduced compared to that from the age-matched non-osteoporotic group (Sterck et al., 1998). Therefore, in this study, it is hypothesized that decreasing osteocyte density (assuming a normal level of mechanosensitivity for the osteocytes) can cause spongy bone loss in healthy old adults, and in the case of osteoporotic bones, a reduction in osteocyte mechanosensitivity is one of the main contributing factors in bone loss. To investigate our hypotheses, a two dimensional finite element model of spongy bone was developed (Figure 4.1), implementing a semi-mechanistic bone remodeling theory (Huiskes et al., 2000). Three series of simulations were performed. In the first series of simulations, osteocytes were assumed to be distributed uniformly within the bone domain. A trabeculae-like architecture was obtained from our initial computer model (Figure 4.2). The orientation of trabecular structure and also the

thickness of trabeculae changed according to alterations of the external loading direction and magnitude (Figures 4.3-4.5). The first simulation results are all in agreement with Wolff's Law (Wolff, 1892). In the second series of simulations, based on the experimental evidence (Mullender et al., 1996), the osteocyte density was reduced for healthy older adults, and the osteocytes were assumed to be non-uniformly distributed in the bone region (Marotti et al., 1985; Baiotto and Zidi, 2004). Our simulation results showed that by decreasing the osteocyte density, bone loss will occur (Figure 4.7), and so average relative bone density will decrease (Figure 4.8). These results are in favor of the first part of our hypotheses which states that a reduction in osteocyte density will cause the bone loss in healthy adults. In the third series of simulations, based on the experimental evidence (Mullender et al., 1996), we increased the osteocyte density for osteoporotic bones compared to healthy adults, but decrease osteocyte mechanosensitivity (Sterck et al., 1998). Again, the osteocytes were randomly distributed in the bone region (Marotti et al., 1985; Baiotto and Zidi, 2004). The simulation results showed that the reduction of osteocyte mechanosensitivity can cause bone loss (Figure 4.9), and so will decrease the average relative bone density (Figure 4.10). When osteocyte mechanosensitivity is less than a certain level, osteoporotic patients lose more bone than healthy old adults (Figure 4.10), even though the number of osteocytes in osteoporotic patients is greater than that in healthy adults. These results support the last part of our hypotheses stating that reducing osteocyte mechanosensitivity could be one of the crucial factors causing bone loss in an osteoporotic bone. Comparing results of the first simulation series (Figures 4.2-4.5) with the results of the second and third simulations (Figure 4.7 and Figure 4.9), we find that the final architectures with the uniform osteocyte distribution are more regular than those with a non-uniform osteocyte distribution.

6.1.2. A three-dimensional computer model to simulate spongy bone remodeling under overload

In chapter 5, considering the effects of the microcracks on bone remodeling process, we extended Huiskes et al.'s semi-mechanistic bone remodeling theory (Huiskes et al., 2000) for the case of overloaded bone, and also developed a three-dimensional finite element model to simulate spongy bone remodeling under overload. Overload has been suggested to be a contributing factor for bone loss at the bone-implant interface (Huiskes et al., 1987; McNamara et al., 1997). Many mathematical models have been proposed to model bone adaptation, but very few considered bone resorption due to overload (Li et al., 2007). As many other mathematical models, Huiskes et al.'s semi-mechanistic model (Huiskes et al., 2000) cannot predict the overload resorption because in their theory it is assumed that the resorption probability and the amount of bone resorbed by each osteoclast to be constants (Eqs. 3.6 and 3.7). Some researchers have suggested that osteoclastic resorption can be enhanced when osteocytic network within bone matrix is blocked due to microdamage (e.g. Martin, 2003; Tanck et al., 2006). Considering the experimental evidence of the accumulating microcracks caused by overload (Hazelwood et al., 2001), in this study, it is hypothesized that overload can increase osteoclast activities: the probability of bone resorption, and also the amount of bone resorbed by each osteoclast (see Table 5). Moreover, we hypothesized that the osteocyte influence distance will reduce due to the accumulation of microdamage under overloading conditions (see Table 5). Based on experimental results which shows a positive quadratic relationship between microdamage and local strain energy density (Nagaraja et al., 2005), it is

assumed here that resorption probability caused by overload was a quadratic function of total remodeling stimulus (Eq. 5.2). In order to investigate the validity of our hypothesis, a three-dimensional computer model of spongy bone was developed (Figure 5.1) and three series of simulations were performed. The results of our first (see Figure 5.3.A) and second (see Figures 5.3.B-5.3.E) series of simulations were in agreement with Wolff's Law (Wolff, 1892). A trabecular-like structure was obtained, and the orientation of trabecular structure and thickness of trabeculae changed according to alterations of the external load direction and magnitude. The third series was related to the spongy bone remodeling under overload. In the third series, it was observed that spongy bone remodeling under overload will result in significant and sharp decreases in the trabecular thickness (see Figure 5.3.F), and also a considerable reduction in the average relative bone density (see Figure 5.4). This trend is observed in clinical situation as well (Nyström et al., 2004; Lin et al., 2009), also a similar behavior can be seen in some other studies which were based on two-dimensional simulations of the bone remodeling process (Tanaka et al., 1999; Tanck et al., 2006; Li et al., 2007). Our simulation results imply that the integration of our hypotheses with the pre-existing regulatory mechanisms does not cause any disruption in the bone remodeling processes. Moreover, the modified algorithm in this study shows a great sensitivity to overload.

6.2. Conclusions

From chapter 4, it is concluded that, by decreasing osteocyte density, there will be a net bone loss with aging in the healthy adults. Different from many possible explanations for the excessive bone loss in osteoporotic bones (Eriksen and Kassem, 1992; Mullender et al., 1996; Ruimerman et al., 2001), which mostly consider the influence of bone making cells, i.e.

osteoblasts, our study shows that the decrease of osteocyte mehanosensitivity might be one of the crucial causes for abnormal bone loss in osteoporotic patients. Also, based on our study, one can conclude that not only the osteocytes density and mechanosensitivity, but also their spatial distribution can have a noticeable effect on the final geometry, and configuration of spongy bone.

From our simulations for spongy bone remodeling under overload, chapter 5, it is concluded that overload can cause bone loss in spongy bone. Overload might increase the osteoclasts' activities, i.e. osteoclast resorption probability and also the amount of bone resorbed by each osteoclast. Moreover, the osteocyte influence distance might decrease under overloading conditions. The integration of our hypotheses (the effects of microcracks caused by overload) and Huiskes et al.'s semi-mechanistic remodeling theory (Huiskes et al., 2000) will offer reasonable results, which are in agreement with some clinical situations.

6.3. Future directions

Most parameters used in our formulations have physical meanings. However, some parameters' values are assumed hypothetically due to lack of experimental data. One of the most important efforts in the future can be measuring these data using experimental techniques. In this thesis, bone elements were assumed to be isotropic and linearly elastic. It is well known that trabecular bone is an anisotropic and a viscoelastic material (van Rietbergen and Huiskes, 2001). It might worth investigating the effects of anisotropy, as well as viscoelasticity on the spongy bone remodeling in the future. Moreover, the FEA model of spongy bone analyzed in this study was relatively small, restricted by our computer capacity.

Also, for the sake of simplicity, just sinusoidal external loads with a constant frequency have been applied to our models in this study, which are not the real loading pattern. When there is no computer restriction, an increase in the size of the three-dimensional model for simulating the spongy bone remodeling around prosthetic implant under realistic loading patterns can be a great addition to this work.

References

Aarden, E.M., Burger. E.H., and Nijweide, P.J. (1994). Function of osteocytes in bone, J. Cell. Biochem., 55, 287-299.

Ahlborg, H.G., Johnell, O., Nilsson, B.E., Jeppsson, S., Rannevik, G., and Karlsson, M.K. (2001). Bone loss in relation to menopause: a prospective study during 16 years, Bone, 28 (3), 327-331.

Baiotto, S., Zidi, M. (2004). Theoretical and numerical study of a bone remodeling model: The effect of osteocyte cells distribution, Biomechan Model Mechanobiol, 3, 6-16.

Basso, N., Heersche, J.N.M. (2006). Effects of hind limb unloading and reloading on nitric oxide synthase expression and apoptosis of osteocytes and chondrocytes, Bone, 39, 807-814.

Bendavid, E.J., Shan, J., and Barrett-Connor, E. (1996). Factors associated with bone mineral density in middle-aged men, J. Bone Miner. Res., 11 (8), 1185-1190.

Bilezikian, J.P., Raiz, L.G., and Rodan, R.A. (1996). Principles of bone biology, New York: Academic Press, chap. Biomechanics of Bone, 25-37.

Bonewald, L.F. (2006a). Mechanosensation and transduction in osteocytes, Bonekey Osteovision, 3(10): 7-15.

Bonewald, L.F. (2006b). Osteocytes as multifunctional cells, J. Musculoskelet Neuronal Interact, 6 (4), 331-333.

Bono, M., Einhorn, A. (2003). Overview of osteoporosis: pathophysiology and determinants of bone strength, Eur Spine J., 12 (Suppl. 2), S90–S96.

Brown, T.D., DiGioia III, A.M. (1984). A contact-coupled finite element analysis of the natural adult hip, Journal of Biomechanics, 17, 437-448.

Buckwalter, J.A., Glimcher, M.J., Cooper, R.R., and Recker, R. (1995). Bone biology. Part I and Part II. Structure, blood supply, cells, matrix, and mineralization. J Bone Joint Surg., 77A, No. 8, 1255-1290.

Burger, E.H., Klein-Nulend, J., Van Der Plas, A., and Nijweide, P.J. (1995). Function of osteocytes in bone-their role in mechanotransduction. J. Nutr., 125 (Suppl. 7), 2020S-2023S.

Burger, E.H. and Klein-Nulend, J. (1999). Mechanotransduction in bone-role of the lacuno-canalicular network, FASEB J., 13, S101-S112.

Burger, E.H. (2001). Experiments on cells mechanosensitivity: bone cells as mechanical engineers, In: Cowin S.C., ed. Bone mechanics Handbook (2nd edn.), CRC Press, chap. 28.

Calbet, J.A.L., Moysi, J.S., Dorado, C., and Rodriguez, L.P. (1998). Bone mineral content and density in professional tennis players, Calcif. Tissue Int., 62 (6), 491–496.

Calbet, J.A.L., Herrera P.D., and Rodriguez, L.P. (1999). High bone mineral density in male elite professional volleyball players, Osteoporosis Int., 10 (6), 468–474.

Carter, D.R. and Hayes, W.C. (1977). The compressive behavior of bone as a two-phase structure, J. Bone Joint Surg. (Am.), 59, 954-962.

Carter, D.R. (1984). Mechanical loading histories and cortical bone remodeling, Calcified Tissue Int., 36. S19-S24.

Chan, K.M., Anderson, M., and Lau, E.M.C. (2003). Exercise interventions: defusing the world's osteoporosis time bomb, B. World Health Organ., 81 (11), 827–830.

Cheng, B., Zhao, S., Luo, J., Sprague, E., Bonewald, L.F. and Jiang, J.X. (2001). Expression of functional gap junctions and regulation by fluid flow in osteocyte-like MLO-Y4 cells, J. Bone Miner Res., 16, 249-259.

Ciarelli, M.J., Goldstein, S.A., Kuhn, J.L., Cody, D.D., Brown, M.B. (1991). Evaluation of orthogonal mechanical properties and density of human trabecular bone from the major metaphyseal regions with materials testing and computed tomography. Journal of Orthopaedic Research, 9, 674–682.

Compston, J.E., Rosen, C.J. (2002). Fast facts-osteoporosis, UK: Health Press, 3rd edn..

Cowin, C.S. and Hegedus, D.H. (1976). Bone remodeling I: a theory of adaptive elasticity, J. Elasticity, 6 (3), 313-326.

Cowin, S.C. and Firoozbakhsh, K. (1981). Bone remodeling of diaphysial surfaces under constant load: theoretical predictions, J. Biomechanics, 7, 471-484.

Cowin, S.C., Moss-Salentijn, L., and Moss, M.L. (1991). Candidates for the mechanosensory system in bone, Journal of Biomechanical Engineering, 113, 191-197.

Cowin, S.C. (1998). On mechanosensation in bone under microgravity, Bone, 22 (Suppl. 5), S119-S125.

Cowin, S.C. (2003). Adaptive elasticity: a review and critique of a bone tissue adaptation model, Eng. Transactions, polish academy of science, 51(2-3), 113-193.

Culmann, K. (1866). Die graphische Statik. Zurich: Auflage, Meyer und Zeller.

Currey, J.D. (1984). The mechanical adaptations of bones, Princeton University Press, New Jersey.

Currey, J.D. (1988). The effect of porosity and mineral content on the Young's modulus of elasticity of compact bone, J. Biomech., 21 (2), 131-139.

Dallas, S.L., Zaman, G., Read, M.J., and Lanyon, L.E. (1993). Early strain-related changes in cultured embryonic chick tibiotarsi parallel those associated with adaptive modeling in vivo, J. Bone Miner Res., 8, 251-259;

Dawson-Hughes, B., Harris, S.S., Krall, E.A., and Dallal, G.E. (1997). Effect of calcium and

vitamin D supplementation on bone, density in men and women 65 years of age or older, New England J. Med., 337 (10), 670-676.

Dickenson, R.P., Hutton, W.C., Stott, R. (1981). The mechanical properties of bone in osteoporosis, J Bone and Joint Surgery, 63-B (2), 233-238.

Doblaré, M., García, J.M. (2002). Anisotropic bone remodelling model based on a continuum damage-repair theory, Journal of Biomechanics, 35, 1-17.

Edward Guo, X. (2001). Mechanical properties of cortical bone and cancellous bone tissue, in Bone mechanics Handbook (Ed. Cowin SC), CRC Press, chap.10.

Einhorn T.A. (1996). The bone organ system: Form and function. In: Osteoporosis, Eds. R Marcus, D Feldman and J kelsey, Academic Press, New York, 3-22.

Elisabeth, M.A., Elisabeth, H.B., and Peter, J.N. (1994). Function of osteocytes in Bone, Journal of Cellular Biochemistry, 55, 287-299.

El-Haj, A.J., Minter, S.L., Rawlinson, S.C.F., Suswillo, R., and Lanyon, L.E. (1990). Cellular responses to mechanical loading in vitro, J. Bone Miner Res., 5, 923-932.

Eriksen, E.F. and Kassem, M. (1992). The cellular basis of bone remodeling, Triangle, Sandoz Journal of Medical Science, 31 (2/3), 45-57.

Fazzalari, N.L., Kuliwaba, J.S. and Forwood, M.R. (2002). Cancellous bone microdamage in the proximal femur: influence of age and osteoarthritis on damage morphology and regional distribution, Bone, 31, 697-702.

Faulkner, R.A., Forwood, M.R., Beck, T.J., Mafukidze, J.C., Russell, K., and Wallace, W. (2003). Strength indices of the proximal femur and shaft in prepubertal female gymnasts, Med. Sci. Sport. Exer., 35 (3), 513–518.

Firoozbakhsh, K. and Cowin, S.C. (1980). Devolution of inhomogeneities in bone structure predictions of adaptive elasticity theory, J. Biomecha. eng., 102 (4), 287-293.

Fischer, T.G. (2007). Bone structure, http://faculty.irsc.edu/FACULTY/TFischer/AP1/.

Foldes, I., Rapcsak, M., Szilagyi, T., and Oganov, V.S. (1990). Effects of space flight on bone formation and resorption, Acta. Physiol. Hung., 75 (4), 271–285.

Forwood, M.R., Kelly, W.L., Worth, N.F. (1998). Localization of prostaglandin endoperoxidase H synthase (PGHS)-1 and PGHS-2 in bone following mechanical loading in vivo, Anat. Rec., 252, 580-586.

Fritton, S.P., McLeod, K.J., and Rubin, C.T. (2000). Quantifying the strain history of bone: spatial uniformity and self-similarity of low magnitude strains, J. Biomech., 33, 317-325.

Frost, H.M. (1960). In vivo osteocyte death, Am. J. Orthop., 42, 138-143.

Frost, H.M. (1964a). Dynamics of bone remodeling, In: Frost H.M., ed. Bone biodynamics, Boston: Little, Brown and Company, 315-333.

Frost, H.M. (1964b). Mathematical Elements of Lamellar Bone Remodeling, Charles C. Thomas Publisher.

Frost, H.M. (1987). Bone "mass" and the "mechanostat": a proposal, Ant. Rec., 219, 1-9.

Frost, H.M. (1988). Vital biomechanics: proposed general concepts for skeletal adaptations to mechanical usage, Calcif Tissue Int., 42 (3), 145-156.

Frost, H.M. (1990). Skeletal structural adaptations to mechanical usage (SATMU): 2. Redefining Wolff's Law: the bone remodeling problem. Anat. Rec., 226, 414-422.

Frost, H.M. (1994). Wolff's Law and bone's structural adaptation to mechanical usage: an overview for clinicians, Angle Orthod., 64 (3), 175-188.

Fyhrie, D.P., and Schaffler, M.B. (1994). Failure mechanisms in human vertebral cancellous bone, Bone, 15, 105-109.

Gorski, J.P. (1998). Is all bone the same? Distinctive distributions and properties of non-collagenous matrix proteins in lamellar vs. woven bone imply the existence of different underlying osteogenic mechanisms. Crit Rev Oral Biol Med, 9(2): 201-223.

Goulet, R.W., Goldstein, S.A., Giarelli, M.J., Kuhn, J.L., Brown, M.B., and Feldkamp, L.A. (1994). The relationship between the structural and orthogonal compressive properties of trabecular bone, J. Biomech., 27, 375.

Greendale, G.A., Barrett-Connor, E., Edelstein, S., Ingles, S., and Haile, R. (1995). Life-time leisure exercise and osteoporosis- the rancho-bernardo study. Am. J. Epidemiol., 141 (10), 951–959.

Grosland, N.M., Goel, V.K., Lakes, R.S. (2001). Techniques and applications of adaptive bone remodeling concepts, In: Leondes, C., ed. Musculoskeletal models and techniques: Biomechanical systems techniques and applications (Vol. III), CRC Press LLC, Chapter 2.

Gunnes, M. (1995). Determinants of peak bone mass and bone mineralization rates in 470 healthy children, adolescents and young adults: A prospective study, Norsk Epidemiology, 5 (2), 178,.

Haase, K. (2010). Finite element analysis of orthopaedic plates and screws to reduce the effects of stress shielding, M.A.Sc. Thesis, University of Ottawa.

Hadjidakis, D.J., Androulakis, I.I. (2006). Bone remodeling, Ann. N. Y. Acad. Sci., 1092, 385-396.

Hayes, W.C. and Bouxsein, M.L. (1997). Biomechanics of cortical and trabecular bone: Implications for assesment of fracture risk. In Mow, V. C. and Hayes, W. C., editors, Basic Orthopaedic Biomechanics, pages 69–111. Lippincott-Raven, Philadelphia, 2 edition.

Hazelwood, S.J., Martin, R.B., Rashid, M.M., and Rodrigo, J.J. (2001). A mechanistic model for internal bone remodeling exhibits different dynamic responses in disuse and overload, Journal of Biomechanics, 34, 299-308.

Hegedus, D.H. and Cowin, C.S. (1976). Bone remodeling II: small strain adaptive elasticity, J. Elasticity, 6 (4), 337-352.

Heino, T.J., Kurata, K., Higaki, H., and Vaananen H.K. (2009). Evidence for the role of osteocytes in the initiation of targeted remodeling, Technology and Health Care, 17, 49-56.

Hernandez, C.J. (2001). Simulation of bone remodeling during the development and treatment of osteoporosis, Ph.D. Thesis, Stanford University.

Hernandez, C.J., Beaupré, G.S., Keller, T.S., Carter, D.R. (2001). The influence of bone volume fraction and ash fraction on bone strength and modulus, Bone, 29 (1), 74-78.

Hert, J., Liskova, M., and Landgrot, B. (1969). Influence of the long-term continuous bending on the bone. An experimental study on the bibia of the rabbit, Fol. Morphol., 17, 389-399.

Hodgskinson, R. and Currey, J.D. (1992). Young's modulus, density and material properties in cancellous bone over a large density range, J. Mater. Sci. Mater. Med., 3, 377.

Holbrook, T.L., Barrett-Connor, E. (1993). A prospective study of alcohol consumption and bone mineral density, BMJ., 306 (6891), 1506–1509.

Hollenbach, K.A., Barrett-Connor, E., Edelstein, S.L., and Holbrook, T.L. (1993). Cigarette-smoking and bone-mineral density in older men and women. Am. J. Public Health, 83 (9), 1265–1270.

Hollister, S.J., Brennan, S.J., Kikuchi, N. (1994). A homogenization sampling procedure for calculating trabecular bone effective stiffness and tissue level stress, Journal of Biomechanics, 27, 433-444.

Huiskes, R., Nunamaker, D. (1984). Local stresses and bone adaption around orthopaedic implants, Calcif. Tissue Int., 36, S110-S117.

Huiskes, R., Weinans, H., Grootenboer, J., Dalstra, M., Fudala, M., Slooff, T.J. (1987). Adaptive bone remodeling theory applied to prosthetic-design analysis. J. Biomech., 20, 1135–1150.

Huiskes, R., Ruimerman, R., van Lenthe, G.H., Janssen, J.D. (2000). Effects of mechanical forces on maintenance and adaptation of form in trabecular bone, Nature, 405 (6787), 704–706.

Huiskes, R. and van Rietbergen, B. (2005). Biomechanics of bone, In: van Mow C., and Huiskes R., ed. Basic orthopaedic biomechanics and mechano-biology (3rd edn.), Lippincott Williams & Wilkins, Chapter 4.

Hutton, D.V. (2005). Fundamentals of Finite Element Analysis, Tata McGraw-Hill Edition.

Jacobs, C.R. (1994). Numerical simulation of bone adaption to mechanical loading, Ph.D. Thesis, Stanford University.

Jacobs, C.R. (2000). The mechanobiology of cancellous bone structural adaptation, Journal of Rehabilitation Research & Development, 37 (1).

Jee, W.S.S. (2001). Integrated bone tissue physiology: Anatomy and physiology. In Cowin, S. C., editor, Bone Mechanics Handbook. CRC Press.

Kabel, J., van Rietbergen, B., Dalstra, M., Odgaard, A. and Huiskes, R. (1999). The role of an effective isotropic tissue modulus in the elastic properties of cancellous bone, Journal of biomechanics, 32, 673-680.

Keller, T.S. (1994). Predicting the compressive mechanical behavior of bone, J. Biomech., 27, 1159.

Kenzora, J.E., Steele, R.E., Yosipovitch, Z.H., and Glimcher, M.J. (1978). Experimental osteonecrosis of the femoral head in adult rabbits, Clin. Orthop., 130, 8.

Klein-Nulend, J., van der Plas, A., Semeins, C.M., Ajubi, N.E., Frangos, J.A., Nijweide, P.J., Burger, E.H. (1995). Sensitiviy of osteocytes to biomechanical stress in vitro, FASEB J., 9, 441-445.

Klein-Nulend, J. and Bakker, A.D. (2007). Osteocytes: mechanosensors of bone and orchestrators of mechanical adaptation, Clinic Rev. Bone Miner Metab., 5, 195-209.

Knothe-Tate, M.L., Steck, R., Forwood, M.R., Niederer, P. (2000). In vivo demonstration of load-induced fluid flow in the rat tibia and its potential implications for processes associated with functional adaptation, J. Exp, Biol., 203, 2737-2745.

Kuhn, J.L., Goldstein, S.A., Feldkamp, L.A., Goulet, R.W., and Jesion, G. (1990). Evaluation of a microcomputed tomography system to study trabecular bone structure. Journal of Orthopaedic Research, 8(6), 833–842.

Ladd, A.J., Kinney, J.H., Haupt, D.L., and Goldstein, S.A. (1998). Finite-element modeling of trabecular bone: comparison with mechanical testing and determination of tissue modulus, J. Orthop. Res., 16, 622.

Lakes, R. (2001). Viscoelastic properties of cortical bone, In: Cowin, S.C., ed. Bone mechanics handbook , CRC Press LLC, chapter 11.

Landrigan, M., Penninger, C., Post, M.J. (2006). Experimental and computational investigations in bone structure and adaptation, http://www.nd.edu/~malber/multi_scale_06/bone.pdf.

Lang, T., LeBlanc, A., Evans, H., Lu, Y., Genant, H., and Yu, A. (2004). Cortical and trabecular bone mineral loss from the spine and hip in long-duration spaceflight, J. Bone Miner. Res., 19 (6), 1006–1012.

Lanyon, L.E. (1993). Osteocytes, strain detection, bone modeling and remodeling, Calcif. Tissue Int., 53 (suppl. 1), S103-S106.

Laoise, M.M., Patrick, J.P. (2007). Bone remodeling algorithms incorporating both strain and microdamage stimuli, Journal of Biomechanics, 40, 1381-1391.

Lee, D.A., Einhorn, T. (2001). In: Marcus, Feldman, and Kelsey, eds, Osteoporosis, 3-20.

Lean, J.M., Jagger, C.J., Chambers, T.J., and Chow, J.W. (1995). Increased insulin-like growth factor I mRNA expression in rat osteocytes in response to mechanical stimulation. Am. J. Physiol., 268, E318-327.

Li, J., Li, H., Shi, Li, Fok, Alex S.L., Ucer, C., Devlin, H., Horner, K., and Silikas, N. (2007). A mathematical model for simulating the bone remodeling process under mechanical stimulus, Dental Materials, 23, 1073-1078.

Lin, D., Li, Q., Li, W., Rungsiyakull, P. and Swain, M. (2009). Bone resorption induced by dental implants with ceramics crowns, Journal of the Australian Ceramic Society, 45 (2), 1-7.

Linde, F., Nørgaard, P., Hvid, I., Odgaard, A., and Søballe, K. (1991). Mechanical properties of trabecular bone: dependency on strain rate, J. Biomech., 24, 803.

Liu, G.R. and Quek, S.S. (2003). The Finite Element Method: A Practical Course, Butterworth-Heinemann.

Marotti, G., Remaggi, F., and Zaffe, D. (1985). Quantitative investigation on osteocyte canaliculi in human compact and spongy bone. Bone, 6, 335–337.

Marotti, G., Cané, V., Palazzini, S., and Palumbo, C. (1990). Structure-function relationships in the osteocyte, Ital. J. Miner Electrolyte Metab., 1990, 4, 93-106.

Marotti, G., Ferretti, M., Muglia, M.A., Palumbo, C., Palazzini, S. (1992). A quantitative evaluation of osteoblast-osteocyte relationships on growing endosteal surface of rabbit tibiae, Bone, 13, 363-368.

Martin, R.B., and Burr, D.B. (1982). A hypothetical mechanism for the stimulation of osteonal remodeling by fatigue damage, J. Biomech., 15, 1137-1139.

Martin, R.B., Burr, D.B., and Sharkey, N.A. (1998). Skeletal tissue mechanics, Springer, New York.

Martin, R.B. (2000). Toward a unifying theory of bone remodeling, Bone, 26, 1-6.

Martin, R.B. (2003). Fatigue microdamage as an essential element of bone mechanics and biology, Calcified Tissue Int., 73 (2), 101-107.

McNamara, B.P., Taylor, D., and Prendergast, P.J. (1997). Computer prediction of adaptive bone remodeling around noncemented femoral prostheses: the relationship between damage-based and strain-based algorithms, Med. Eng. Phys., 19, 454-463.

Mosekilde, L., Bentzen, S.M., Ortoft, G., and Jorgensen, J. (1989). The predictive value of quantitative computed tomography for vertebral body compressive strength and ash density. Bone, 10(6): 465–470.

Mosekilde, L. (1990). Consequences of the remodelling process for vertebral trabecular bone structure: a scanning electron microscopy study (uncoupling of unloaded structures), Bone Miner, 10, 13-35.

Mullender, M.G., Huiskes, R., and Weinans, H. (1994). A physiological approach to the simulation of bone remodeling as a self-organization control process [technical note], J. Biomech., 27, 1389-1394.

Mullender, M.G. and Huiskes, R. (1995). A proposal for the regulatory mechanism of Wolff's law, J. Orthop. Res., 13, 503-512.

Mullender, M.G., van Der MEER, D.D., Huiskes, R. and Lips, P. (1996). Osteocyte density changes in aging and osteoporosis, Bone, 18 (2), 109-113.

Mulvihill, B.M. and Prendergast, P.J. (2008). An algorithm for bone mechanoresponsiveness: implementation to study the effect of patient-specific cell mechanosensitivity on trabecular bone loss, Computer Methods in Biomechanics and Biomedical Engineering, 11 (5), 443-451.

Nagaraja, S., Couse, T.L., Guldberg, R.E. (2005). Trabecular bone microdamage and microstructural stresses under uniaxial compression, Journal of Biomechanics, 38, 707-716.

Nijweide, P.J., Burger, E.H., Klein-Nulend, J., and Van der Plas, A. (1996). The osteocyte, in Principles of Bone Biology, Bilezikian, J.P., Raisz, L.G., and Rodan, G.A., Eds., Academic Press, San Diego, chap. 9.

Noble, B. (2003). Bone microdamage and cell apoptosis, European Cells and Materials, 6, 46-56.

Nyman, J.S., Roy, A., Shen, X., Acuna, R.L., Tyler, J.H. and Wang, X. (2006), The influence of water removal on the strength and toughness of cortical bone. J Biomech, 39(5): 931-938.

Nyström, E., Ahlqvist, J., Kahnberg, K.E. (2004). 10-year follow-up of onlay bone grafts and implants in severely resorbed maxillae, Int. J. Oral Maxillofac Surg., 33, 258-262.

Oleson, C.V., Busconi, B.D., and Baran, D.T. (2002). Bone density in competitive figure skaters, Arch. Phys. Med. Rehab., 83 (1), 122–128.

Osteoporosis Canada (2008). Breaking barriers, not bones: 2008 national report on osteoporosis, http://www.osteoporosis.ca/.

Parfitt, A.M. (1977). The cellular basis of bone turnover and bone loss: a rebuttal of the osteocytic resorption-bone flow theory. Clin Orthop Relat Res., 127: 236–47.

Parfitt, A.M., Mathews, C.H.E., Villanueva, A.R., and Kleerekoper, M. (1983). Relationships between surface, volume, and thickness of iliac trabecular bone in aging and osteoporosis, J. Clin. Invest, 72, 1396-1409.

Parfitt, A.M. (1993). Bone age, mineral density, and fatigue damage, Calcified Tissue International, 53 (Supplement 1), S82-S86.

Parfitt, A.M. (1994). Osteonal and hemi-osteonal remodeling: the spatial and temporal framework for signal traffic in adult human bone, J. Cell Biochem., 55, 273-286.

Pazzaglia, U.E., Andrini, L. and Di Nucci, A. (1997). The effects of mechanical forces on bones and joints, J. Bone Jt Surg., 79-B, 1025-1030.

Prendergast, P.J., and Maher, S.A. (2001). Issues in pre-clinical testing of implants, J. Mater. Process. Tech., 118 (1-3), 337–342.

Pugh, J.W., Rose, R.M., and Radin, E.L. (1973). Elastic and viscoelastic properties of trabecular bone: dependency or structure, J. Biomecha., 6, 475.

Qiu, S., Rao, D.S., Palnitkar, S. and Parfitt, A.M. (2002). Age and distance from the surface but not menoause reduce osteocyte density in human cancellous bone, Bone, 31 (2), 313-318.

Quirynen, M., Naert, I., van Steenberghe, D. (1992). Fixture design and overload influence marginal bone loss and fixture success in the Branemark system, Clin. Oral Implants Res., 3, 104-111.

Rauch, F., Glorieux, F.H. (2004). Osteogenesis imperfecta, Lancet, 363 (9418), 1377-1385.

Reilly, G.C., and Currey, J.D. (1999). The development of microcracking and failure in bone depends on the loading mode to which it is adapted, J. Exp. Biol., 2002, 543-552.

Roche Facet, Distributed balance in bone remodeling, http://www.roche.com/pages/facets/11/ostedefe.htm.

Rodan, G.A. (1991). Mechanical loading, estrogen deficiency, and the coupling of bone formation to bone resorption, Journal of Bone and Mineral Research, 6 (6), 527-530.

Roesler, H. (1987). The history of some fundamental concepts in bone biomechanics, J. Biomech., 20, 1025-34.

Rouhi, G., Herzog, W., Sudak, L., Firoozbakhsh, K. and Epstein, M. (2004). Free surface density instead of volume fraction in the bone remodeling equation: theoretical considerations, Forma, 19 (3), 165-182.

Rouhi, G. (2006). Theoretical aspects of bone remodeling and resorption processes, PhD Thesis, University of Calgary.

Rouhi, G., Epstein, M., Herzog,W., Sudak, L. (2006). Free surface density and microdamage in the bone remodeling equation: theoretical considerations. Int. J. Eng. Sci., 44 (7), 456–469.

Rouhi, G., Epstein, M., Sudak, L., Herzog, W. (2007). Modeling bone resorption using mixture theory with chemical reactions. J. Mech. Mater. Struct., 2 (6),1141–1156.

Rubin, C.T., Lanyon, L.E. (1984). Regulation of bone formation by applied dynamic loads, Journal of Bone and Joint Surgery, Am 66, 397-402.

Ruimerman, R., Huiskes, R., van Lenthe, G.H. and Janssen, J.D. (2001). A computer-simulation model relating bone-cell metabolism to mechanical adaptation of trabecular architecture, Computer Methods in Biomechanics and Biomedical Engineering, 4, 433-448.

Ruimerman, R., van Rietbergen, B., Hilbers, P., and Huiskes, R. (2003). A 3-dimensional computer model to simulate trabecular bone metabolism, Biorheology, 40, 315-320.

Ruimerman, R. (2005). Modeling and remodeling in bone tissue, Technische Universiteit Eindhoven, ISBN 90-386-2856-0.

Ruimerman, R., Hibers, P., van Rietbergen, B. and Huiskes, R. (2005). A theoretical framework for strain-related trabecular bone maintenance and adaptation, Journal of Biomechanics, 38 (4), 931-941.

Ruimerman, R., Huiskes, R. (2005). Development of a unifying theory for mechanical adaptation and maintenance of trabecular bone, Theoretical Issues in Ergonomics, 6 (3/4), 225-238.

Schaffler, M.B., Radin, E.L., and Burr, D.B. (1989). Mechanical and morphological effects of strain rate on fatigue of compact bone, Bone, 10, 207-214.

Schaffler, M.B. (2003). Role of bone turnover in microdamage, Osteoporosis International, 14 (Suppl. 5), 73-80.

Skerry, T.M., Bitensky, L., Chayen, J., and Lanyon L.E. (1989). Early strain-related changes in enzyme activity in osteocytes following bone loading in vivo, J. Bone Miner Res., 4, 783-788.

Silva, J.A.P., Dias, F.C., Fonseca, J.E., Canhao, H., Resende, C., and Queiroz, M.V. (2004). Low bone mineral density in professional scuba divers, Clin. Rheumatol., 23 (1), 19–20.

Slomka, N., Diamant, I., and Gefen, A. (2008). Tissue-level failure accumulate on in vertebral cancellous bone: A theoretical model, Technology and Health Care, 16 (1), 47–60.

Smith, I.M. and Griffiths, D.V. (2004). Programming the Finite Element Method, John Wiley & Sons, Ltd..

Smith, J.W. and Walmsley, R. (1959). Factors affecting the elasticity of bone. J Anat, 93: 503-523.

Sohit, J. and Parma, R. (2007). Evolution, http://www.tqnyc.org/2007/NYC074568/.

Sterck, J.G.H., Klein-Nulend, J., Lips, P., and Burger, E.H. (1998). Response of normal and osteoporotic human bone cells to mechanical stress *in vitro*, Am J Physiol Endocrinol Metab, 274 (6), 1113-1120.

Stolk, J., Maher, S.A., Verdonschot, N., Prendergast, P.J., and Huiskes, R. (2003). Can finite element models detect clinically inferior cemented hip implants? Clin. Orthop. Relat. R., 409, 138–150.

Tan, S.D., de Vries, T.J., Kuijpers-Jagtman, A.M., Semeins, C.M., Everts, V., Klein-Nulend, J. (2007). Osteocytes subjected to fluid flow inhibit osteoclast formation and bone resorption, Bone, 41, 745-751.

Tanaka, E., Yamamoto, S., Nishida, T., Aoki, Y. (1999). A mathematical model of bone remodeling under overload and its application to evaluation of bone resorption around dental implants, Acta of Bioengineering and Biomechanics, 1 (1), 117-121.

Tanck, E., Homminga, J., Van Lenthe, G.H., Huiskes, R. (2001). Increase in bone volume fraction precedes architectural adaptation in growing bone, Bone, 28, 650-654.

Tanck, E., Ruimerman, R., and Huiskes, R. (2006). Trabecular architecuture can remain intact for both disuse and overload enhanced resorption characteristics, J. Biomech., 39, 2631-2637.

Taylor, D. (1997). Bone maintenance and remodeling: a control system based on fatigue damage, J. Orthop. Res., 15, 601-606.

Terai, K., Takano-Yamamoto, T., Ohba, Y., Hiura, K., Sugimoto, M., Sato, M., Kawahata, H., Inaguma, N., Kitamura, Y., Nomura, S. (1999). Role of osteopontin in bone remodeling caused by mechanical stress, J. Bone Miner Res., 14, 839-849.

Thompson, M. (2007). What is osteoporosis? Understanding what causes bone loss in osteoporosis, http://womenshealth.suite101.com/article.cfm/what_is_osteoporosis.

Tovar, A. (2004). Bone remodeling as a hybrid cellular automation optimization process, PhD Thesis, University of Notre Dame.

Turner, C.H. (1997). The relationship between cancellous bone architecture and mechanical properties at a continuum level, Forma, 12 (3, 4) 225-233.

Turner, C.H. (2002). Biomechanics of bone: determinants of skeletal fragility and bone quality, Osteoporosis International, 13 (2), 97-104.

Uten'Kin, A.A. and Ashkenazi, E.K. (1972). The anisotropy of compact bone material, Mechanics of Composite Materials, 8 (4), 614-618.

Vahdati, A. and Rouhi, G. (2009). A model for mechanical adaptation of trabecular bone incorporating cellular accommodation and effects of microdamage and disuse, Mech. Res. Comm., 36 (3), 284-293.

van der Linden, J.C., Verhaar, J.A., and Weinans, H. (2001). A three-dimensional simulation of age-related remodeling in trabecular bone, J. Bone Miner. Res., 16 (4), 688–696.

van der Linden, J.C., Verhaar, J.A., Pols, H.A., and Weinans, H. (2003). A simulation model at trabecular level to predict effects of antiresorptive treatment after menopause. Calcif. Tissue Int., 73 (6), 537–544.

van der Linden, J.C., Day, J.S., Verhaar, J.A., and Weinans, H. (2004). Altered tissue properties induce changes in cancellous bone architecture in aging and diseases, J. Biomech., 37 (3), 367–374.

van Rietbergen, B., Huiskes, R., Weinans, H., Sumner, D.R., Turner, T.M. and Galante, J.O. (1993). The mechanism of bone remodeling and resorption around press-fitted THA stems, J. Biomechanics., 26, 369-382.

van Rietbergen, B., Weinans, H., Huiskes, R., Odgaard, A. (1995). A new method to determine trabecular bone elastic properties and loading using micromechanical finite-element models. Journal of Biomechanics, 28, 69-81.

van Rietbergen, B., Weinans, H., Polman, B.J.W., Huiskes, R. (1996). Computational strategies for iterative solutions of large FEM applications employing voxel data. International Journal of Numerical Methods in Engineering, 39, 2743-2767.

van Rietbergen, B. and Huiskes, R. (2001). Elastic constants of cancellous bone, In: Cowin, S.C., ed. Bone mechanics handbook , CRC Press LLC, chapter 15.

Vashishth, D., Koontz, J., Qiu, S.J., Lundin-Cannon, D., Yeni, Y.N., and Schaffler, M.B. (2000). In vivo diffuse damage in human vertebral trabecular bone, Bone, 26, 147-152.

Vezeridis, P.S., Semeins, C.M., Chen, Q., Klein-Nulend, J. (2005). Osteocytes subjected to pulsating fluid flow regulate osteoblast proliferation and differentiation, Biochem. Biophys. Res. Commum., 348, 1082-1088.

Vogel, J.M. (1975). Bone mineral measurement: Skylab experiment M-078, Acta Astronaut., 2 (1-2), 129–139.

von Meyer, G. H. (1867). Die Architektur der Spongiosa. Arch Anat. Physiol. Med., 34, 615-628.

Wachtel, E.F., and Keaveny, T.M. (1997). Dependence of trabecular damage on mechanical strain, J. Orthop. Res., 15, 781-787.

Wageningen ur, (2009). Skeletal tissue differentiation in fish, http://www.ezo.wur.nl/UK/MSc+projects/Skeletal+tissue+differentiation+in+fish/.

Wagner, H., Wagner, M., The transfemoral approach in total hip revision arthoplasty, http://www.maitrise-orthop.com/corpusmaitri/orthopaedic/mo71_wagner/wagner_us.shtml.

Wang, X. (2004). Measurement and analysis of microdamage in bone, PhD Thesis, University of Notre Dame.

Weaver, J.K. and Chalmers, J. (1966). Cancellous bone: its strength and changes with aging and an evaluation of some methods for measuring mineral content, age changes in cancellous bone, J. Bone and Joint Surg., 48A: 289-298.

Weinans, H., Huiskes, R., van Rietbergen, B., Summer, D.R., Turner, T.M., Galante, J.O. (1993). Adaptive bone remodeling around bonded noncemented total hip arthroplasty: a comparison between animal experiments and computer simulation, J., Orthop. Res., 11, 500-513.

Weinbaum, S., Cowin, S.C., Zeng, Y. (1994). A model for the excitation of osteocytes by mechanical loading-induced bone fluid shear stresses, J. Biomech., 27, 339-360.

Wenzel, T.E., Schaffler, M.B., and Fyhrie, D.P. (1996). In vivo trabecular microcracks in human vertebral bone, Bone, 19, 89-95.

Whalen, R. (1993). Musculoskeletal adaptation to mechanical forces on earth and in space, Physiologist, 36 (1), 127–130.

Whitehouse, W.J., Dyson, E.D. and Jackson, C.K. (1971). The scanning electron microscope in studies of trabecular bone from the human vertebral body, J. Anat., 108, 481-496.

Wolff, J. (1892). Das gesetz der transformation der knochen, Berlin A. Hirchwild (1892) translated as "The law of bone remodeling", Maquet P. and Furlong R., Springer-Verlag, Berlin, 1986.

You, L., Temiyasathis, S., Lee, P., Kim, C.H., Tummala, P., Yao, W., Kingery, W., Malone, A.M., Kwon, R.Y., Jacobs, C.R. (2008). Osteocytes as mechanosensors in the inhibition of bone resorption due to mechanical loading, Bone, 2008, 42, 172-179.

Yuehuei. H.A. and Robert A.D. (2000). Mechanical testing of bone and the bone-implant interface, Taylor & Francis, Inc..

Yuan, H.A., Brown, C.W., and Phillpis, F.M. (2004). Osteoporotic spinal deformity: A biomechanical rationale for the linicalconsequences and treatment of vertebral body compression fractures, J. Spinal Disord, 17 (3), 236–242.

Zhao, Y. (2009). Osteocytes as mechanosensory cells: from extracellular structure to intracellular signals, Master Thesis, University of Toronto.

Zilch, H., Rohlmann, A., Bergman, G., and Kölbel, R. (1980). Material properties of femoral cancellous bone in axial loading. Part II : Time dependent properties, Arch. Orthop. Traumat. Surg., 97, 257.

Publications Arising from This Thesis

Journal Papers

Xianjie Li, Gholamreza Rouhi, Investigation into the reasons for bone loss in aging and osteoporotic individuals using a semi-mechanistic bone model, Acta Mechanica Sinica, (Submitted in Sep. 2010, currently under review)

Xianjie Li, Gholamreza Rouhi, A three-dimensional computer model to simulate spongy bone remodeling under overload using a semi-mechanistic bone remodeling theory, (Submitted in Dec. 2010, currently under review)

Conference Posters

Xianjie Li, Gholamreza Rouhi, An Investigation on the Spongy Bone Remodeling Using a Semi-Mechanistic Bone Remodeling Theory, ASM, Carleton University, Ottawa, February 2009-----1st Prize graduate poster

Xianjie Li, Gholamreza Rouhi, Effects of Non-Uniform Osteocyte Distribution and Anisotropic Spongy Bone Property Bone Remodeling Process, CMBEC32, Calgary, May 2009

Xianjie Li, Gholamreza Rouhi, Theoretical Simulation of Spongy Bone Remodeling under Overload using A Semi-Mechanistic Bone Remodeling Theory, CSB2010, Kingston, June 2010

Appendix I

Finite element methods

I.1. Equations for two-dimensional (2D) finite elements

In our finite element study, 4-node square elements were used in 2D computer bone model. Figure I.1 shows a mesh of elements, together with the node, element and global freedom numbering. It is assumed that the sides of the square elements are parallel to the global Cartesian axes. Figure I.2 gives the node numbering system adopted for the 4-node square element. By convention, we number the nodes in each element 1, 2, 3 and 4 in a clockwise direction. Note that, since each node has two degrees of freedom (DOFs), the total DOFs for a 4-node square element would be eight.

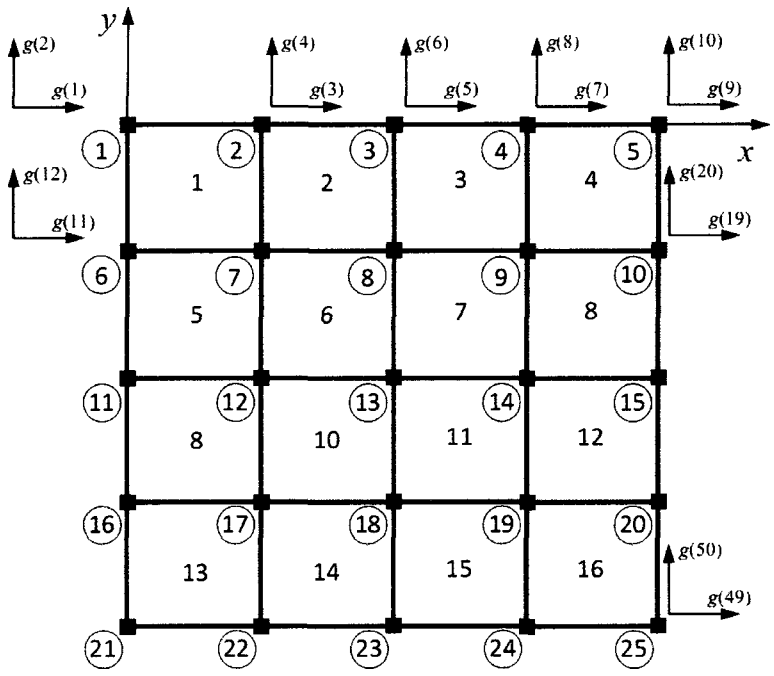

Figure I.1 Global node, element and global freedom numbering for a mesh of 4-node square elements.

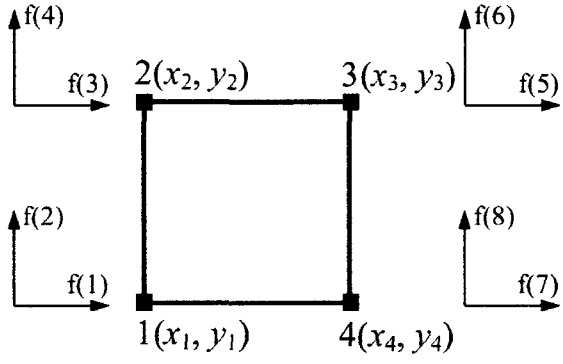

Figure I.2 Local node, freedom numbering for the 4-node square element.

In order to make the expression of the shape functions very much easier, a local natural coordinate system (r, s) with its origin located at the center of the square element is defined (see Figure I.3.b). The relationship between the global coordinate (x, y) and the local natural coordinate system (r, s) is given by:

$$r = \frac{x - \bar{x}}{a} \qquad s = \frac{y - \bar{y}}{a} \tag{I.1}$$

where $2a$ is the length of the square side, and the coordinates of the centroid are:

$$\bar{x} = \frac{x_1 + x_4}{2} \qquad \bar{y} = \frac{y_1 + y_2}{2} \tag{I.2}$$

Eq. (I.1) and (I.2) define a very simple coordinate mapping between global and natural coordinate systems for square elements as shown in Figure I.3. Therefore, r and s are such that the values range from -1 to +1, and the nodal coordinates in natural coordinate system are as in Figure I.3.b.

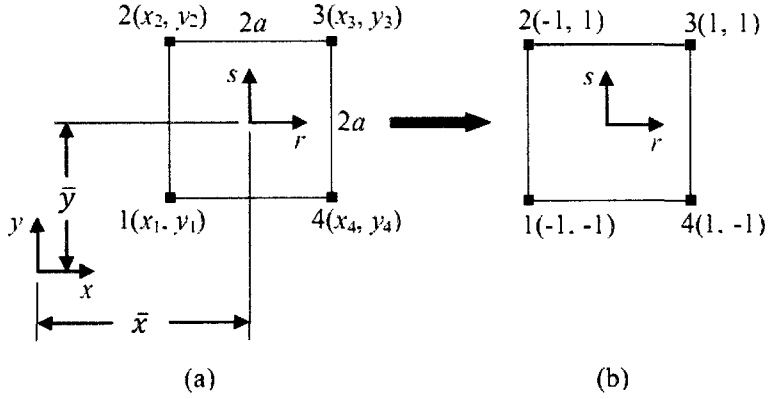

Figure I.3 Square element and the coordinate systems. (a) Square element in global coordinate system; (b) square element in natural coordinate system.

I.1.1. The matrix of shape function [*N*]

The shape functions (or interpolation functions) corresponding to four nodes of the element in Figure I.3 can be written as follows:

$$N_1 = \frac{1}{4}(1 - r)(1 - s)$$

$$N_2 = \frac{1}{4}(1 - r)(1 + s) \tag{I.3}$$

$$N_3 = \frac{1}{4}(1+r)(1+s)$$

$$N_4 = \frac{1}{4}(1+r)(1-s)$$

where (r, s) is the natural coordinates of an interior point located in the element of Figure I.3.b.

For a general field problem, the field variable on an element basis is described as:

$$\phi(x,y) = \sum_{i=1}^{4} N_i(r,s)\phi_i \qquad \text{(I. 4)}$$

The global coordinates of the element of Figure I.3.a can be expressed as:

$$x = \sum_{i=1}^{4} N_i(r,s)x_i \qquad y = \sum_{i=1}^{4} N_i\,(r,s)y_i \qquad \text{(I. 5)}$$

where (r, s) is the natural coordinates of an interior point located in the element of Figure I.3(b), (x, y) is the global coordinates of an corresponding interior point located in the element of Figure I.3.a, and (x_i, y_i) $(i=1, 2, 3, 4)$ are global coordinates of element's four nodes in Figure I.3.a.

The displacements of an interior point located at (x, y), which is the global coordinates of an interior point in the element of Figure I.3.a, can be written as:

$$u(x,y) = \sum_{i=1}^{4} N_i(r,s)u_i \qquad v(x,y) = \sum_{i=1}^{4} N_i(r,s)v_i \qquad \text{(I. 6)}$$

where u and v are displacements of a point (x, y) in the global x and y direction respectively, and u_i and v_i $(i=1, 2, 3, 4)$ are displacements of element's four nodes in Figure I.3. In matrix form, the displacement function within the element is:

$$\begin{Bmatrix} u \\ v \end{Bmatrix} = \begin{bmatrix} N_1 & 0 & N_2 & 0 & N_3 & 0 & N_4 & 0 \\ 0 & N_1 & 0 & N_2 & 0 & N_3 & 0 & N_4 \end{bmatrix} \begin{Bmatrix} u_1 \\ v_1 \\ u_2 \\ v_2 \\ u_3 \\ v_3 \\ u_4 \\ v_4 \end{Bmatrix} \tag{I.7}$$

In compact matrix form, Eq. (I.7) can be expressed as:

$$\begin{Bmatrix} u \\ v \end{Bmatrix} = [N]\{U^e\} \tag{I.8}$$

where

$$[N] = \left[\begin{array}{cc|cc|cc|cc} N_1 & 0 & N_2 & 0 & N_3 & 0 & N_4 & 0 \\ 0 & N_1 & 0 & N_2 & 0 & N_3 & 0 & N_4 \end{array}\right] \tag{I.9}$$

is shape function matrix; $\{U^e\}$ is the nodal displacement vector of element in Figure I.3.

I.1.2. The Jacobian matrix [*J*]

The Jacobian matrix is given by:

$$[J] = \begin{bmatrix} \dfrac{\partial x}{\partial r} & \dfrac{\partial y}{\partial r} \\ \dfrac{\partial x}{\partial s} & \dfrac{\partial y}{\partial s} \end{bmatrix} \tag{I.10}$$

Using Eq. (I.3) and Eq. (I.5) in Eq. (I.10), we can get:

$$[J] = \begin{bmatrix} \displaystyle\sum_{i=1}^{4} \frac{\partial N_i}{\partial r} x_i & \displaystyle\sum_{i=1}^{4} \frac{\partial N_i}{\partial r} y_i \\ \displaystyle\sum_{i=1}^{4} \frac{\partial N_i}{\partial s} x_i & \displaystyle\sum_{i=1}^{4} \frac{\partial N_i}{\partial s} y_i \end{bmatrix}$$

$$= \frac{1}{4}\begin{bmatrix} (1-\mathrm{s})(\mathrm{x}_4-\mathrm{x}_1)+(1+\mathrm{s})(\mathrm{x}_3-\mathrm{x}_2) & (1-\mathrm{s})(\mathrm{y}_4-\mathrm{y}_1)+(1+\mathrm{s})(\mathrm{y}_3-\mathrm{y}_2) \\ (1-\mathrm{r})(\mathrm{x}_2-\mathrm{x}_1)+(1+\mathrm{r})(\mathrm{x}_3-\mathrm{x}_4) & (1-\mathrm{r})(\mathrm{y}_2-\mathrm{y}_1)+(1+\mathrm{r})(\mathrm{y}_3-\mathrm{y}_4) \end{bmatrix} \tag{I.11}$$

I.1.3. The elastic material property matrix $[D]$ for plan stress

External forces are applied only in the *x-y* plane. There are three stress components in total at a point in the 2D element. These stresses are called a stress tensor. They are often written in a vector form of:

$$\sigma^T = \{\sigma_x \quad \sigma_y \quad \tau_{xy}\} \tag{I.12}$$

Corresponding to the three stress tensors, there are three strain components at any point in the element, which can also be written in a similar vector form of:

$$\varepsilon^T = \{\varepsilon_x \quad \varepsilon_y \quad \gamma_{xy}\} \tag{I.13}$$

The stress-strain relation, or constitutive equations, is:

$$\begin{Bmatrix} \sigma_x \\ \sigma_y \\ \tau_{xy} \end{Bmatrix} = \frac{E}{1-v^2} \begin{bmatrix} 1 & v & 0 \\ v & 1 & 0 \\ 0 & 0 & \frac{1-v}{2} \end{bmatrix} \begin{Bmatrix} \varepsilon_x \\ \varepsilon_y \\ \gamma_{xy} \end{Bmatrix} \tag{I.14}$$

or:

$$\{\sigma\} = [D]\{\varepsilon\} \tag{I.15}$$

where E is the modulus of elasticity and v is Poisson' s ratio for the material,

$$[D] = \frac{E}{1-v^2} \begin{bmatrix} 1 & v & 0 \\ v & 1 & 0 \\ 0 & 0 & \frac{1-v}{2} \end{bmatrix} \tag{I.16}$$

is the elastic material property matrix for plane stress.

I.1.4. The strain – nodal displacement matrix $[B]$

For a 4-node square element, the strain components are expressed as:

$$\begin{Bmatrix} \varepsilon_x \\ \varepsilon_y \\ \gamma_{xy} \end{Bmatrix} = \begin{Bmatrix} \dfrac{\partial u}{\partial x} \\ \dfrac{\partial v}{\partial y} \\ \dfrac{\partial u}{\partial y} + \dfrac{\partial v}{\partial x} \end{Bmatrix} = \begin{bmatrix} \dfrac{\partial}{\partial x} & 0 \\ 0 & \dfrac{\partial}{\partial y} \\ \dfrac{\partial}{\partial y} & \dfrac{\partial}{\partial x} \end{bmatrix} \begin{Bmatrix} u \\ v \end{Bmatrix} \tag{I.17}$$

From Eq. (I.1), we know:

$$\frac{\partial}{\partial x} = \frac{\partial}{\partial r}\frac{\partial r}{\partial x} = \frac{1}{a}\frac{\partial}{\partial r}$$

$$\frac{\partial}{\partial y} = \frac{\partial}{\partial s}\frac{\partial s}{\partial y} = \frac{1}{a}\frac{\partial}{\partial s} \tag{I.18}$$

Substituting Eq. (I.7) and Eq. (I.18) into Eq. (I.17), we get:

$$\begin{Bmatrix} \varepsilon_x \\ \varepsilon_y \\ \gamma_{xy} \end{Bmatrix} = \frac{1}{a}\begin{bmatrix} \dfrac{\partial N_1}{\partial r} & 0 & \dfrac{\partial N_2}{\partial r} & 0 & \dfrac{\partial N_3}{\partial r} & 0 & \dfrac{\partial N_4}{\partial r} & 0 \\ 0 & \dfrac{\partial N_1}{\partial s} & 0 & \dfrac{\partial N_2}{\partial s} & 0 & \dfrac{\partial N_3}{\partial s} & 0 & \dfrac{\partial N_4}{\partial s} \\ \dfrac{\partial N_1}{\partial s} & \dfrac{\partial N_1}{\partial r} & \dfrac{\partial N_2}{\partial s} & \dfrac{\partial N_2}{\partial r} & \dfrac{\partial N_3}{\partial s} & \dfrac{\partial N_3}{\partial r} & \dfrac{\partial N_4}{\partial s} & \dfrac{\partial N_4}{\partial r} \end{bmatrix} \begin{Bmatrix} u_1 \\ v_1 \\ u_2 \\ v_2 \\ u_3 \\ v_3 \\ u_4 \\ v_4 \end{Bmatrix} \tag{I.19}$$

As in customary, Eq. (I.19) is written as:

$$\{\varepsilon\} = [B]\{U^e\} \tag{I.20}$$

where $[B]$ represents the strain-nodal displacement matrix.

Substituting Eq. (I.3) into Eq. (I.19), the $[B]$ matrix is found to be a function of r and s, which can be expressed as:

$$[B] = \frac{1}{4a}\begin{bmatrix} -(1-s) & 0 & -(1+s) & 0 & 1+s & 0 & 1-s & 0 \\ 0 & -(1-r) & 0 & 1-r & 0 & 1+r & 0 & -(1+r) \\ -(1-r) & -(1-s) & 1-r & -(1+s) & 1+r & 1+s & -(1+r) & 1-s \end{bmatrix} \tag{I.21}$$

I.1.5. The element stiffness matrix $[K^e]$

For the two-dimensional element, the element stiffness matrix is:

$$[K^e] = \iint [B]^T [D][B]\, dA \tag{I.22}$$

where $[K^e]$ is the element stiffness matrix.

The element in our study is square element, from Eq. (I.1), we get:

$$dA = dxdy = a^2 drds \tag{I.23}$$

Because:

$$dA = |J| drds \tag{I.24}$$

, we get:

$$|J| = a^2 \tag{I.25}$$

where $|J|$ is the determinant of the Jacobian matrix, $[J]$.

Substitution of Eq. (I.24) and Eq. (I.25) into Eq. (I.22) results in:

$$[K^e] = a^2 \int_{-1}^{1} \int_{-1}^{1} [B]^T [D][B]\, drds \tag{I.26}$$

From Eq. (I.21), we know that $[B]^T[D][B]$ is a function of r and s. Hence, using the Gaussian integration procedure, the integration represented by Eq. (I.24) can be approximated by:

$$[k^e] = a^2 \sum_{j=1}^{m} \sum_{i=1}^{n} W_i^r W_j^s \left[B(r_i, s_j)\right]^T [D]\left[B(r_i, s_j)\right] \tag{I.27}$$

where W_i^r and W_j^s denote Gauss weight factors, r_i and s_j denote Gauss points (or sampling points, integrating points), and n and m are the number of Gauss points in the r and s direction, respectively.

In most cases, two Gauss points (or integrating points) in r and s direction lead to accurate estimates of the stiffness matrix of a 4-node general quadrilateral. Therefore, in our

2D finite element analysis, n and m equal to 2. There are 4 integrating points in 4-node square element. Gauss weight factors and Gauss integration points are shown in Table I.1.

Table I.1

Sampling points, weighting factors for 4-node square elements with 4 integrating points

Point	r_i	s_j	W_i^r	W_j^s
1	$-\sqrt{\frac{1}{3}}$	$-\sqrt{\frac{1}{3}}$	1	1
2	$-\sqrt{\frac{1}{3}}$	$\sqrt{\frac{1}{3}}$	1	1
3	$\sqrt{\frac{1}{3}}$	$\sqrt{\frac{1}{3}}$	1	1
4	$\sqrt{\frac{\mathbf{1}}{\mathbf{3}}}$	$-\sqrt{\frac{\mathbf{1}}{\mathbf{3}}}$	1	1

After getting the element stiffness matrix, we can assemble the individual element matrices to obtain the global stiffness matrix $[K]$ for our 2D computer bone model.

I.1.6. The stain energy density u_e

The strain energy per unit area is:

$$u_e = \frac{1}{2}\{\varepsilon\}^T\{\sigma\} = \frac{1}{2}\{\varepsilon\}^T[D]\{\varepsilon\} \quad \text{(I. 28)}$$

or, for a 2D element,

$$u_e = \frac{1}{2}(\sigma_x\varepsilon_x + \sigma_y\varepsilon_y + \tau_{xy}\gamma_{xy}) \quad \text{(I. 29)}$$

I.2. Equations for three-dimensional (3D) finite elements

In our finite element study, 8-node cubic elements were used in 3D computer bone model. Figure I.4 shows a mesh of elements, together with the node, element and global freedom numbering. It is assumed that the sides of the cube elements are parallel to the global Cartesian axes.

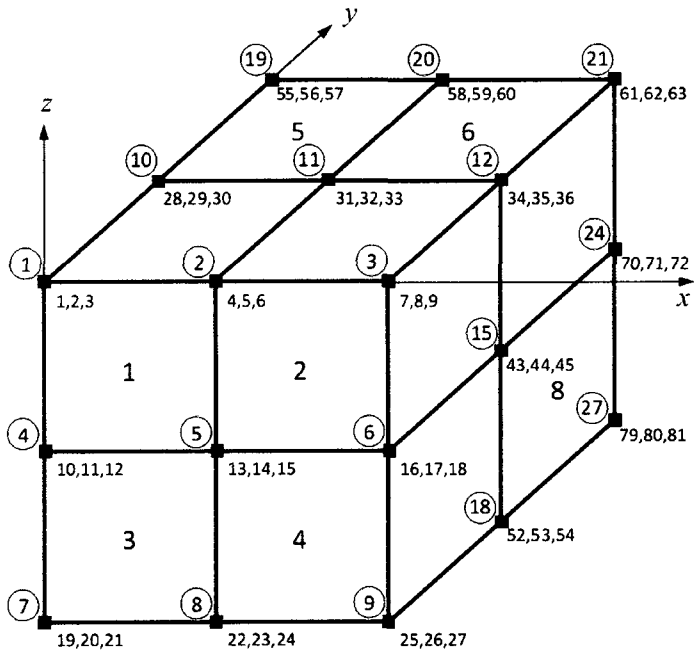

Figure I.4 Global node, element and global freedom numbering for a mesh of 8-node cubic elements.

The 8-node cubic element with the node numbering system is shown in Figure I.5.a in reference to a global Cartesian coordinate system.

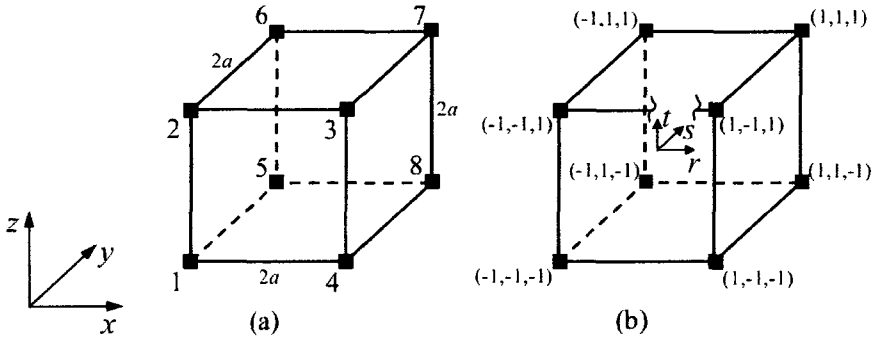

Figure I.5 8-node cubic element: (a) Global Cartesian coordinates. (b) Natural coordinates with an origin at the centroid.

Here, we utilize a local natural coordinates *r, s, t* of Figure I.5.b with its origin located at the center of the cubic element, defined as:

$$r = \frac{x - \bar{x}}{a}, \quad s = \frac{y - \bar{y}}{a}, \quad t = \frac{z - \bar{z}}{a} \tag{I.30}$$

where $2a$ is the length of the cubic side, and:

$$\bar{x} = \frac{x_1 + x_4}{2}, \quad \bar{y} = \frac{y_1 + y_5}{2}, \quad \bar{z} = \frac{z_1 + z_2}{2} \tag{I.31}$$

are the coordinates of the element centroid.

The natural coordinates are defined such that the coordinate value varies between -1 and 1 over the domain of the element.

I.2.1. The matrix of shape function [*N*]

The shape functions (or interpolation functions) corresponding to eight nodes of the element of Figure I.5.b in terms of the natural coordinates are:

$$N_1 = \frac{1}{8}(1 - r)(1 - s)(1 - t)$$

$$N_2 = \frac{1}{8}(1-r)(1-s)(1+t)$$

$$N_3 = \frac{1}{8}(1+r)(1-s)(1+t)$$

$$N_4 = \frac{1}{8}(1+r)(1-s)(1-t) \qquad \text{(I.32)}$$

$$N_5 = \frac{1}{8}(1-r)(1+s)(1-t)$$

$$N_6 = \frac{1}{8}(1-r)(1+s)(1+t)$$

$$N_7 = \frac{1}{8}(1+r)(1+s)(1+t)$$

$$N_8 = \frac{1}{8}(1+r)(1+s)(1-t)$$

where (r, s, t) is the natural coordinates of an interior point located in the element of Figure I.5(b).

The field variable on an element basis is described as:

$$\phi(x,y,z) = \sum_{i=1}^{8} N_i(r,s,t)\phi_i \qquad \text{(I.33)}$$

The global coordinate coordinates of the element of Figure I.5.a can be expressed as:

$$x = \sum_{i=1}^{8} N_i(r,s,t)x_i, \quad y = \sum_{i=1}^{8} N_i(r,s,t)y_i, \quad z = \sum_{i=1}^{8} N_i(r,s,t)z_i \qquad \text{(I.34)}$$

where (r, s, t) is the natural coordinates of an interior point located in the element of Figure I.5.b, (x, y, z) is the global coordinates of an corresponding interior point located in the element of Figure I.5.a, and (x_i, y_i, z_i) (i=1, 2, 3, 4, 5, 6, 7 and 8) are global coordinates of element's eight nodes in Figure I.5.a.

The displacements of an interior point located at (x, y, z), which is the global coordinates of an interior point in the element of Figure I.5.a, can be written as:

$$u(x,y,z)=\sum_{i=1}^{8}N_i(r,s,t)u_i,\quad v(x,y,z)=\sum_{i=1}^{8}N_i(r,s,t)v_i,\quad w(x,y,z)=\sum_{i=1}^{8}N_i(r,s,t)w_i \qquad (I.35)$$

where u, v and w are displacements of a point (x, y, z) in the global x, y and z direction respectively, and u_i, v_i and w_i (i=1, 2, 3, 4, 5, 6, 7 and 8) are displacements of element's eight nodes in Figure I.5. In matrix form, the displacement function within the element is:

$$\begin{Bmatrix}u(x,y,z)\\v(x,y,z)\\w(x,y,z)\end{Bmatrix}=\begin{bmatrix}N_1&0&0&N_2&0&0&N_3&0&0&\cdots&0&N_8&0&0\\0&N_1&0&0&N_2&0&0&N_3&0&\cdots&0&0&N_8&0\\0&0&N_1&0&0&N_2&0&0&N_3&\cdots&N_7&0&0&N_8\end{bmatrix}\begin{Bmatrix}u_1\\v_1\\w_1\\u_2\\v_2\\w_2\\u_3\\v_3\\w_3\\\vdots\\w_7\\u_8\\v_8\\w_8\end{Bmatrix} \qquad (I.36)$$

In compact matrix form, Eq. (I.36) can be expressed as:

$$\begin{Bmatrix}u\\v\\w\end{Bmatrix}=[N]\{U^e\} \qquad (I.37)$$

where

$$[N]=\begin{bmatrix}N_1&0&0&N_2&0&0&N_3&0&0&\cdots&0&N_8&0&0\\0&N_1&0&0&N_2&0&0&N_3&0&\cdots&0&0&N_8&0\\0&0&N_1&0&0&N_2&0&0&N_3&\cdots&N_7&0&0&N_8\end{bmatrix} \qquad (I.38)$$

is the shape function matrix; $\{U^e\}$ is the nodal displacement vector of 8-node cubic element in Figure I.5.

I.2.2. The Jacobian matrix [J]

The Jacobian matrix is given by:

$$[J] = \begin{bmatrix} \frac{\partial x}{\partial r} & \frac{\partial y}{\partial r} & \frac{\partial z}{\partial r} \\ \frac{\partial x}{\partial s} & \frac{\partial y}{\partial s} & \frac{\partial z}{\partial s} \\ \frac{\partial x}{\partial t} & \frac{\partial y}{\partial t} & \frac{\partial z}{\partial t} \end{bmatrix} \tag{I.39}$$

Using Eq. (I.32) and Eq. (I.34) in Eq. (I.39), we can get:

$$[J] = \begin{bmatrix} \sum_{i=1}^{8} \frac{\partial N_i}{\partial r} x_i & \sum_{i=1}^{8} \frac{\partial N_i}{\partial r} y_i & \sum_{i=1}^{8} \frac{\partial N_i}{\partial r} z_i \\ \sum_{i=1}^{8} \frac{\partial N_i}{\partial s} x_i & \sum_{i=1}^{8} \frac{\partial N_i}{\partial s} y_i & \sum_{i=1}^{8} \frac{\partial N_i}{\partial s} z_i \\ \sum_{i=1}^{8} \frac{\partial N_i}{\partial t} x_i & \sum_{i=1}^{8} \frac{\partial N_i}{\partial t} y_i & \sum_{i=1}^{8} \frac{\partial N_i}{\partial t} z_i \end{bmatrix} \tag{I.40}$$

in which

$$\sum_{i=1}^{8} \frac{\partial N_i}{\partial r} x_i = \frac{1}{8}[(1-s)(1-t)(x_4 - x_1) + (1-s)(1+t)(x_3 - x_2) + (1+s)(1-t)(x_8 - x_5) + (1+s)(1+t)(x_7 - x_6)]$$

$$\sum_{i=1}^{8} \frac{\partial N_i}{\partial r} y_i = \frac{1}{8}[(1-s)(1-t)(y_4 - y_1) + (1-s)(1+t)(y_3 - y_2) + (1+s)(1-t)(y_8 - y_5) + (1+s)(1+t)(y_7 - y_6)]$$

$$\sum_{i=1}^{8} \frac{\partial N_i}{\partial r} z_i = \frac{1}{8}[(1-s)(1-t)(z_4 - z_1) + (1-s)(1+t)(z_3 - z_2) + (1+s)(1-t)(z_8 - z_5) + (1+s)(1+t)(z_7 - z_6)]$$

$$\sum_{i=1}^{8} \frac{\partial N_i}{\partial s} x_i = \frac{1}{8}[(1-r)(1-t)(x_5 - x_1) + (1-r)(1+t)(x_6 - x_2) + (1+r)(1+t)(x_7 - x_3) + (1+r)(1-t)(x_8 - x_4)]$$

$$\sum_{i=1}^{8} \frac{\partial N_i}{\partial s} y_i = \frac{1}{8}[(1-r)(1-t)(y_5 - y_1) + (1-r)(1+t)(y_6 - y_2) + (1+r)(1+t)(y_7 - y_3) + (1+r)(1-t)(y_8 - y_4)] \tag{I.41}$$

$$\sum_{i=1}^{8} \frac{\partial N_i}{\partial s} z_i = \frac{1}{8}[(1-r)(1-t)(z_5 - z_1) + (1-r)(1+t)(z_6 - z_2) + (1+r)(1+t)(z_7 - z_3) + (1+r)(1-t)(z_8 - z_4)]$$

$$\sum_{i=1}^{8}\frac{\partial N_i}{\partial t}x_i = \frac{1}{8}[(1-r)(1-s)(x_2-x_1)+(1+r)(1-s)(x_3-x_4)+(1-r)(1+s)(x_6-x_5)+(1+r)(1+s)(x_7-x_8)]$$

$$\sum_{i=1}^{8}\frac{\partial N_i}{\partial t}y_i = \frac{1}{8}[(1-r)(1-s)(y_2-y_1)+(1+r)(1-s)(y_3-y_4)+(1-r)(1+s)(y_6-y_5)+(1+r)(1+s)(y_7-y_8)]$$

$$\sum_{i=1}^{8}\frac{\partial N_i}{\partial t}z_i = \frac{1}{8}[(1-r)(1-s)(z_2-z_1)+(1+r)(1-s)(z_3-z_4)+(1-r)(1+s)(z_6-z_5)+(1+r)(1+s)(z_7-z_8)]$$

I.2.3. The elastic material property matrix $[D]$

In 3D solid, there are six stress components in total at a point. These stresses are often called a stress tensor. They are often written in a vector form of:

$$\sigma^T = \{\sigma_x \quad \sigma_y \quad \sigma_z \quad \tau_{xy} \quad \tau_{xz} \quad \tau_{yz}\} \tag{I.42}$$

Corresponding to the six stress tensors, there are six strain components at any point in the element, which can also be written in a similar vector form of:

$$\varepsilon^T = \{\varepsilon_x \quad \varepsilon_y \quad \varepsilon_z \quad \gamma_{xy} \quad \gamma_{xz} \quad \gamma_{yz}\} \tag{I.43}$$

The stress-strain relations, or constitutive equations, are expressed in matrix form as:

$$\begin{Bmatrix}\sigma_x\\ \sigma_y\\ \sigma_z\\ \tau_{xy}\\ \tau_{xz}\\ \tau_{yz}\end{Bmatrix} = \frac{E}{(1+v)(1-2v)}\begin{bmatrix}1-v & v & v & 0 & 0 & 0\\ v & 1-v & v & 0 & 0 & 0\\ v & v & 1-v & 0 & 0 & 0\\ 0 & 0 & 0 & \frac{1-2v}{2} & 0 & 0\\ 0 & 0 & 0 & 0 & \frac{1-2v}{2} & 0\\ 0 & 0 & 0 & 0 & 0 & \frac{1-2v}{2}\end{bmatrix}\begin{Bmatrix}\varepsilon_x\\ \varepsilon_y\\ \varepsilon_z\\ \gamma_{xy}\\ \gamma_{xz}\\ \gamma_{yz}\end{Bmatrix} \tag{I.44}$$

or:

$$\{\sigma\} = [D]\{\varepsilon\} \tag{I.45}$$

where $[D]$ is a 6×6 matrix involving only the elastic modulus E and Poisson's ratio v for the material.

I.2.4. The strain – nodal displacement matrix [B]

For an 8-node cubic element, the strain-displacement relations can be expressed as:

$$\begin{Bmatrix} \varepsilon_x \\ \varepsilon_y \\ \varepsilon_z \\ \gamma_{xy} \\ \gamma_{xz} \\ \gamma_{yz} \end{Bmatrix} = \begin{Bmatrix} \dfrac{\partial u}{\partial x} \\ \dfrac{\partial v}{\partial y} \\ \dfrac{\partial w}{\partial z} \\ \dfrac{\partial u}{\partial y} + \dfrac{\partial v}{\partial x} \\ \dfrac{\partial u}{\partial z} + \dfrac{\partial w}{\partial x} \\ \dfrac{\partial v}{\partial z} + \dfrac{\partial w}{\partial y} \end{Bmatrix} = \begin{bmatrix} \dfrac{\partial}{\partial x} & 0 & 0 \\ 0 & \dfrac{\partial}{\partial y} & 0 \\ 0 & 0 & \dfrac{\partial}{\partial z} \\ \dfrac{\partial}{\partial y} & \dfrac{\partial}{\partial x} & 0 \\ \dfrac{\partial}{\partial z} & 0 & \dfrac{\partial}{\partial x} \\ 0 & \dfrac{\partial}{\partial z} & \dfrac{\partial}{\partial y} \end{bmatrix} \begin{Bmatrix} u \\ v \\ w \end{Bmatrix} \tag{I.46}$$

From Eq. (I.30), we know:

$$\begin{aligned} \frac{\partial}{\partial x} &= \frac{\partial}{\partial r}\frac{\partial r}{\partial x} = \frac{1}{a}\frac{\partial}{\partial r} \\ \frac{\partial}{\partial y} &= \frac{\partial}{\partial s}\frac{\partial s}{\partial y} = \frac{1}{a}\frac{\partial}{\partial s} \\ \frac{\partial}{\partial z} &= \frac{\partial}{\partial t}\frac{\partial t}{\partial z} = \frac{1}{a}\frac{\partial}{\partial t} \end{aligned} \tag{I.47}$$

Substituting Eq. (I.36) and Eq. (I.47) into Eq. (I.46), we get:

$$\begin{Bmatrix} \varepsilon_x \\ \varepsilon_y \\ \varepsilon_z \\ \gamma_{xy} \\ \gamma_{xz} \\ \gamma_{yz} \end{Bmatrix} = \frac{1}{a} \begin{bmatrix} \dfrac{\partial N_1}{\partial r} & 0 & 0 & \dfrac{\partial N_2}{\partial r} & 0 & 0 & \dfrac{\partial N_3}{\partial r} & 0 & 0 & \cdots & \dfrac{\partial N_8}{\partial r} & 0 & 0 \\ 0 & \dfrac{\partial N_1}{\partial s} & 0 & 0 & \dfrac{\partial N_2}{\partial s} & 0 & 0 & \dfrac{\partial N_3}{\partial s} & 0 & \cdots & 0 & \dfrac{\partial N_8}{\partial s} & 0 \\ 0 & 0 & \dfrac{\partial N_1}{\partial t} & 0 & 0 & \dfrac{\partial N_2}{\partial t} & 0 & 0 & \dfrac{\partial N_7}{\partial t} & \cdots & 0 & 0 & \dfrac{\partial N_8}{\partial t} \\ \dfrac{\partial N_1}{\partial s} & \dfrac{\partial N_1}{\partial r} & 0 & \dfrac{\partial N_2}{\partial s} & \dfrac{\partial N_2}{\partial r} & 0 & \dfrac{\partial N_3}{\partial s} & \dfrac{\partial N_3}{\partial r} & 0 & \cdots & \dfrac{\partial N_8}{\partial s} & \dfrac{\partial N_8}{\partial r} & 0 \\ \dfrac{\partial N_1}{\partial t} & 0 & \dfrac{\partial N_1}{\partial r} & \dfrac{\partial N_2}{\partial t} & 0 & \dfrac{\partial N_2}{\partial r} & \dfrac{\partial N_3}{\partial t} & 0 & \dfrac{\partial N_7}{\partial r} & \cdots & \dfrac{\partial N_8}{\partial t} & 0 & \dfrac{\partial N_8}{\partial r} \\ 0 & \dfrac{\partial N_1}{\partial t} & \dfrac{\partial N_1}{\partial s} & 0 & \dfrac{\partial N_2}{\partial t} & \dfrac{\partial N_2}{\partial s} & 0 & \dfrac{\partial N_3}{\partial t} & \dfrac{\partial N_7}{\partial s} & \cdots & 0 & \dfrac{\partial N_8}{\partial t} & \dfrac{\partial N_8}{\partial s} \end{bmatrix} \begin{Bmatrix} u_1 \\ v_1 \\ w_1 \\ u_2 \\ v_2 \\ w_2 \\ u_3 \\ v_3 \\ \vdots \\ w_7 \\ u_8 \\ v_8 \\ w_8 \end{Bmatrix} \tag{I.48}$$

As in customary, Eq. (I.48) is written as:

$$\{\varepsilon\} = [B]\{U^e\} \tag{I.49}$$

where

$$[B]=\frac{1}{a}\begin{bmatrix} \frac{\partial N_1}{\partial r} & 0 & 0 & \frac{\partial N_2}{\partial r} & 0 & 0 & \frac{\partial N_3}{\partial r} & 0 & \cdots & 0 & \frac{\partial N_8}{\partial r} & 0 & 0 \\ 0 & \frac{\partial N_1}{\partial s} & 0 & 0 & \frac{\partial N_2}{\partial s} & 0 & 0 & \frac{\partial N_3}{\partial s} & & 0 & 0 & \frac{\partial N_8}{\partial s} & 0 \\ 0 & 0 & \frac{\partial N_1}{\partial t} & 0 & 0 & \frac{\partial N_2}{\partial t} & 0 & 0 & & \frac{\partial N_7}{\partial t} & 0 & 0 & \frac{\partial N_8}{\partial t} \\ \frac{\partial N_1}{\partial s} & \frac{\partial N_1}{\partial r} & 0 & \frac{\partial N_2}{\partial s} & \frac{\partial N_2}{\partial r} & 0 & \frac{\partial N_3}{\partial s} & \frac{\partial N_3}{\partial r} & & 0 & \frac{\partial N_8}{\partial s} & \frac{\partial N_8}{\partial r} & 0 \\ \frac{\partial N_1}{\partial t} & 0 & \frac{\partial N_1}{\partial r} & \frac{\partial N_2}{\partial t} & 0 & \frac{\partial N_2}{\partial r} & \frac{\partial N_3}{\partial t} & 0 & & \frac{\partial N_7}{\partial r} & \frac{\partial N_8}{\partial t} & 0 & \frac{\partial N_8}{\partial r} \\ 0 & \frac{\partial N_1}{\partial t} & \frac{\partial N_1}{\partial s} & 0 & \frac{\partial N_2}{\partial t} & \frac{\partial N_2}{\partial s} & 0 & \frac{\partial N_3}{\partial t} & & \frac{\partial N_7}{\partial s} & 0 & \frac{\partial N_8}{\partial t} & \frac{\partial N_8}{\partial s} \end{bmatrix} \quad \text{(I.50)}$$

represents the strain-nodal displacement matrix.

Substituting Eq. (I.32) into Eq. (I.50), we can find that the $[B]$, 6 by 24 matrix, is a function of r, s and t.

I.2.5. The stiffness matrix $[K^e]$

For the three-dimensional element, the element stiffness matrix is:

$$[K^e]=\iiint [B]^T[D][B]dV \quad \text{(I.51)}$$

where $[K^e]$ is the element stiffness matrix.

The element in our study is cubic element, from Eq. (I.30), we get:

$$dV = dxdydz = a^3 drdsdt \quad \text{(I.52)}$$

Because

$$dV = |J|drdsdt \quad \text{(I.53)}$$

, we get:

$$|J| = a^3 \quad \text{(I.54)}$$

where $|J|$ is the determinant of the Jacobian matrix, $[J]$.

Substitution of Eq. (I.53) and Eq. (I.54) into Eq. (I.51) results in:

$$[K^e] = a^3 \int_{-1}^{1}\int_{-1}^{1}\int_{-1}^{1} [B]^T[D][B]\, drdsdt \tag{I.55}$$

From Eq. (I.50), we know that $[B]^T[D][B]$ is a function of r and s. Hence, using the Gaussian integration procedure, the integration represented by Eq. (I.55) can be approximated by:

$$[k^e] = a^3 \sum_{k=1}^{m}\sum_{j=1}^{n}\sum_{i=1}^{l} W_i^r W_j^s W_k^t \left[B(r_i, s_j, t_k)\right]^T [D]\left[B(r_i, s_j, t_k)\right] \tag{I.56}$$

where W_i^r, W_j^s and W_i^r denote Gauss weight factors, r_i and s_j denote Gauss points (or sampling points, integrating points), and n and m are the number of Gauss points in the r and s direction, respectively.

In most cases, two Gauss points (or integrating points) in r, s and t direction lead to accurate estimates of the stiffness matrix of a 8-node general hexahedron. Therefore, in our 3D finite element analysis, we use two Gauss points for l, m and n. There are 8 integrating points in total in our 8-node cubic element. Gauss weight factors and Gauss integration points are shown in Table I.2.

After getting the element stiffness matrix, we can assemble the individual element matrices to obtain the global stiffness matrix $[K]$ for our 3D computer bone model.

Table I.2 Sampling points, weighting factors for 8-node cubic elements with 8 integrating points

Point	r_i	s_j	t_k	W_i^r	W_j^s	W_k^t
1	$-\sqrt{\frac{1}{3}}$	$-\sqrt{\frac{1}{3}}$	$-\sqrt{\frac{1}{3}}$	1	1	1
2	$-\sqrt{\frac{1}{3}}$	$-\sqrt{\frac{1}{3}}$	$\sqrt{\frac{1}{3}}$	1	1	1
3	$\sqrt{\frac{1}{3}}$	$-\sqrt{\frac{1}{3}}$	$\sqrt{\frac{1}{3}}$	1	1	1
4	$\sqrt{\frac{\mathbf{1}}{\mathbf{3}}}$	$-\sqrt{\frac{\mathbf{1}}{\mathbf{3}}}$	$-\sqrt{\frac{1}{3}}$	1	1	1
5	$-\sqrt{\frac{1}{3}}$	$\sqrt{\frac{1}{3}}$	$-\sqrt{\frac{1}{3}}$	1	1	1
6	$-\sqrt{\frac{1}{3}}$	$\sqrt{\frac{1}{3}}$	$\sqrt{\frac{1}{3}}$	1	1	1
7	$\sqrt{\frac{1}{3}}$	$\sqrt{\frac{1}{3}}$	$\sqrt{\frac{1}{3}}$	1	1	1
8	$\sqrt{\frac{\mathbf{1}}{\mathbf{3}}}$	$\sqrt{\frac{\mathbf{1}}{\mathbf{3}}}$	$-\sqrt{\frac{\mathbf{1}}{\mathbf{3}}}$	1	1	1

I.2.6. The stain energy density u_e

The strain energy per unit volume is:

$$u_e = \frac{1}{2}\{\varepsilon\}^T\{\sigma\} = \frac{1}{2}\{\varepsilon\}^T[D]\{\varepsilon\} \tag{I.57}$$

or, for a 3D element,

$$u_e = \frac{1}{2}(\sigma_x\varepsilon_x + \sigma_y\varepsilon_y + \sigma_z\varepsilon_z + \tau_{xy}\gamma_{xy} + \tau_{xz}\gamma_{xz} + \tau_{yz}\gamma_{yz}) \tag{I.58}$$

Appendix II

Simulation programs for spongy bone remodeling

This appendix describes some programs used in our computer simulations. They are input file (input_2D.dat or input _3D.dat), main program (main_2D.f90 or main_3D.f90), which are FORTRAN90 codes, subroutines (main.f90 and geom.f90), and output file (twoD_elements.m or threeD_elements.m, threeD_surface.m), which are MATLAB codes. Input file (input_2D.dat or input _3D.dat) includes the parameters needed in main program (main_2D.f90 or main_3D.f90) which simulates the spongy bone remodeling with finite element analysis (FEA). Output file (twoD_elements.m or threeD_elements.m, threeD_surface.m) generates image which helps visualize the data obtained from main program.

II.1. Input files

Input files describe the parameters for geometry of the computer model, mathematical functions of spongy bone remodeling, and external loads. These parameters can be adjusted before running main program (main_2D.f90 or main_3D.f90).

II.1.1.input_2D.dat

```
4  40  40  4
0.00004
0.01  1.0  5e+9  0.3  3
3000
0.0001  2  1.0
20  0.001  0.1  0.3
0.00996  -0.018  -0.018


--------------- Structure of data ----------------------
(units:N,m,N/m²)
nod  nxe  nye  nip
dx
mindens  maxdens  emax  v  gama
iteration
Dinfl  ninfe  mechanosensitivity
profactor  threshold  resorptionchance  resorptionamount
ftop(1)  ftop(2)  fleft(1)
```

II.1.2.input_3D.dat

```
8
25  25  25  8
0.000063
0.01  1  5.0e+9  0.3  3.0
500
0.000126  2  1.0
15e-9  10e+5  0.2  0.3
0.0  0.0  -0.016675  -0 016675  0 0  -0.016675


---------- Structure of data ----------
(units N, m, N/m²)
nod
nxe  nye  nze  nip
dx
mindens  maxdens  emax  v  gama
iteration
Dinfl  ninfe  mechanosensitivity
profactor  threshold  resorptionchance  resorptionamount
ftop(1)  ftop(2)  ftop(3)  fleft(1)  fleft(2)  ffront(2)
```

II.2. Main programs

II.2.1.main_2D.f90

```
PROGRAM main_2D
! -------  ------------  ------------  -----------  ------------  -------------  -------------
! main_2D is a two- diemsional spongy bone remodeling program with uniform osteocyte distribution
!      Four-node rectangular quadrilaterals are used for the finite element analysis  This program
!      reads data from input_2D dat  After calculation, it generates two files  output_2D res and
!      densities_final2D dat  In output_2D res, there are stress and strain at the center of each
!      element, elements' SED and density for some specific iteration  In densities_final2D dat,
!      each element's relative density for the final configuration is listed
!------  ------------------------------------------------------------------  --------------------
 USE main
 USE geom
 IMPLICIT NONE
 INTEGER, PARAMETER  iwp=SELECTED_REAL_KIND(15)
 INTEGER  i, iel, k, ndim=2, ndof, nels, neq, nip, nn, nod, nodof=2, nst=3, nxe, nye,   &
   a, b, al, bl, n, nl, nipcenter, iteration, counter, ninfe, deltaa, deltab, iell,    &
   counter2
 REAL(iwp)  det, one=1 0_iwp, zero=0 0_iwp, dx, dy, tl, delta, mindens, maxdens,   &
   profactor, threshold, resorptionchance, resorptionamount, dinfl, emax, , e, v,  &
   gama, formation, resorption, distance, randnumber, mechanosensitivity
 CHARACTER(LEN=15)  element=' quadrilateral'
!----------------------dynamic arrays------  ------------  -------------  --
 INTEGER, ALLOCATABLE  g( ), g_g( , ), g_num( , ), kdiag( ), nf( , ), no( ),    &
   node( ), num( ), nr( )
 REAL(iwp), ALLOCATABLE  bee( , ), coord( , ), dee( , ), der( , ), deriv( , ),  &
   eld( ), fun( ), gc( , ), g_coord( , ), jac( , ), km( , ), kv( ), loads( ),     &
   loads1( ), points( , ), sigma( ), value( ), weights( ), x_coords( ),          &
   y_coords( ), ftop( ), fbottom( ), fleft( ), fright( ), epsilon1( ),           &
   sed( ), stimulus( ), ostnum( ), dens( ), densities1( )
!----------------------input and initialisation--------------------------
 tl=secnds(0 0)
 counter2=0
 OPEN(10, FILE=' input_2D dat')
 OPEN(11, FILE=' output_2D res')
 open(12, file=' densities_final2D dat')
 READ(10, *) nod, nxe, nye, nip
 read(10, *) dx
 read(10, *) mindens, maxdens, emax, v, gama
 read(10, *) iteration
 read(10, *) Dinfl, ninfe, mechanosensitivity
 read(10, *) profactor, threshold, resorptionchance, resorptionamount
 CALL mesh_size(element, nod, nels, nn, nxe, nye)
 ndof=nod*nodof
 ALLOCATE(nf(nodof, nn), g(ndof), g_coord(ndim, nn), fun(nod), coord(nod, ndim),  &
   jac(ndim, ndim), g_num(nod, nels), der(ndim, nod), deriv(ndim, nod),          &
   bee(nst, ndof), eld(ndof), g_g(ndof, nels), num(nod), x_coords(nxe+1),        &
   y_coords(nye+1), gc(ndim, nels), dee(nst, nst), sigma(nst), ftop(ndim),       &
   fbottom(ndim), fleft(ndim), fright(ndim), epsilon1(nst), ostnum(nels),        &
   dens(nels), nr(2), densities1(31))
```

```
 read(10,*)ftop(1),ftop(2),fleft(1)
 dy=dx
 call coord_xy(x_coords,y_coords,nxe,nye,dx,dy)
 nf=1
 nr(1)=nye*(nxe+1)+1
 nr(2)=(nye+1)*(nxe+1)
 nf(1,nr(1))=0
 nf(2,nr(1))=0
 nf(1,nr(2))=1
 nf(2,nr(2))=0
 CALL formnf(nf)
 neq=MAXVAL(nf)
!----- global node number,nodal and centroid coordinates and g vector -----
!----------------------loop the elements to find global arrays sizes-----
 nipcenter=1
 allocate(points(nipcenter,ndim),weights(nipcenter),kdiag(neq))
 CALL sample(element,points,weights)
 kdiag=0
 elements  DO iel=1,nels
   CALL geom_rect(iel,x_coords,y_coords,coord,num)
   int_points  DO i=1,nipcenter
     call shape_fun(fun,points,i)
     gc(,iel)=matmul(fun,coord)
   end do int_points
   call num_to_g(num,nf,g)
   g_num(,iel)=num
   g_coord(,num)=TRANSPOSE(coord)
   g_g(,iel)=g
   call fkdiag(kdiag,g)
 END DO elements
 DO i=2,neq
   kdiag(i)=kdiag(i)+kdiag(i-1)
 END DO
 WRITE(11,'(2(A,I8))')                                                    &
   " There are",neq," equations and the skyline storage is",kdiag(neq)
!----------------------initial densities---------------------------------
 dens=mindens
 do a=1,nxe,3
   do b=1,nye
     dens((b-1)*nxe+a)=maxdens
   end do
 end do
 do b=1,nye,3
   do a=1,nxe
     dens((b-1)*nxe+a)=maxdens
   end do
 end do
 counter2=counter2+1
 densities1(counter2)=sum(dens)/(nxe*nye)
!----------------------starting loads------------------------------------
 allocate (loads1(0 neq))
 loads1=zero
 fleft(2)=-1*ftop(1)
 fbottom=-1*ftop
 fright=-1*fleft
```

```
!the loads on the top and bottom sides
 do a=2,nxe
   b=1
   n=(b-1)*(nxe+1)+a
   loads1(nf( ,n))=ftop
   b1=nye+1
   n1-(b1-1)*(nxe+1)+a
   loads1(nf( ,n1))=fbottom
 end do
!the loads on the left and right sides
 do b=2,nye
   a=1
   n-(b-1)*(nxe+1)+a
   loads1(nf( ,n))-fleft
   a1=nxe+1
   n1=(b-1)*(nxe+1)+a1
   loads1(nf( ,n1))=fright
 end do
!---------- ------------iterations start------------------------  - --------
 Iterations do counter-1,iteration
   ALLOCATE(loads(0 neq),km(ndof,ndof),kv(kdiag(neq)),sed(nels),stimulus(nels))
   if (counter-=100 or counter==200 or counter=-300 or counter=-400 or counter--500 or       &
       counter==600 or counter--700 or counter--800 or counter==900 or counter=-1000 or      &
       counter==1100 or counter==1200 or counter==1300 or counter=-1400 or counter==1500 or  &
       counter==1600 or counter-=1700 or counter==1800 or counter==1900 or counter-=2000 or  &
       counter==2100 or counter==2200 or counter==2300 or counter--2400 or counter==2500 or  &
       counter==2600 or counter-=2700 or counter--2800 or counter==2900 or counter-=3000)Then
     write(11,'(/A,15)')"Iterations  ",counter
   end if
   loads=loads1                                                          !loads1  starting loads
!-------- --------------element stiffness integration and assembly--------
   deallocate(points,weights)
   allocate(points(nip,ndim),weights(nip))
   CALL sample(element,points,weights)
   kv=zero
   elements_2  DO iel=1,nels
     e=emax*(dens(iel)**gama)
     call deemat(dee,e,v)
     num=g_num( ,iel)
     g=g_g( ,iel)
     coord-TRANSPOSE(g_coord( ,num))
     km-zero
     int_pts_1  DO i-1,nip
       CALL shape_der(der,points,i)
       jac=MATMUL(der,coord)
       det=determinant(jac)
       CALL invert(jac)
       deriv=MATMUL(jac,der)
       CALL beemat(bee,deriv)
       km=km+MATMUL(MATMUL(TRANSPOSE(bee),dee),bee)*det*weights(i)
     END DO int_pts_1
     CALL fsparv(kv,km,g,kdiag)
   END DO elements_2
!-------- --------------equation solution---------------------------- --
   CALL sparin(kv,kdiag)
```

```
  CALL spabac(kv, loads, kdiag)
  loads(0)=zero
  if (counter==100 or counter==200 or counter==300 or counter==400 or counter--500 or       &
      counter--600 or counter==700 or counter--800 or counter==900 or counter==1000 or      &
      counter=-1100 or counter==1200 or counter=-1300 or counter==1400 or counter==1500 or  &
      counter=-1600 or counter==1700 or counter==1800 or counter==1900 or counter==2000 or  &
      counter==2100 or counter==2200 or counter==2300 or counter==2400 or counter==2500 or  &
      counter-=2600 or counter==2700 or counter==2800 or counter==2900 or counter==3000)Then
    WRITE(11,'(/A)')" Node   x-disp      y-disp"
    DO k=1,nn
      WRITE(11,'(I5,2E12 4)')k,loads(nf( ,k))                  !here, loads are displacements
    END DO
  end if
!-----------------------recover stresses at nip integrating points--------
  nipcenter=1
  DEALLOCATE(points,weights)
  ALLOCATE(points(nipcenter,ndim),weights(nipcenter))
  CALL sample(element,points,weights)
  if (counter==100 or counter=-200 or counter==300 or counter==400 or counter--500 or       &
      counter--600 or counter==700 or counter==800 or counter==900 or counter==1000 or      &
      counter==1100 or counter--1200 or counter==1300 or counter--1400 or counter==1500 or  &
      counter=-1600 or counter=-1700 or counter--1800 or counter==1900 or counter==2000 or  &
      counter==2100 or counter==2200 or counter=-2300 or counter==2400 or counter==2500 or  &
      counter--2600 or counter=-2700 or counter--2800 or counter=-2900 or counter=-3000)Then
    WRITE(11,'(/A,I2,A)')" The integration point (nip=",nipcenter,") stresses/strain are "
    WRITE(11,'(A,A,A)')" Element x-coord     y-coord",                                     &
      "      sig_x       sig_y       tau_xy" ,                                            &
      "      eps_x       eps_y       eps_xy"
  end if
  elements_3  DO iel=1,nels
    e=emax*(dens(iel)**gama)
    call deemat(dee,e,v)
    num=g_num( ,iel)
    coord-TRANSPOSE(g_coord( ,num))
    g=g_g( ,iel)
    eld-loads(g)
    int_pts_2  DO i=1,nipcenter
      CALL shape_der(der,points,i)
      jac=MATMUL(der,coord)
      CALL invert(jac)
      deriv=MATMUL(jac,der)
      CALL beemat(bee,deriv)
      epsilon1=matmul(bee,eld)
      sigma=MATMUL(dee,epsilon1)
      sed(iel)=0 5*(sigma(1)*epsilon1(1)+sigma(2)*epsilon1(2)+sigma(3)*epsilon1(3))
      if (counter==100 or counter==200 or counter==300 or counter--400 or counter==500 or       &
          counter=-600 or counter==700 or counter--800 or counter==900 or counter==1000 or      &
          counter==1100 or counter--1200 or counter==1300 or counter==1400 or counter==1500 or  &
          counter==1600 or counter==1700 or counter==1800 or counter=-1900 or counter==2000 or  &
          counter==2100 or counter==2200 or counter==2300 or counter==2400 or counter==2500 or  &
          counter==2600 or counter=-2700 or counter==2800 or counter==2900 or counter==3000)Then
        WRITE(11,'(I5,8E12 4)')iel,gc( ,iel),sigma,epsilon1
      end if
    END DO int_pts_2
  END DO elements_3
```

```
  if (counter==100 or counter==200 or counter==300 or counter==400 or counter==500 or       &
      counter==600 or counter==700 or counter==800 or counter==900 or counter==1000 or      &
      counter==1100 or counter==1200 or counter==1300 or counter==1400 or counter==1500 or  &
      counter==1600 or counter==1700 or counter==1800 or counter==1900 or counter==2000 or  &
      counter==2100 or counter==2200 or counter==2300 or counter==2400 or counter==2500 or  &
      counter==2600 or counter==2700 or counter==2800 or counter==2900 or counter==3000)Then
    write(11,'(/A)')"Strain Energy Density "
    WRITE(11,'(8E12.4)')sed
  end if
!  ---------- - -------calculate stimulus--- -- ----------  ---
  ostnum=1.0
  stimulus=0.0
  do a=1,nxe
    do b=1,nye
      iel=(b-1)*nxe+a
      do deltaa=-1*ninfe,ninfe
        do deltab=-1*ninfe,ninfe
          if ((a+deltaa)>=1 and (a+deltaa)<=nxe)Then
            if ((b+deltab)>=1 and (b+deltab)<=nye)Then
              iel1=(b+deltab-1)*nxe+(a+deltaa)
              distance=sqrt((gc(1,iel)-gc(1,iel1))**2.0+(gc(2,iel)-gc(2,iel1))**2.0)
              if (distance<=Dinfl)Then
                stimulus(iel)=stimulus(iel)+mechanosensitivity*ostnum(iel1)*sed(iel1)      &
                              *exp(-1*distance/Dinfl)
              end if
            end if
          end if
        end do
      end do
    end do
  end do
  if (counter==100 or counter==200 or counter==300 or counter==400 or counter==500 or       &
      counter==600 or counter==700 or counter==800 or counter==900 or counter==1000 or      &
      counter==1100 or counter==1200 or counter==1300 or counter==1400 or counter==1500 or  &
      counter==1600 or counter==1700 or counter==1800 or counter==1900 or counter==2000 or  &
      counter==2100 or counter==2200 or counter==2300 or counter==2400 or counter==2500 or  &
      counter==2600 or counter==2700 or counter==2800 or counter==2900 or counter==3000)Then
    write(11,'(/A)')"Stimulus "
    write(11,'(8e12.4)')stimulus
  end if
!---------- ----------  update densities----------  ----------
  call random_seed()
  do a=2,(nxe-1)
    do b=2,(nye-1)
      iel=(b-1)*nxe+a
      formation=0.0
      resorption=0.0
      if ((dens(iel)<maxdens and dens(iel)>=mindens) or                &
          ((iel+1<=nels and dens(iel+1)==maxdens) or                   &
          (iel-1>0 and dens(iel-1)==maxdens) or                        &
          (iel+nxe<=nels and dens(iel+nxe)==maxdens) or                &
          (iel-nxe>0 and dens(iel-nxe)==maxdens)))Then
        if (stimulus(iel)>threshold)Then
          formation=profactor*(stimulus(iel)-threshold)
        end if
```

```
        end if
        if ((dens(iel)<=maxdens and dens(iel)>mindens) or              &
            ((iel+1<=nels and dens(iel+1)<0 4) or                      &
            (iel-1>0 and dens(iel-1)<0 4) or                           &
            (iel+nxe<=nels and dens(iel+nxe)<0 4) or                   &
            (iel-nxe>0 and dens(iel-nxe)<0 4)))Then
          call random_number(randnumber)
          if (randnumber<=resorptionchance)Then
            resorption=resorptionamount
          end if
        end if
        dens(iel)=dens(iel)+formation-resorption
        if (dens(iel)<mindens) dens(iel)=mindens
        if (dens(iel)>maxdens) dens(iel)=maxdens
      end do
    end do
    if (counter=-100 or counter=-200 or counter--300 or counter==400 or counter==500 or      &
        counter==600 or counter==700 or counter==800 or counter--900 or counter--1000 or     &
        counter=-1100 or counter-=1200 or counter=-1300 or counter==1400 or counter=-1500 or &
        counter==1600 or counter=-1700 or counter==1800 or counter==1900 or counter==2000 or &
        counter--2100 or counter==2200 or counter-=2300 or counter=-2400 or counter==2500 or &
        counter=-2600 or counter--2700 or counter=-2800 or counter==2900 or counter==3000)Then
      write(11,'(/A)')'Densities "
      write(11,'(8f12 3)')dens
      counter2-counter2+1
      densities1(counter2)=sum(dens)/(nxe*nye)
    end if
!
    deallocate(loads, km, kv, sed, stimulus)
  end do iterations
! -------- ---------------- ------  -------- ------------------ ------- --
  write(11,'(/A)')"Relative Density "
  write(11,'(8f12 4)')densities1
  write(12,'(f12 3)')dens
  delta=secnds(t1)
  write(11,'(/A,f12 3,A)')"The analysis took",delta,"s "
  STOP
END PROGRAM main_2D
```

II.2.2.main_3D.f90

```
PROGRAM main_3D
!-----------------------------------------------------------------------------------------------
! main_3D is a three- diemsional spongy bone remodeling program with uniform osteocyte distribution
!       Eight-node cubic elements are used for the finite element analysis  This program reads data
!       from input_3D dat  After calculation, it generates two files  output_3D res and
!       densities_final3D dat  In output_3D res, there are stress and strain at the center of each
!       element, elements' SED and density for some specific iteration  In densities_final3D dat,
!       each element's relative density for the final configuration is listed
!-----------------------------------------------------------------------------------------------
 USE main
 USE geom
 IMPLICIT NONE
 INTEGER, PARAMETER  iwp=SELECTED_REAL_KIND(15)
 INTEGER  i, iel, k, ndim=3, ndof, nels, neq, nip, nn, loaded_nodes, nod, nodof=3,    &
   nod, nodof-3, nst=6, nxe, nye, nze, ninfle, a, b, c, al, bl, cl, kl, nipcenter,    &
   counter, iteration, ninfe, deltaa, deltab, deltac, iell, counter2
 REAL(iwp)  det, zero=0 0_iwp, dx, dy, dz, Dinfl, mindens, maxdens, v, distance,    &
   resorptionchance, threshold, resorptionamount, profactor, formation, gama,    &
   formation, resorption, randnumber, tl, delta, mechanosensitivity, emax, e
 CHARACTER(LEN=15)  element='hexahedron'
!-----------------------dynamic arrays---------------- -  ---------------
 INTEGER, ALLOCATABLE  g( ), g_g( , ), g_num( , ), kdiag( ), nf( , ), num( ),    &
   nr( )
 REAL(iwp), ALLOCATABLE  bee( , ), coord( , ), dee( , ), der( , ), deriv( , ),  &
   eld( ), fun( ), gc( , ), g_coord( , ), jac( , ), km( , ), kv( ), loads( ),    &
   loadsl( ), points( , ), sigma( ), value( ), weights( ), x_coords( ),          &
   y_coords( ), z_coords( ), epsilonl( ), dens( ), sed( ), ostnum( ),            &
   stimulus( ), ftop( ), fbottom( ), fleft( ), fright( ), ffront( ), fback( ),   &
   densitiesl( )
!- ----------------- ----input and initialisation---------- --------------
 tl=secnds(0 0)
 counter2=0
 OPEN(10, FILE='input_3D dat')
 OPEN(11, FILE='output_3D res')
 OPEN(12, FILE='densities_final3D res')
 READ(10, *)nod, nxe, nye, nze, nip
 read(10, *)dx
 read(10, *)mindens, maxdens, emax, v, gama
 read(10, *)iteration
 read(10, *)Dinfl, ninfe, mechanosensitivity
 read(10, *)profactor, threshold, resorptionchance, resorptionamount
 CALL mesh_size(element, nod, nels, nn, nxe, nye, nze)  !generate "nels" and "nn"
ndof=nod*nodof
 ALLOCATE(nf(nodof, nn), dee(nst, nst), coord(nod, ndim), jac(ndim, ndim),       &
   der(ndim, nod), deriv(ndim, nod), g(ndof), bee(nst, ndof), eld(ndof),         &
   sigma(nst), g_g(ndof, nels), g_coord(ndim, nn), g_num(nod, nels), num(nod),   &
   x_coords(nxe+1), y_coords(nye+1), z_coords(nze+1), fun(nod),                  &
   gc(ndim, nels), ostnum(nels), dens(nels), epsilonl(nst), ftop(ndim),          &
   fbottom(ndim), fleft(ndim), fright(ndim), ffront(ndim), fback(ndim), nr(4),   &
   densitiesl(15))
 read(10, *)ftop(1), ftop(2), ftop(3), fleft(1), fleft(2), ffront(2)
```

```
dy=dx
dz=dx
call coord_xyz(x_coords, y_coords, z_coords, nxe, nye, nze, dx, dy, dz)
nf=1
nr(1)=nze*(nxe+1)+1
nr(2)=(nze+1)*(nxe+1)
nr(3)=(nze+1)*(nxe+1)*(nye+1)-nxe
nr(4)=(nze+1)*(nxe+1)*(nye+1)
nf(1,nr(1))=0
nf(2,nr(1))=0
nf(3,nr(1))=0
nf(1,nr(2))=1
nf(2,nr(2))=0
nf(3,nr(2))=0
nf(1,nr(3))=0
nf(2,nr(3))=1
nf(3,nr(3))=0
nf(1,nr(4))=1
nf(2,nr(4))=1
nf(3,nr(4))=0
CALL formnf(nf)
neq=MAXVAL(nf)
!----- global node number, nodal and centroid coordinates and g vector -   -
!-------------  ------loop the elements to find global arrays sizes-----
nipcenter=1
allocate(points(nipcenter,ndim),weights(nipcenter),kdiag(neq))
call sample(element,points,weights)
kdiag=0
elements_1  DO iel=1,nels
  CALL hexahedron_xz(iel,x_coords,y_coords,z_coords,coord,num)
  gauss_pts_1  DO i=1,nipcenter
    CALL shape_fun(fun,points,i)
    gc(,iel)=matmul(fun,coord)
  END DO gauss_pts_1
  CALL num_to_g(num,nf,g)
  g_num(,iel)=num                    !num  element node number vector
  g_coord(,num)=TRANSPOSE(coord)     !coord   element nodal coordinates
  g_g(,iel)=g
  call fkdiag(kdiag,g)
END DO elements_1
DO i=2,neq
  kdiag(i)=kdiag(i)+kdiag(i-1)
END DO
WRITE(11,'(2(A,I12))')                                                    &
  " There are",neq," equations and the skyline storage is",kdiag(neq)
!-----  ---------------  initial element relative density -----------------
dens=mindens
do a=1,nxe
  do b=1,nze,3
    do c=1,nye,3
      dens((c-1)*nxe*nze+(b-1)*nxe+a)=maxdens
    end do
  end do
end do
do b=1,nze
```

```
    do a=1,nxe,3
      do c=1,nze,3
        dens((c-1)*nxe*nze+(b-1)*nxe+a)=maxdens
      end do
    end do
  end do
  do c=1,nye
    do a=1,nxe,3
      do b=1,nze,3
        dens((c-1)*nxe*nze+(b-1)*nxe+a)=maxdens
      end do
    end do
  end do
   do a=1,nxe
    do b=1,nze
      dens((b-1)*nxe+a)=maxdens
      dens((nye 1)*nxe*nze+(b-1)*nxe+a)=maxdens
    end do
  end do
  do a=1,nxe
    do c=1,nye
      dens((c-1)*nxe*nze+a)=maxdens
      dens((c 1)*nxe*nze+(nze-1)*nxe+a)=maxdens
    end do
  end do
  do b=1,nze
    do c=1,nye
      dens((c-1)*nxe*nze+(b-1)*nxe+1)=maxdens
      dens((c-1)*nxe*nze+(b-1)*nxe+nxe)=maxdens
    end do
  end do
  counter2=counter2+1
  densities1(counter2)=sum(dens)/(nxe*nye*nze)
!--------  -------------iterations start---------------   -----------------
  Iterations do counter=1,iteration
    if (counter==50 or counter==100 or counter==150 or counter==200 or counter==250 or  &
      counter==300 or counter==350 or counter==400 or counter==450 or counter==500 or   &
      counter==550 or counter==600 or counter==650 or counter==700)Then
      write(11,'(/A,15)')"Iteration  ",counter
    end if
    ALLOCATE(loads(0 neq),km(ndof,ndof),kv(kdiag(neq)),sed(nels),stimulus(nels))
!-----------------------starting loads----------------- -----------------
    loads=zero
    fleft(3)=-1*ftop(1)
    ffront(1)=fleft(2)
    ffront(3)=-1*ftop(2)
    fbottom=-1*ftop
    fright=-1*fleft
    fback=-1*ffront
!the loads in the top and bottom surfaces
    do a=2,nxe
      do c=2,nye
        b=1
        k=(c-1)*(nxe+1)*(nze+1)+(b-1)*(nxe+1)+a
        loads(nf( ,k))=ftop
```

```
      b1=nze+1
      k1=(c-1)*(nxe+1)*(nze+1)+(b1-1)*(nxe+1)+a
      loads(nf( ,k1))=fbottom
    end do
  end do
!the loads in the left and right surfaces
  do b=2,nze
    do c=2,nye
      a=1
      k=(c-1)*(nxe+1)*(nze+1)+(b-1)*(nxe+1)+a
      loads(nf( ,k))=fleft
      a1=nxe+1
      k1=(c-1)*(nxe+1)*(nze+1)+(b-1)*(nxe+1)+a1
      loads(nf( ,k1))=fright
    end do
  end do
!the loads in the front and back surfaces
  do a=2,nxe
    do b=2,nze
      c=1
      k=(c-1)*(nxe+1)*(nze+1)+(b-1)*(nxe+1)+a
      loads(nf( ,k))=ffront
      c1=nye+1
      k1=(c1-1)*(nxe+1)*(nze+1)+(b-1)*(nxe+1)+a
      loads(nf( ,k1))=fback
    end do
  end do
!----------------------element stiffness integration and assembly--------
  deallocate(points,weights)
  allocate(points(nip,ndim),weights(nip))
  CALL sample(element,points,weights)
  kv=zero
  elements_2: DO iel=1,nels
    e=emax*(dens(iel)**gama)
    call deemat(dee,e,v)
    num=g_num( ,iel)
    g=g_g( ,iel)
    coord=TRANSPOSE(g_coord( ,num))
    km=zero
    gauss_pts_2  DO i=1,nip
      CALL shape_der(der,points,i)
      jac=MATMUL(der,coord)
      det=determinant(jac)
      CALL invert(jac)
      deriv=MATMUL(jac,der)
      CALL beemat(bee,deriv)
      km=km+MATMUL(MATMUL(TRANSPOSE(bee),dee),bee)*det*weights(i)
    END DO gauss_pts_2
    CALL fsparv(kv,km,g,kdiag)
  END DO elements_2
!-----------------------equation solution-----------------------------------
  CALL sparin(kv,kdiag)
  CALL spabac(kv,loads,kdiag)
  loads(0)=zero
  if (counter==50 or.counter==100.or counter==150.or.counter==200.or.counter==250.or. &
```

```
    counter==300. or. counter==350. or. counter==400 or. counter==450 or. counter==500. or.  &
    counter==550. or counter==600. or. counter==650. or. counter==700) Then
    WRITE(11,'(/A)')"  Node    x-disp       y-disp       z-disp"
    DO k=1,nn
      WRITE(11,'(I8,3E12.4)')k,loads(nf(:,k))
    END DO
  end if
!-----------------------recover stresses at nip integrating points--------
  nipcenter=1
  DEALLOCATE(points,weights)
  ALLOCATE(points(nipcenter,ndim),weights(nipcenter))
  CALL sample(element,points,weights)
  if (counter==50. or. counter==100. or. counter==150 or counter==200 or counter==250 or. &
    counter==300. or. counter==350. or counter==400 or counter==450. or. counter==500 or.  &
    counter==550. or. counter==600. or counter==650. or. counter==700) Then
    WRITE(11,'(/A,I2,A)')" The integration point (nip=",nipcenter,") stresses/strains are."
    WRITE(11,'(/A,/,A,/,A)')"    Element     x-coord     y-coord     z-coord",     &
      "     sig_x       sig_y       sig_z       tau_xy      tau_yz      tau_zx",     &
      "     eps_x       eps_y       eps_z       eps_xy      eps_yz      eps_zx"
  end if
  elements_3  DO iel=1,nels
    e=emax*(dens(iel)**gama)
    call deemat(dee,e,v)
    num=g_num(:,iel)
    coord=TRANSPOSE(g_coord(:,num))
    g=g_g(:,iel)
    eld=loads(g)
    gauss_pts_3: DO i=1,nipcenter
      CALL shape_der(der,points,i)
      jac=MATMUL(der,coord)
      CALL invert(jac)
      deriv=MATMUL(jac,der)
      CALL beemat(bee,deriv)
      epsilon1=matmul(bee,eld)
      sigma=MATMUL(dee,epsilon1)
      sed(iel)=0.5*(sigma(1)*epsilon1(1)+sigma(2)*epsilon1(2)+sigma(3)*epsilon1(3)  &
               +sigma(4)*epsilon1(4)+sigma(5)*epsilon1(5)+sigma(6)*epsilon1(6))
      if (counter==50. or. counter==100. or. counter==150. or. counter==200. or. counter==250. or. &
        counter==300 or. counter==350. or counter==400. or. counter==450 or. counter==500. or. &
        counter==550. or. counter==600. or. counter==650 or counter==700) Then
        WRITE(11,'(I8,4X,3E12.4)')iel,gc(:,iel)
        WRITE(11,'(6E12.4)')sigma
        write(11,'(6e12.4)')epsilon1
      end if
    END DO gauss_pts_3
  END DO elements_3
  if (counter==50. or. counter==100. or. counter==150. or. counter==200. or counter==250. or. &
    counter==300. or. counter==350. or. counter==400. or counter==450. or. counter==500 or. &
    counter==550 or. counter==600. or. counter==650. or. counter==700) Then
    write(11,'(/A)')"Strain energy densityies."
    write(11,'(8e12.4)')sed
  end if
!-------------------------calculate stimulus--------------------------
  ostnum=11
  stimulus=zero
```

```
  do a=1,nxe
    do b=1,nze
      do c=1,nye
        iel=(c-1)*nxe*nze+(b-1)*nxe+a
        do deltaa=-1*ninfe,ninfe
          do deltab=-1*ninfe,ninfe
            do deltac=-1*ninfe,ninfe
              if ((a+deltaa)>=1 and. (a+deltaa)<=nxe)Then
                if ((b+deltab)>=1. and. (b+deltab)<=nze)Then
                  if ((c+deltac)>=1. and. (c+deltac)<=nye)Then
                    iell=(c+deltac-1)*nxe*nze+(b+deltab-1)*nxe+(a+deltaa)
                    distance=sqrt((gc(1,iel)-gc(1,iell))**2 0+(gc(2,iel)-gc(2,iell))**2 0+    &
                                  (gc(3,iel)-gc(3,iell))**2.0)
                    if (distance<=Dinfl)Then
                      stimulus(iel)=stimulus(iel)+mechanosensitivity*ostnum(iell)*sed(iell)*  &
                                    exp(-1*distance/Dinfl)
                    end if
                  end if
                end if
              end if
            end do
          end do
        end do
      end do
    end do
  end do
  if (counter==50 or. counter==100. or counter==150. or. counter==200. or. counter==250. or          &
    counter==300. or. counter==350. or counter==400. or. counter==450. or. counter==500. or          &
    counter==550 or. counter==600. or. counter==650. or counter==700)Then
    write(11,'(/A)')"Stimulus·"
    write(11,'(8e12.4)')stimulus
  end if
!-----------------------------update density-----------------------------
  do a=2,(nxe-1)
    do b=2,(nze-1)
      do c=2,(nye-1)
        iel=(c-1)*nxe*nze+(b-1)*nxe+a
        formation=0.0
        resorption=0.0
        if ((dens(iel)<maxdens. and. dens(iel)>=mindens). or.                &
            (iel+1<=nels. and. dens(iel+1)==maxdens). or.                    &
            (iel-1>0. and. dens(iel-1)==maxdens). or.                        &
            (iel+nxe<=nels. and. dens(iel+nxe)==maxdens). or.                &
            (iel-nxe>0. and. dens(iel-nxe)==maxdens). or.                    &
            (iel+nxe*nze<=nels and. dens(iel+nxe*nze)==maxdens). or          &
            (iel-nxe*nze>0. and. dens(iel-nxe*nze)==maxdens))Then
          if (stimulus(iel)>threshold)Then
            formation=profactor*(stimulus(iel)-threshold)
          end if
        end if
        if ((dens(iel)<=maxdens. and. dens(iel)>mindens). or                 &
            (iel+1<=nels. and. dens(iel+1)<0 4) or                           &
            (iel-1>0. and. dens(iel-1)<0.4). or                              &
            (iel+nxe<=nels and. dens(iel+nxe)<0 4). or                       &
            (iel-nxe>0. and. dens(iel-nxe)<0 4). or                          &
```

```
            (iel+nxe*nze<=nels.and.dens(iel+nxe*nze)<0.4).or.              &
            (iel-nxe*nze>0.and.dens(iel-nxe*nze)<0.4))Then
          call random_number(randnumber)
          if (randnumber<=resorptionchance)Then
            resorption=resorptionamount
          end if
        end if
        dens(iel)=dens(iel)+formation-resorption
        if (dens(iel)<mindens) dens(iel)=mindens
        if (dens(iel)>maxdens) dens(iel)=maxdens
      end do
    end do
  end do
  if (counter==50.or.counter==100.or.counter==150.or.counter==200.or.counter==250.or. &
    counter==300.or.counter==350.or.counter==400.or.counter==450.or.counter==500.or. &
    counter==550.or.counter==600.or.counter==650.or.counter==700)Then
    write(11,'(/A)')"Densities:"
    write(11,'(8f12.4)')dens
    counter2=counter2+1
    densitiesl(counter2)=sum(dens)/(nxe*nye*nze)
  end if
  deallocate(loads,km,kv,sed,stimulus)
  write(*,*)counter
 end do Iterations
!-------------------------------------------------------------------------------
 write(11,'(/A)')"Relative Density:"
 write(11,'(8f12.3)')densitiesl
 write(12,'(f12.3)')dens
 delta=secnds(t1)
 write(11,'(/A,f12.3,A)')"The analysis took",delta,"s."
 STOP
END PROGRAM main_3D
```

II.3. Subroutines

II.3.1.main.f90

```
MODULE main
!
contains
!
SUBROUTINE beemat(bee,deriv)
!
! This subroutine forms the bee matrix in 2-d (ih=3 or 4) or 3-d (ih=6)
!
 IMPLICIT NONE
 INTEGER,PARAMETER  iwp=SELECTED_REAL_KIND(15)
 REAL(iwp),INTENT(IN)  deriv( , )
 REAL(iwp),INTENT(OUT)  bee( , )
 INTEGER  k,l,m,n,ih,nod
 REAL  x,y,z
 bee=0 0_iwp
 ih-UBOUND(bee,1)
 nod=UBOUND(deriv,2)
 SELECT CASE (ih)
 CASE(3,4)
   DO m-1,nod
     k=2*m
     l-k 1
     x=deriv(1,m)
     y=deriv(2,m)
     bee(1,1)=x
     bee(3,k)=x
     bee(2,k)=y
     bee(3,1)=y
   END DO
 CASE(6)
   DO m=1,nod
     n-3*m
     k=n-1
     l=k-1
     x=deriv(1,m)
     y=deriv(2,m)
     z=deriv(3,m)
     bee(1,1)=x
     bee(4,k)=x
     bee(6,n)=x
     bee(2,k)=y
     bee(4,1)=y
     bee(5,n)=y
     bee(3,n)=z
     bee(5,k)=z
     bee(6,1)=z
   END DO
 CASE DEFAULT
```

```
   WRITE(*,*)'wrong dimension for nst in bee matrix'
 END SELECT
RETURN
END SUBROUTINE beemat
!
!
SUBROUTINE deemat(dee,e,v)
!
! This subroutine returns the elastic dee matrix for ih=3 (plane strain),
! ih=4 (axisymmetry or plane strain elastoplasticity) or ih=6
! (three dimensions)
!
 IMPLICIT NONE
 INTEGER,PARAMETER  iwp=SELECTED_REAL_KIND(15)
 REAL(iwp),INTENT(IN)  e,v
 REAL(iwp),INTENT(OUT)  dee( , )
 REAL(iwp)  v1,v2,c,vv,zero=0 0_iwp,pt5=0 5_iwp,one=1 0_iwp,two=2 0_iwp
 INTEGER  i,ih
 dee=zero
 ih=UBOUND(dee,1)
 v1=one-v
 c=e/((one+v)*(one-two*v))
 SELECT CASE(ih)
 CASE(3)
   dee(1,1)=v1*c
   dee(2,2)=v1*c
   dee(1,2)=v*c
   dee(2,1)=v*c
   dee(3,3)=pt5*c*(one-two*v)
 CASE(4)
   dee(1,1)=v1*c
   dee(2,2)=v1*c
   dee(4,4)=v1*c
   dee(3,3)=pt5*c*(one-two*v)
   dee(1,2)=v*c
   dee(2,1)=v*c
   dee(1,4)=v*c
   dee(4,1)=v*c
   dee(2,4)=v*c
   dee(4,2)=v*c
 CASE(6)
   v2=v/(one-v)
   vv=(one-two*v)/(one-v)*pt5
   DO i=1,3
     dee(i,i)=one
   END DO
   DO i=4,6
     dee(i,i)=vv
   END DO
   dee(1,2)=v2
   dee(2,1)=v2
   dee(1,3)=v2
   dee(3,1)=v2
   dee(2,3)=v2
   dee(3,2)=v2
```

```
    dee=dee*e/(two*(one+v)*vv)
  CASE DEFAULT
    WRITE(*,*)'wrong size for dee matrix'
  END SELECT
RETURN
END SUBROUTINE deemat
!
!
FUNCTION determinant(jac)RESULT(det)
!
! This function returns the determinant of a 1x1, 2x2 or 3x3
! Jacobian matrix
!
  IMPLICIT NONE
  INTEGER,PARAMETER  iwp=SELECTED_REAL_KIND(15)
  REAL(iwp),INTENT(IN)  jac( , )
  REAL(iwp)  det
  INTEGER  it
  it=UBOUND(jac,1)
  SELECT CASE(it)
  CASE(1)
    det=1.0_iwp
  CASE(2)
    det=jac(1,1)*jac(2,2)-jac(1,2)*jac(2,1)
  CASE(3)
    det=jac(1,1)*(jac(2,2)*jac(3,3)-jac(3,2)*jac(2,3))
    det=det-jac(1,2)*(jac(2,1)*jac(3,3)-jac(3,1)*jac(2,3))
    det=det+jac(1,3)*(jac(2,1)*jac(3,2)-jac(3,1)*jac(2,2))
  CASE DEFAULT
    WRITE(*,*)' wrong dimension for Jacobian matrix'
  END SELECT
RETURN
END FUNCTION determinant
!
!
SUBROUTINE fkdiag(kdiag,g)
!
! This subroutine computes the skyline profile
!
  IMPLICIT NONE
  INTEGER,INTENT(IN)  g( )
  INTEGER,INTENT(OUT)  kdiag( )
  INTEGER  idof,i,iwpl,j,im,k
  idof=SIZE(g)
  DO i=1,idof
    iwpl=1
    IF(g(i)/=0)THEN
      DO j=1,idof
        IF(g(j)/=0)THEN
          im=g(i)-g(j)+1
          IF(im>iwpl)iwpl=im
        END IF
      END DO
      k=g(i)
      IF(iwpl>kdiag(k))kdiag(k)=iwpl
```

```
    END IF
  END DO
RETURN
END SUBROUTINE fkdiag
!
!
SUBROUTINE formnf(nf)
!
! This subroutine forms the nf matrix
!
 IMPLICIT NONE
 INTEGER, INTENT(IN OUT)  nf( , )
 INTEGER  i, j, m
 m=0
 DO j=1, UBOUND(nf, 2)
   DO i=1, UBOUND(nf, 1)
     IF(nf(i, j)/=0) THEN
       m=m+1
       nf(i, j)=m
     END IF
   END DO
 END DO
RETURN
END SUBROUTINE formnf
!
!
SUBROUTINE fsparv(kv, km, g, kdiag)
!
! This subroutine assembles element matrices into a symmetric skyline
! global matrix
!
 IMPLICIT NONE
 INTEGER, PARAMETER  iwp=SELECTED_REAL_KIND(15)
 INTEGER, INTENT(IN)  g( ), kdiag( )
 REAL(iwp), INTENT(IN)  km( , )
 REAL(iwp), INTENT(OUT)  kv( )
 INTEGER  i, idof, k, j, iw, ival
 idof=UBOUND(g, 1)
 DO i=1, idof
   k=g(i)
   IF(k/=0) THEN
     DO j=1, idof
       IF(g(j)/=0) THEN
         iw=k-g(j)
         IF(iw>=0) THEN
           ival=kdiag(k)-iw
           kv(ival)=kv(ival)+km(i, j)
         END IF
       END IF
     END DO
   END IF
 END DO
RETURN
END SUBROUTINE fsparv
!
```

```
!
SUBROUTINE invert(matrix)
!
! This subroutine inverts a small square matrix onto itself
!
 IMPLICIT NONE
 INTEGER,PARAMETER  iwp=SELECTED_REAL_KIND(15)
 REAL(iwp),INTENT(IN OUT)  matrix( , )
 REAL(iwp)  det,j11,j12,j13,j21,j22,j23,j31,j32,j33,con
 INTEGER  ndim,i,k
 ndim=UBOUND(matrix,1)
 IF(ndim==2)THEN
   det=matrix(1,1)*matrix(2,2)-matrix(1,2)*matrix(2,1)
   j11=matrix(1,1)
   matrix(1,1)=matrix(2,2)
   matrix(2,2)=j11
   matrix(1,2)=-matrix(1,2)
   matrix(2,1)=-matrix(2,1)
   matrix=matrix/det
 ELSE IF(ndim==3)THEN
   det=matrix(1,1)*(matrix(2,2)*matrix(3,3)-matrix(3,2)*matrix(2,3))
   det=det-matrix(1,2)*(matrix(2,1)*matrix(3,3) matrix(3,1)*matrix(2,3))
   det=det+matrix(1,3)*(matrix(2,1)*matrix(3,2)-matrix(3,1)*matrix(2,2))
   j11=matrix(2,2)*matrix(3,3)-matrix(3,2)*matrix(2,3)
   j21=-matrix(2,1)*matrix(3,3)+matrix(3,1)*matrix(2,3)
   j31=matrix(2,1)*matrix(3,2)-matrix(3,1)*matrix(2,2)
   j12=-matrix(1,2)*matrix(3,3)+matrix(3,2)*matrix(1,3)
   j22=matrix(1,1)*matrix(3,3)-matrix(3,1)*matrix(1,3)
   j32=-matrix(1,1)*matrix(3,2)+matrix(3,1)*matrix(1,2)
   j13=matrix(1,2)*matrix(2,3)-matrix(2,2)*matrix(1,3)
   j23=-matrix(1,1)*matrix(2,3)+matrix(2,1)*matrix(1,3)
   j33=matrix(1,1)*matrix(2,2)-matrix(2,1)*matrix(1,2)
   matrix(1,1)=j11
   matrix(1,2)=j12
   matrix(1,3)=j13
   matrix(2,1)=j21
   matrix(2,2)=j22
   matrix(2,3)=j23
   matrix(3,1)=j31
   matrix(3,2)=j32
   matrix(3,3)=j33
   matrix=matrix/det
 ELSE
   DO k=1,ndim
     con=matrix(k,k)
     matrix(k,k)=1 0_iwp
     matrix(k, )=matrix(k, )/con
     DO i=1,ndim
       IF(i/=k)THEN
         con=matrix(i,k)
         matrix(i,k)=0 0_iwp
         matrix(i, )=matrix(i, )-matrix(k, )*con
       END IF
     END DO
   END DO
```

```
 END IF
RETURN
END SUBROUTINE invert
!
!
SUBROUTINE num_to_g(num,nf,g)
!
! This subroutine finds the g vector from num and nf
!
 IMPLICIT NONE
 INTEGER,INTENT(IN)  num( ),nf( , )
 INTEGER,INTENT(OUT)  g( )
 INTEGER  i,k,nod,nodof
 nod=UBOUND(num,1)
 nodof=UBOUND(nf,1)
 DO i=1,nod
   k=i*nodof
   g(k-nodof+1 k)=nf( ,num(i))
 END DO
RETURN
END SUBROUTINE num_to_g
!
!
SUBROUTINE sample(element,s,wt)
!
! This subroutine returns the local coordinates and weighting coefficients
! of the integrating points
!
 IMPLICIT NONE
 INTEGER,PARAMETER  iwp=SELECTED_REAL_KIND(15)
 REAL(iwp),INTENT(OUT)  s( , )
 REAL(iwp),INTENT(OUT),OPTIONAL  wt( )
 CHARACTER(*),INTENT(IN)  element
 INTEGER  nip
 REAL(iwp)  root3,r15,w(3),v(9),b,c
 root3=1 0_iwp/SQRT(3 0_iwp)
 r15=0 2_iwp*SQRT(15 0_iwp)
 nip=UBOUND(s,1)
 w=(/5 0_iwp/9 0_iwp,8 0_iwp/9 0_iwp,5 0_iwp/9 0_iwp/)
 v=(/5 0_iwp/9 0_iwp*w,8 0_iwp/9 0_iwp*w,5 0_iwp/9 0_iwp*w/)
 SELECT CASE(element)
 CASE('quadrilateral')
   SELECT CASE(nip)
   CASE(1)
     s(1,1)=0 0_iwp
     s(1,2)=0 0_iwp
     wt(1)=4 0_iwp
   CASE(4)
     s(1,1)=-root3
     s(1,2)= root3
     s(2,1)- root3
     s(2,2)= root3
     s(3,1)=-root3
     s(3,2)=-root3
     s(4,1)- root3
```

```
      s(4,2)=-root3
      wt=1.0_iwp
    CASE DEFAULT
      WRITE(*,*)"wrong number of integrating points for a quadrilateral"
    END SELECT
CASE('hexahedron')
    SELECT CASE(nip)
    CASE(1)
      s(1,1:3)=0.0_iwp
      wt(1)=8.0_iwp
    CASE(8)
      s(1,1)= root3
      s(1,2)= root3
      s(1,3)= root3
      s(2,1)= root3
      s(2,2)= root3
      s(2,3)=-root3
      s(3,1)= root3
      s(3,2)=-root3
      s(3,3)= root3
      s(4,1)= root3
      s(4,2)=-root3
      s(4,3)=-root3
      s(5,1)=-root3
      s(5,2)= root3
      s(5,3)= root3
      s(6,1)=-root3
      s(6,2)=-root3
      s(6,3)= root3
      s(7,1)=-root3
      s(7,2)= root3
      s(7,3)=-root3
      s(8,1)=-root3
      s(8,2)=-root3
      s(8,3)=-root3
      wt=1.0_iwp
    CASE DEFAULT
      WRITE(*,*)"wrong number of integrating points for a hexahedron"
    END SELECT
 CASE DEFAULT
    WRITE(*,*)"not a valid element type"
 END SELECT
RETURN
END SUBROUTINE sample
!
!
SUBROUTINE shape_der(der,points,i)
!
!   This subroutine produces derivatives of shape functions with respect
!   to local coordinates.
!
 IMPLICIT NONE
 INTEGER,PARAMETER::iwp=SELECTED_REAL_KIND(15)
 INTEGER,INTENT(IN)::i
 REAL(iwp),INTENT(IN)::points(:,:)
```

```
REAL(iwp), INTENT(OUT)  der( , )
REAL(iwp)  eta, x1, zeta, x10, eta0, zeta0, etam, etap, x1m, x1p, c1, c2, c3
REAL(iwp)  t1, t2, t3, t4, t5, t6, t7, t8, t9, x2p1, x2m1, e2p1, e2m1, zetam, zetap
REAL, PARAMETER  zero=0.0_iwp, pt125=0.125_iwp, pt25=0.25_iwp, pt5=0.5_iwp,   &
  pt75=0.75_iwp, one=1.0_iwp, two=2.0_iwp, d3=3.0_iwp, d4=4.0_iwp, d5=5.0_iwp,&
  d6=6.0_iwp, d8=8.0_iwp, d9=9.0_iwp, d10=10.0_iwp, d11=11.0_iwp,             &
  d12=12.0_iwp, d16=16.0_iwp, d18=18.0_iwp, d27=27.0_iwp, d32=32.0_iwp,       &
  d36=36.0_iwp, d54=54.0_iwp, d64=64.0_iwp, d128=128.0_iwp
INTEGER  x11(20), eta1(20), zeta1(20), l, ndim, nod
ndim=UBOUND(der, 1)
nod= UBOUND(der, 2)
SELECT CASE(ndim)
CASE(2)       ! two dimensional elements
  x1=points(1, 1)
  eta=points(1, 2)
  c1 x1
  c2=eta
  c3=one-c1-c2
  etam=pt25*(one eta)
  etap=pt25*(one+eta)
  x1m= pt25*(one-x1)
  x1p= pt25*(one+x1)
  x2p1=two*x1+one
  x2m1=two*x1-one
  e2p1=two*eta+one
  e2m1=two*eta-one
  SELECT CASE(nod)
  CASE (4)
    der(1, 1)=-etam
    der(1, 2)=-etap
    der(1, 3)=etap
    der(1, 4)=etam
    der(2, 1)=-x1m
    der(2, 2)=x1m
    der(2, 3)=-x1p
    der(2, 4)=-x1p
  CASE DEFAULT
    WRITE(*, *)"wrong number of nodes in shape_der"
  END SELECT
CASE(3)  ! 3 dimensional elements
  x1=points(1, 1)
  eta=points(1, 2)
  zeta=points(1, 3)
  etam=one-eta
  x1m=one-x1
  zetam=one-zeta
  etap=eta+one
  x1p=x1+one
  zetap=zeta+one
  SELECT CASE(nod)
  CASE(8)
    der(1, 1)= pt125*etam*zetam
    der(1, 2)=-pt125*etam*zetap
    der(1, 3)= pt125*etam*zetap
    der(1, 4)= pt125*etam*zetam
```

```
      der(1,5)= pt125*etap*zetam
      der(1,6)=-pt125*etap*zetap
      der(1,7)- pt125*etap*zetap
      der(1,8)- pt125*etap*zetam
      der(2,1)=-pt125*xim*zetam
      der(2,2)=-pt125*xim*zetap
      der(2,3)= pt125*xip*zetap
      der(2,4)=-pt125*xip*zetam
      der(2,5)= pt125*xim*zetam
      der(2,6)- pt125*xim*zetap
      der(2,7)= pt125*xip*zetap
      der(2,8)= pt125*xip*zetam
      der(3,1)- pt125*xim*etam
      der(3,2)= pt125*xim*etam
      der(3,3)= pt125*xip*etam
      der(3,4)=-pt125*xip*etam
      der(3,5)= pt125*xim*etap
      der(3,6)= pt125*xim*etap
      der(3,7)- pt125*xip*etap
      der(3,8)=-pt125*xip*etap
    CASE DEFAULT
      WRITE(*,*)"wrong number of nodes in shape_der"
    END SELECT
  CASE DEFAULT
    WRITE(*,*)"wrong number of dimensions in shape_der"
  END SELECT
RETURN
END SUBROUTINE shape_der
!
!
SUBROUTINE shape_fun(fun,points,i)
!
!   This subroutine computes the values of the shape functions
!   to local coordinates
!
 IMPLICIT NONE
 INTEGER,PARAMETER  iwp=SELECTED_REAL_KIND(15)
 INTEGER,INTENT(in)  i
 REAL(iwp),INTENT(IN)  points( , )
 REAL(iwp),INTENT(OUT)  fun( )
 REAL(iwp)  eta,xi,etam,etap,xim,xip,zetam,zetap,c1,c2,c3
 REAL(iwp)  t1,t2,t3,t4,t5,t6,t7,t8,t9
 REAL(iwp)  zeta,xi0,eta0,zeta0
 INTEGER  xi1(20),etai(20),zetai(20),l,ndim,nod
 REAL,PARAMETER  pt125=0.125_iwp,pt25=0.25_iwp,pt5=0.5_iwp,pt75=0.75_iwp,  &
   one=1.0_iwp,two=2.0_iwp,d3=3.0_iwp,d4=4.0_iwp,d8=8.0_iwp,d9=9.0_iwp,    &
   d16=16.0_iwp,d27=27.0_iwp,d32=32.0_iwp,d64=64.0_iwp,d128=128.0_iwp
 ndim=UBOUND(points,2)
 nod=UBOUND(fun,1)
 SELECT CASE(ndim)
 CASE(2) ! two dimensional case
   c1=points(i,1)
   c2=points(i,2)
   c3=one-c1-c2
   xi=points(i,1)
```

```
    eta=points(1,2)
    etam=pt25*(one-eta)
    etap=pt25*(one+eta)
    x1m=pt25*(one-x1)
    x1p=pt25*(one+x1)
    SELECT CASE(nod)
    CASE(4)
      fun=(/d4*x1m*etam, d4*x1m*etap, d4*x1p*etap, d4*x1p*etam/)
    CASE DEFAULT
      WRITE(*,*)"wrong number of nodes in shape_fun"
    END SELECT
  CASE(3) ! d3 dimensional case
    x1=points(1,1)
    eta=points(1,2)
    zeta=points(1,3)
    etam=one-eta
    x1m=one-x1
    zetam=one-zeta
    etap=eta+one
    x1p=x1+one
    zetap=zeta+one
    SELECT CASE(nod)
    CASE(8)
      fun=(/pt125*x1m*etam*zetam, pt125*x1m*etam*zetap,                    &
            pt125*x1p*etam*zetap, pt125*x1p*etam*zetam,                    &
            pt125*x1m*etap*zetam, pt125*x1m*etap*zetap,                    &
            pt125*x1p*etap*zetap, pt125*x1p*etap*zetam/)
    CASE DEFAULT
      WRITE(*,*)"wrong number of nodes in shape_fun"
    END SELECT
  CASE DEFAULT
    WRITE(*,*)"wrong number of dimensions in shape_fun"
  END SELECT
RETURN
END SUBROUTINE shape_fun
!
!
SUBROUTINE spabac(kv, loads, kdiag)
!
! This subroutine performs Cholesky forward and back-substitution
! on a symmetric skyline global matrix
!
 IMPLICIT NONE
 INTEGER, PARAMETER  iwp=SELECTED_REAL_KIND(15)
 REAL(iwp), INTENT(IN)  kv( )
 REAL(iwp), INTENT(IN OUT)  loads(0 )
 INTEGER, INTENT(IN)  kdiag( )
 INTEGER  n, i, k1, l, m, j, it, k
 REAL(iwp)  x
 n=UBOUND(kdiag,1)
 loads(1)=loads(1)/kv(1)
 DO i=2,n
   k1=kdiag(i)-i
   l=kdiag(i 1)-k1+1
   x=loads(i)
```

```
    IF(l/=i)THEN
      m=i-l
      DO j=l,m
        x=x-kv(k1+j)*loads(j)
      END DO
    END IF
    loads(i)=x/kv(k1+i)
  END DO
  DO it=2,n
    i=n+2-it
    k1=kdiag(i)-i
    x=loads(i)/kv(k1+i)
    loads(i)=x
    l=kdiag(i-1)-k1+1
    IF(l/=i)THEN
      m=i-l
      DO k=l,m
        loads(k)=loads(k)-x*kv(k1+k)
      END DO
    END IF
  END DO
  loads(1)=loads(1)/kv(1)
RETURN
END SUBROUTINE spabac
!
!
SUBROUTINE sparin(kv,kdiag)
!
! This subroutine performs Cholesky factorisation on a symmetric
! skyline global matrix
!
 IMPLICIT NONE
 INTEGER,PARAMETER  iwp=SELECTED_REAL_KIND(15)
 REAL(iwp),INTENT(IN OUT)  kv( )
 INTEGER,INTENT(IN)  kdiag( )
 INTEGER  n,i,k1,l,kj,j,ll,m,k
 REAL(iwp)  x
 n=UBOUND(kdiag,1)
 kv(1)=SQRT(kv(1))
 DO i=2,n
   k1=kdiag(i)-i
   l=kdiag(i-1)-k1+1
   DO j=l,i
     x=kv(k1+j)
     kj=kdiag(j)-j
     IF(j/=1)THEN
       ll=kdiag(j-1)-kj+1
       ll=max(l,ll)
       IF(ll/=j)THEN
         m=j-1
         DO k=ll,m
           x=x-kv(k1+k)*kv(kj+k)
         END DO
       END IF
     END IF
```

```
      kv(k1+j)=x/kv(kj+j)
    END DO
    kv(k1+1)=SQRT(x)
  END DO
RETURN
END SUBROUTINE sparin
!
END MODULE main
```

II.3.2.geom.f90

```
MODULE geom
!
contains
!
subroutine coord_xy(x coords, y_coords, nxe, nye, dx, dy)
!
!generate x_coords, y_coords
!
implicit none
integer, parameter  iwp=selected_real_kind(15)
integer, intent(in)  nxe, nye
real(iwp), intent(in)  dx, dy
real(iwp), intent(out)  x_coords( ), y coords( )
integer  i
x_coords(1)=0 0
y_coords(1)=0 0
xcoords do i=2, nxe+1
  x_coords(i)=x_coords(i-1)+dx  !dx is the dimension in x-direction
end do xcoords
ycoords do i=2, nye+1
  y_coords(i)=y_coords(i 1)-dy  !dy is the dimension in y direction
end do ycoords
return
end subroutine coord_xy
!
!
subroutine coord_xyz(x_coords, y_coords, z coords, nxe, nye, nze, dx, dy, dz)
!
!generate x_coords, y_coords and z_coords
!
implicit none
integer, parameter  iwp=selected_real_kind(15)
integer, intent(in)  nxe, nye, nze
real(iwp), intent(in)  dx, dy, dz
real(iwp), intent(out)  x_coords( ), y_coords( ), z_coords( )
integer  i
x_coords(1)=0 0
y_coords(1)=0 0
z coords(1)=0 0
xcoords do i=2, nxe+1
  x_coords(i)=x_coords(i 1)+dx  !dx is the dimension in x-direction
end do xcoords
ycoords do i=2, nye+1
  y_coords(i)=y_coords(i 1)+dy  !0 00004 is the dimension in y-direction
end do ycoords
zcoords do i=2, nze+1
  z_coords(i)=z_coords(i-1)-dz  !0 00004 is the dimension in z-direction
end do zcoords
return
end subroutine coord_xyz
!
```

```
!
SUBROUTINE geom_rect(iel, x_coords, y_coords, coord, num)
!
! This subroutine forms the coordinates and connectivity for a
! rectangular mesh of quadrilateral elements (4-node) counting in the
! x-dir
!
 IMPLICIT NONE
 INTEGER, PARAMETER  iwp=SELECTED_REAL_KIND(15)
 REAL(iwp), INTENT(IN)  x_coords( ), y_coords( )
 REAL(iwp), INTENT(OUT)  coord( , )
 INTEGER, INTENT(IN)  iel
 INTEGER, INTENT(OUT)  num( )
 INTEGER  ip, iq, jel, fac1, nod, nxe, nye
 REAL(iwp)  pt5=0 5_iwp, two=2 0_iwp, d3=3 0_iwp
 nxe=UBOUND(x_coords, 1)-1
 nod=UBOUND(num, 1)
 nye=UBOUND(y_coords, 1)-1
 iq=(iel-1)/nxe+1
 ip=iel (iq-1)*nxe
 SELECT CASE(nod)
 CASE(4)
    num(1)=iq*(nxe+1)+ip
    num(2)=(iq-1)*(nxe+1)+ip
    num(3)=num(2)+1
    num(4)=num(1)+1
!
    coord(1 2, 1)=x_coords(ip)
    coord(3 4, 1)=x_coords(ip+1)
    coord(1, 2)=y_coords(iq+1)
    coord(2 3, 2)=y_coords(iq)
    coord(4, 2)=coord(1, 2)
!
 CASE DEFAULT
    WRITE(11,'(a)')"Wrong number of nodes for quadrilateral element"
 STOP
 END SELECT
RETURN
END SUBROUTINE geom_rect
!
!
SUBROUTINE hexahedron_xz(iel, x_coords, y_coords, z_coords, coord, num)
!
! This subroutine generates nodal coordinates and numbering for
! 8-node "bricks" counting x-z planes in the y-direction
!
 IMPLICIT NONE
 INTEGER, PARAMETER  iwp=SELECTED_REAL_KIND(15)
 INTEGER, INTENT(IN)  iel
 REAL(iwp), INTENT(IN)  x_coords( ), y_coords( ), z_coords( )
 REAL(iwp), INTENT(OUT)  coord( , )
 INTEGER, INTENT(OUT)  num( )
 REAL(iwp)  pt5=0 5_iwp
 INTEGER  fac1, fac2, ip, iq, is, iplane, nod, nxe, nze
 nxe=UBOUND(x_coords, 1)-1
```

```
 nze=UBOUND(z_coords,1)-1
 nod=UBOUND(num,1)
 iq=(iel-1)/(nxe*nze)+1
 iplane=iel-(iq-1)*nxe*nze
 is=(iplane-1)/nxe+1
 ip=iplane-(is-1)*nxe
 SELECT CASE(nod)
 CASE(8)
   fac1=(nxe+1)*(nze+1)*(iq-1)
   num(1)=fac1+is*(nxe+1)+ip
   num(2)=fac1+(is-1)*(nxe+1)+ip
   num(3)=num(2)+1
   num(4)=num(1)+1
   num(5)=(nxe+1)*(nze+1)*iq+is*(nxe+1)+ip
   num(6)=(nxe+1)*(nze+1)*iq+(is-1)*(nxe+1)+ip
   num(7)=num(6)+1
   num(8)=num(5)+1
!
   coord(1 2,1)=x_coords(ip)
   coord(5 6,1)=x_coords(ip)
   coord(3 4,1)=x_coords(ip+1)
   coord(7 8,1)=x_coords(ip+1)
!
   coord(1 4,2)=y_coords(iq)
   coord(5 8,2)=y_coords(iq+1)
!
   coord(2 3,3)=z_coords(is)
   coord(6 7,3)=z_coords(is)
   coord(1 4 3,3)=z_coords(is+1)
   coord(5 8 3,3)=z_coords(is+1)
!
 CASE DEFAULT
   WRITE(11,'(a)')"Wrong number of nodes for hexahedral element"
   STOP
 END SELECT
RETURN
END SUBROUTINE hexahedron_xz
!
!
SUBROUTINE mesh_size(element,nod,nels,nn,nxe,nye,nze)
!
!  This subroutine returns the number of elements (nels) and the number
!  of nodes (nn) in a 2- or 3-d geometry-created mesh
!
 IMPLICIT NONE
 CHARACTER(LEN=15),INTENT(IN)  element
 INTEGER,INTENT(IN)  nod,nxe,nye
 INTEGER,INTENT(IN),OPTIONAL  nze
 INTEGER,INTENT(OUT)  nels,nn
 IF(element=="quadrilateral")THEN
   nels=nxe*nye
   IF(nod==4)nn=(nxe+1)*(nye+1)
 ELSE IF(element=="hexahedron")THEN
   nels=nxe*nye*nze
   IF(nod==8)nn=(nxe+1)*(nye+1)*(nze+1)
```

```
 END IF
RETURN
END SUBROUTINE mesh_size
!
END MODULE geom
```

II.4. Output files

II.4.1.Two-dimension

II.4.1.1. twoD_elements.m

```
function [dens]=twod_elements(nelx, nely, densities, iteration)

%-------------------------------------------------------------------------
% This file generates image according to the elements' densities
% in the densities_final2D dat, which is generated from main_2D f90
%
% nelx  number of elements in x-axis,
% nely  number of elements in y-axis,
% densities  column vector of elements' density,
% iteration  number of iteration
%-------------------------------------------------------------------------

dens=zeros(nely,nelx),
for i=1 nely
    dens(i, )=densities((i-1)*nelx+1 i*nelx),
end

colormap(bone1)
image(256*dens)
axis square
title(strcat('morphology for iteration-',int2str(iteration)))
drawnow
```

II.4.2. Three-dimension

II.4.2.1. threeD_elements.m

```
function threeD_elements(nxe, nye, nze, dx, dy, dz, densities, density)

%-------------------------------------------------------------------------
%  This file generates image composed of elements according to the
%  elements' densities in the densities_final3D dat, which is generated
%  from main_3D f90
%
%  nelx  number of elements in x-axis,
%  nely  number of elements in y-axis,
%  nelz  number of elements in z-axis,
%  dx  dimension of element in x-axis,
%  dy  dimension of element in y-axis
%  dz  dimension of element in z-axis,
%  densities  column vector of elements' density,
%  density  minimal density of element which can be shown in the image
%-------------------------------------------------------------------------

for a=2 (nxe-1)
   for b=2 (nze-1)
      for c=2 (nye-1)
         iel=(c-1)*nxe*nze+(b-1)*nxe+a,
         if densities(iel)>density
           x=dx*[a-1  a    a    a-1  a-1  a-1,...
                 a    a    a-1  a-1  a    a,...
                 a    a    a-1  a-1  a    a,...
                 a-1  a    a    a-1  a-1  a-1],
           y=dy*[c-1  c-1  c    c    c-1  c-1,...
                 c-1  c    c    c-1  c-1  c-1,...
                 c-1  c    c    c-1  c    c,...
                 c-1  c-1  c    c    c    c],
           z=-1*dz*[b-1  b-1  b-1  b-1  b-1  b,...
                    b-1  b-1  b-1  b-1  b-1  b,...
                    b    b    b    b    b-1  b,...
                    b    b    b    b    b-1  b],
           clr=[0.4861  0.5486  0.6111],
           patch(x, y, z, clr),
           view(3)
           axis equal
           hold on
         end
      end
   end
end
```

II.4.2.2. threeD_surface.m

```
function threeD_surface(nxe,nye,nze,dens)

%-------------------------------------------------------------------------
%  This file generates the surfaces of structure according to the
%  elements' densities in the densities_final3D.dat, which is generated
%  from main_3D.f90.
%
%  nelx: number of elements in x-axis;
%  nely: number of elements in y-axis;
%  nelz: number of elements in z-axis;
%  dens: column vector of elements' density.
%-------------------------------------------------------------------------

dens1=zeros(nze-2,nxe-2,nye-2);
for b=1:(nze-2)
   for a=1:(nxe-2)
      for c=1:(nye-2)
         dens1(c,b,a)=dens((c+1)*(nze*nxe)-(a+1)*nxe+(b+1));
      end
   end
end

clr=[0.4861   0.5486   0.6111];
dens1=smooth3(dens1,'gaussian',5);
p1=patch(isosurface(dens1,.4),'facecolor',clr,'edgecolor','none');
patch(isocaps(dens1,.4),'facecolor',clr,'edgecolor','none');
isonormals(dens1,p1)
view(3);
axis vis3d tight
camlight;
lighting phong
```

II.5. Glossary of main variable names

Scalar integers:

iteration	number of total iteration times
ndim	number of dimensions
ndof	number of degrees of freedom per element
nels	number of elements
neq	number of degrees of freedom in the mesh
nip	number of integrating points per elements
ninfe	number of elements which are influenced in x-,or y-,or z-direction
nn	number of nodes in the mesh
nod	number of nodes per element
nodof	number of degree of freedom per node
nr	number of restrained nodes
nst	number of stress (strain) terms (3, 4, or 6)
nxe	number of elements in x-direction
nye	number of elements in y-direction
nze	number of elements in z-direction

Scalar reals:

det	determinant of Jacobian matrix
Dinfl	distance of influence
emax	maximal Young's modulus of the trabecular tissue
gama	exponent of the Young's modulus calculating function
one	set to 1.0
maxdens	maximal relative density of bone elements
mechanosensitivity	mechanosensitivity of osteocytes
mindens	minimal relative density of bone elements

profactor	proportionality factor that regulates the formation rate
resorptionamount	amount of bone resorbed by osteoclasts
resorptionchance	probability (%) of bone resorption
threshold	threshold of bone formation
v	poisson's ratio of trabecular tissue
zero	set to 0.0

Scalar characters:

element	element type

Dynamic integer arrays:

g	element steering vector
g_g	global element steering matrix
g_num	global element node numbers matrix
kdiag	diagonal term location vector
nf	nodal freedom matrix
no	fixed freedom numbers vector
node	fixed nodes vector
num	element node number vector

Dynamic real arrays:

bee	strain-displacement matrix
coord	element nodal coordinates
d	preconditioned rhs vector
dee	stress-strain matrix
der	shape function derivatives with respect to local coordinates
deriv	shape function derivatives with respect to global coordinates
dx	dimension of element in x direction
eld	element nodal displacements

fback	external loads on the back surface
fbottom	external loads on the bottom surface
ffront	external loads on the front surface
fleft	external loads on the left surface
fright	external loads on the right surface
ftop	external loads on the top surface
fun	shape functions
gc	integrating point coordinates
g_coord	global nodal coordinates
jac	Jacobian matrix
km	element stiffness matrix
kv	global stiffness matrix
loads	nodal loads and displacements
points	integrating point local coordinates
sigma	stress terms
weights	weighting coefficients
x_coords	x-coordinates of mesh layout
y_coords	y-coordinates of mesh layout
z_coords	z-coordinates of mesh layout